ABSTRACT

Title of Dissertation:	IDENTIFICATION OF KEY MOLECULES IN PLACODE-DERIVED NEURONS THAT COORDINATE CHICK TRIGEMINAL GANGLIOGENESIS
	Margaret Hines, Doctor of Philosophy, 2024
Dissertation directed by:	Professor, Lisa Taneyhill, Department of Animal and Avian Sciences

The trigeminal nerve is the largest of the cranial nerves, possessing three main branches (ophthalmic, maxillary, and mandibular) and relaying sensations of pain, touch, and temperature from the face and head to the brain. Cell bodies of this nerve are positioned in the trigeminal ganglion, which arises from the coalescence of neural crest cells and placode cells. These progenitor cells give rise to trigeminal sensory neurons, with placode cell differentiation occurring first. While the dual cellular origin of the trigeminal ganglion has been known for decades, the molecular mechanisms controlling trigeminal ganglion development remain obscure. To elucidate molecules involved in this process, we performed RNAsequencing on the forming chick trigeminal ganglion when only placode cells contribute neurons and identified *Neurogenin2* (*Neurog2*), *Neuronal Differentiation 1* (*NeuroD1*), and *Elongator acetyltransferase complex subunit 1* (*Elp1*) for further study. While Neurog2, NeuroD1, and Elp1 have established roles in neurogenesis in other systems, their functions in placode cells during trigeminal

gangliogenesis had yet to be investigated. To address this, we used the chick embryo due to experimental advantages afforded by this model for the study of trigeminal placode cells and trigeminal ganglion development. Using morpholino antisense oligonucleotides, we depleted Neurog2, NeuroD1, or Elp1 from trigeminal placode cells and demonstrated each are essential for proper trigeminal ganglion development. Knockdown of Neurog2, NeuroD1, or Elp1 reduced trigeminal ganglion size and led to aberrant innervation of the eye by the ophthalmic branch. While depletion of Neurog2 and NeuroD1 had opposite effects on the width of the ophthalmic branch, Elp1 reduction appeared to have no effect. However, Elp1 knockdown led to less compact trigeminal ganglion nerve branches, decreased axon projections, and general disorganization of neurons and neural crest cells. Taken together with prior findings, our results suggest a novel interrelationship among Neurog2, NeuroD1, and Elp1 during trigeminal gangliogenesis. Our results have potential high significance for providing new insights into the function of Neurog2, NeuroD1, and Elp1 in trigeminal ganglion development and the etiology of human and animal diseases arising from defects in neural crest cells and/or placode cells.

IDENTIFICATION OF KEY MOLECULES IN PLACODE-DERIVED NEURONS THAT COORDINATE CHICK TRIGEMINAL GANGLIOGENESIS

by

Margaret Hines

Dissertation submitted to the Faculty of the Graduate School of the
University of Maryland, College Park, in partial fulfillment
of the requirements for the degree of
Doctor of Philosophy
2024

Advisory Committee:
Professor Lisa Taneyhill, Chair
Professor Carol Keefer
Professor Leslie Pick
Associate Professor Sougata Roy
Assistant Professor Andrew Schiffmacher

Foreword

The Examining Committee determined that Margaret Hines made a substantial contribution to the relevant aspects of the jointly authored work presented in Chapter 3 of this dissertation.

Dedication

I would like to dedicate this thesis to my guardian angels, my great grandfather Roland Jacobs, great aunt Wendy Jacobs, uncle Mark McKay, grandmother Patricia Hines and dogs Cooper and Finnegan. While you all may no longer be with us on earth, I have felt your presence every day since you have left. Thank you for everything you all have taught me during our time together.

Acknowledgements

I wish to extend my heartfelt appreciation to the individuals who have played pivotal roles in my academic journey, shaping me into the researcher and individual I am today.

First and foremost, I would like to thank my thesis mentor, Lisa Taneyhill, for seeing my potential and taking a chance on me despite my lack of laboratory experience. She has continued to support and encourage me to grow as a scientist. I am immensely grateful for her wisdom and guidance throughout this journey.

I also want to express my deepest gratitude to my postdoc mentor and close friend, Carrie Leonard. Carrie's impact on my life over the past six years has been immeasurable. Her mentorship, friendship, and support have helped me flourish both professionally and personally. I am forever thankful for her guidance and the opportunity to be part of her extended family.

To my committee members, Carol Keefer, Sougata Roy, Leslie Pick, Andrew Schiffmacher, and Arpita Upadhyaya, thank you for your dedication and invaluable support throughout my academic journey. Their guidance and encouragement have been instrumental in shaping me into the researcher I am today. I am truly fortunate to have had the opportunity to work with such a distinguished group of individuals.

While scheduling conflicts impacted the "official" inclusion on my dissertation committee, Arpita Upadhyaya has been an instrumental part of my committee throughout this journey. Thank you for your support over the years. I am truly grateful for your contributions to my research endeavors.

I would also like to thank the past and present members of the Taneyhill Lab, Chyong-Yi Wu, Ashrifia Adomako-Ankomah, Mashood Wani, Karyn Jourdeuil, Linda Farley, Ankita Shah, Seth Hannah, Parinaz Bina, Carrie Leonard, Caroline Halmi, Johena Sanyal, and Lesly Sejas for

creating a welcoming environment, dedicated to the success of one another. You all have been more like family than coworkers.

To my wonderful officemates, Grace Markley and Elizabeth Cooper, thank you for your friendship, support, and camaraderie throughout this journey. I am grateful to have shared this experience with both of you.

My deepest gratitude goes to my family for their unwavering support throughout this journey. To my mother, Lisa, who has been my greatest supporter since day one. She has been there for all my ups and downs throughout my life, and I can always count on her to be there for me. Next, my father, Dan, has been inspiration from day one. He is the reason I fell in love with science and has continued to be a great supporter of my science journey. Lastly, my sister, Sarah, while we may have had our differences growing up, I am grateful for the relationship we have today. Thank you for always being there for me.

Finally, to my beloved grandmother, Karen Haensch, whose love, admiration, and support has been a constant source of strength and inspiration throughout my academic journey. I cherish every moment we share together, and your presence in my life means the world to me. Lastly, I would like to acknowledge my dog, Navy, who has been by my side throughout this challenging academic journey.

Table of Contents

This Table of Contents is automatically generated by MS Word, linked to the Heading formats used within the Chapter text.

List of Tables

List of Figures

List of Abbreviations

bHLH	Basic Helix-Loop-Helix
CKO	Conditional knockout
CN	Cranial nerve
E	Embryonic day
e	Ectoderm
E-Cad	E-Cadherin
EMT	Epithelial-to-mesenchymal transition
en	External nostrils
Elp	Elongator acetyltransferase complex
Elp1	Elongator acetyltransferase complex subunit 1
FD	Familial dysautonomia
FRUIT	Fructose and urea solution
gcil	ciliary ganglion
GSP	Gene specific primer
HH	Hamburger and Hamilton
HTSS	Heat-treated sheep serum
IHC	Immunohistochemistry
IV	Trochlear nerve
MmV	Maxillomandibular lobe
MO	Morpholino antisense oligonucleotide
NeuroD1	Neuronal Differentiation Factor 1
Neurog	Neurogenin
NT	Neural tube
OpV	Ophthalmic lobe
PBase	PiggyBac helper transposase
PBS	Phosphate-buffered saline
PBS-Tx	Phosphate-buffered saline with 0.1% TritonX-100
PFA	paraformaldehyde
PTW	Phosphate-buffered saline with 0.1% Tween-20
PVDF	Polyvinylidene fluoride membrane
qPCR	Quantitative polymerase chain reaction
RACE	Rapid amplification of cDNA ends
rax	Ramus alveolaris maxillaris
rce	Rami cutanei externi
rln	Lateral nasal branch of V1
rmd	Mandibular nerve
rmn	Medial nasal branch of V1
rmxe	External part of maxillary nerve
ropht	Ophthalmic profundal nerve of V1
rplt	Palantine branch of VII
SDS-PAGE	Sodium dodecyl sulfate–polyacrylamide gel electrophoresis
Sox10	SRY-box transcription factor 10
TG	Trigeminal ganglion
Trk	Tropomyosin receptor kinase
TUBB3	Beta Tubulin III

TUNEL	Terminal deoxynucleotidyl transferase dUTP nick end labeling
UTR	Untranslated region
V1	Ophthalmic nerve
V23	Trochlear nerve
VII + VIII	Facial nerve and acoustic nerve
WB	Immunoblotting

Chapter 1: Literature Review

1.1 Cranial Sensory Ganglia

Cranial sensory nerves are components of the peripheral nervous system, located in the head, that are responsible for relaying sensory information to the central nervous system. The structure that houses the neuronal cell bodies and supporting glia of the sensory nerves is termed the ganglion (Figure 1). In the head, these include the trigeminal (V) and epibranchial (geniculate (facial VII), petrosal (glossopharyngeal IX) and nodose (vagal X)) ganglia. Nerves arising from these ganglia innervate diverse structures including the face, tongue, mouth, and digestive tract, and are derived from two embryonic cell populations, cranial neural crest cells and neurogenic placodes. The geniculate, petrosal, and nodose ganglia have neurons derived from neural crest and placode origin in anatomically distinct, segregated regions (D'Amico-Martel & Noden, 1983; Steventon et al., 2014). The trigeminal ganglion, however, has neurons originating from both neural crest cells and cranial placodes that are intermixed, with supporting glial cells solely derived from neural crest cells (D'Amico-Martel & Noden, 1983).

The trigeminal ganglion is the first, and largest, cranial ganglion to form, making it an ideal model to study the interactions between neural crest cells and placode cells that must take place to build a complex structure. Neural crest cells from the midbrain and rostral hindbrain regions, along with placode cells from the trigeminal placode (Figure 1), migrate together and interact to form a tightly integrated structure. In the chick, the trigeminal ganglion initially possesses a bi-lobed shape that eventually resolves into a nerve with three main branches (ophthalmic, maxillary, and mandibular) (Higashiyama & Kuratani, 2014). These branches are

comprised of smaller nerves such as the frontal nerve, medial and lateral nasal nerves, and infraorbital nerve (Figure 2).

The trigeminal nerve detects pain sensations from common sources such as the jaw and teeth (toothaches), head (migraines), and the temporomandibular joint, all affecting countless individuals daily. Additionally, trigeminal neuralgia (Tic douloureux) is the most common disorder of the trigeminal nerve, occurring in approximately 150,000 people per year (Cleveland Clinic). This disorder is characterized by unilateral, sudden, intense facial pain that often has no clear cause. Understanding how the trigeminal nerve develops can thus inform treatments for many types of pain in the head and face region.

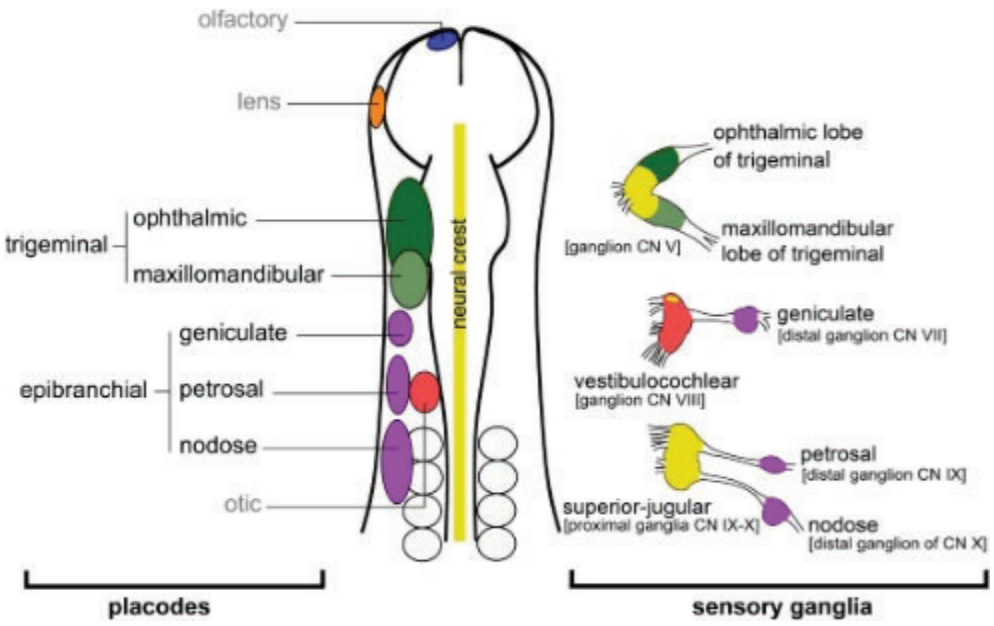

Figure 1: Cranial sensory ganglia are composed of neural crest cells and placode cells. This cartoon shows the anatomical locations of cranial placodes (left, multiple colors) and neural crest cells (middle, yellow) in vertebrate embryos. The respective contribution of these cell types to each sensory ganglia is depicted on the right. Adapted from Park and Saint-Jeannet, 2010.

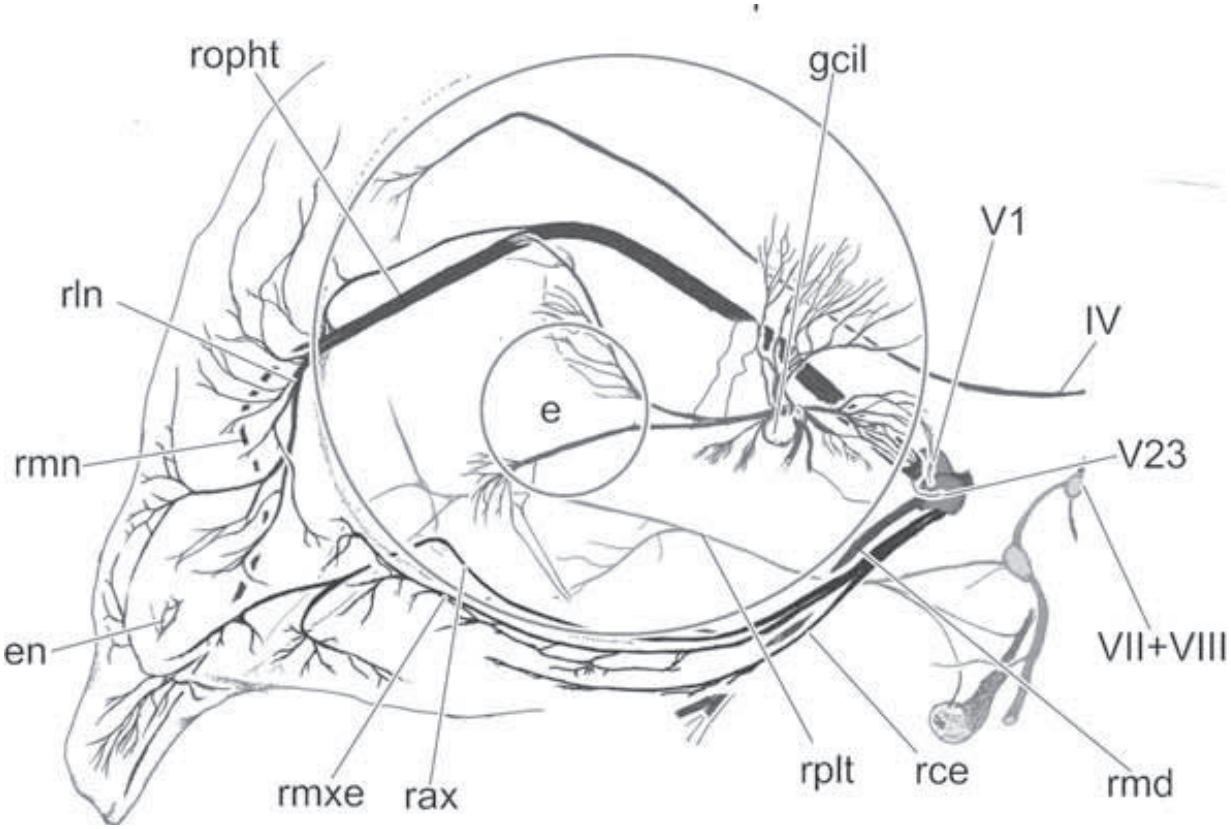

Figure 2: The anatomy of the embryonic chicken trigeminal nerve reveals a highly complex structure that innervates the face. Cartoon depiction of the trigeminal nerve in an embryonic day (E) 4.5 or Hamburger and Hamilton (HH) 25 embryo. Abbreviations are as follows (from top left, clockwise): ropht – ophthalmic profundal nerve of V1, gcil – ciliary ganglion, V1 – ophthalmic nerve, IV – trochlear nerve, V23 – maxillomandibular nerve, VII + VIII – facial nerve and acoustic nerve, rmd – mandibular nerve, rce – rami cutanei externi, rplt – palantine branch of VII, rax – ramus alveolaris maxillaris, rmxe – external part of maxillary nerve, en – external nostrils, rmn – medial nasal branch of V1, rln – lateral nasal branch of V1. Adapted from Higashiyama and Kuratani, 2014.

1.2 Neural Crest Cells

Neural crest cells are a multipotent, stem cell-like embryonic cell population unique to vertebrates. During the process of gastrulation, neural crest cells are induced and become situated at the neural plate border, the boundary between the non-neural ectoderm and the neural plate (Figure 3)(Copp et al., 2003; Simões-Costa & Bronner, 2013). This border then elevates, forming the neural folds, with neural crest cells now located in the dorsal most aspect. The neural folds later fuse to form the neural tube, a structure that will become the future brain and spinal cord, with neural crest cells remaining at the dorsal aspect of the neural tube (Theveneau & Mayor, 2012). Either just prior to (*Xenopus* and mouse) or after (chick) fusion of the neural folds, stationary, premigratory neural crest cells become motile through a process called the epithelial-to-mesenchymal transition (EMT) (Duband, 2010). During EMT, premigratory neural crest cells lose their epithelial structure and apico-basal polarity and adopt a mesenchymal morphology through the dissolution and/or rearrangement of tight and adherens junctions (Duband, 2010; Theveneau & Mayor, 2012). In this mesenchymal state, neural crest cells are now able to migrate to their respective locations, often traveling long distances, and eventually differentiate into a diverse range of cell types, such as the craniofacial cartilage and skeleton, skin pigment cells, portions of the heart, and sensory neurons and glia of the peripheral nervous system (Theveneau & Mayor, 2012).

Neural crest cells are divided into four main categories based on their axial level of origin and the types of structures to which they contribute: cranial (cephalic), vagal and sacral, cardiac, and trunk (Achilleos & Trainor, 2012). Depending upon the category, variations among neural crest cells are seen, such as the process by which delamination occurs in cranial versus trunk neural crest cells. In the head, EMT occurs *en masse,* a coordinated event where the cells are all

pushed out of the ectoderm at once (Duband, 2010). In the trunk, however, neural crest cells undergo progressive EMT with a small number of cells undergoing EMT in a "drip-like" fashion, leading to a longer period of EMT (Theveneau & Mayor, 2012). In addition to differences among the neural crest cell categories, species variation is also present. In the chick, neural crest cells undergo EMT and begin migrating at the time of neural fold fusion while in mouse and *Xenopus* this occurs prior to the fusion of the neural folds (Duband & Thiery, 1982; Sadaghiani & Thiébaud, 1987).

Despite these differences, all neural crest cells and their derivatives are formed through five major processes - induction, specification, delamination, migration, and differentiation - with many similarities shared in the context of their gene regulatory networks. Neural crest cell induction begins early in development at the time of gastrulation with progenitors arising in the neural plate border. Through expression of *Wnts*, *BMP*s, and *FGF*s, the neural plate border becomes competent to give rise to neural crest cells (Bronner & LeDouarin, 2012; Méndez-Maldonado et al., 2020). The expression of these molecules then induces expression of "neural plate border specifiers," transcription factors such as *Msx1/2, Pax3/7*, and *Zic1* that in turn activate expression of "neural crest specifiers," including *Snail/Slug, FoxD3, Id, cMyc*, and *Sox9/10*. Lastly, these neural crest specifiers control the expression of effector genes that mediate cell adhesion and motility such as *Cadherins*, *Collagen 2a*, *ADAMs*, and *Integrins* (Betancur et al., 2010; Bronner & LeDouarin, 2012).

Neural crest cells are an important cell type in embryogenesis, with disruptions at any point in their development causing a variety of birth defects and diseases termed neurocristopathies (Pilon, 2021; Vega-Lopez et al., 2018). Examples of neurocristopathies

include albinism, cleft lip and/or palate, melanoma, neuroblastoma, Treacher Collins syndrome, and Hirschsprung's disease, to name a few.

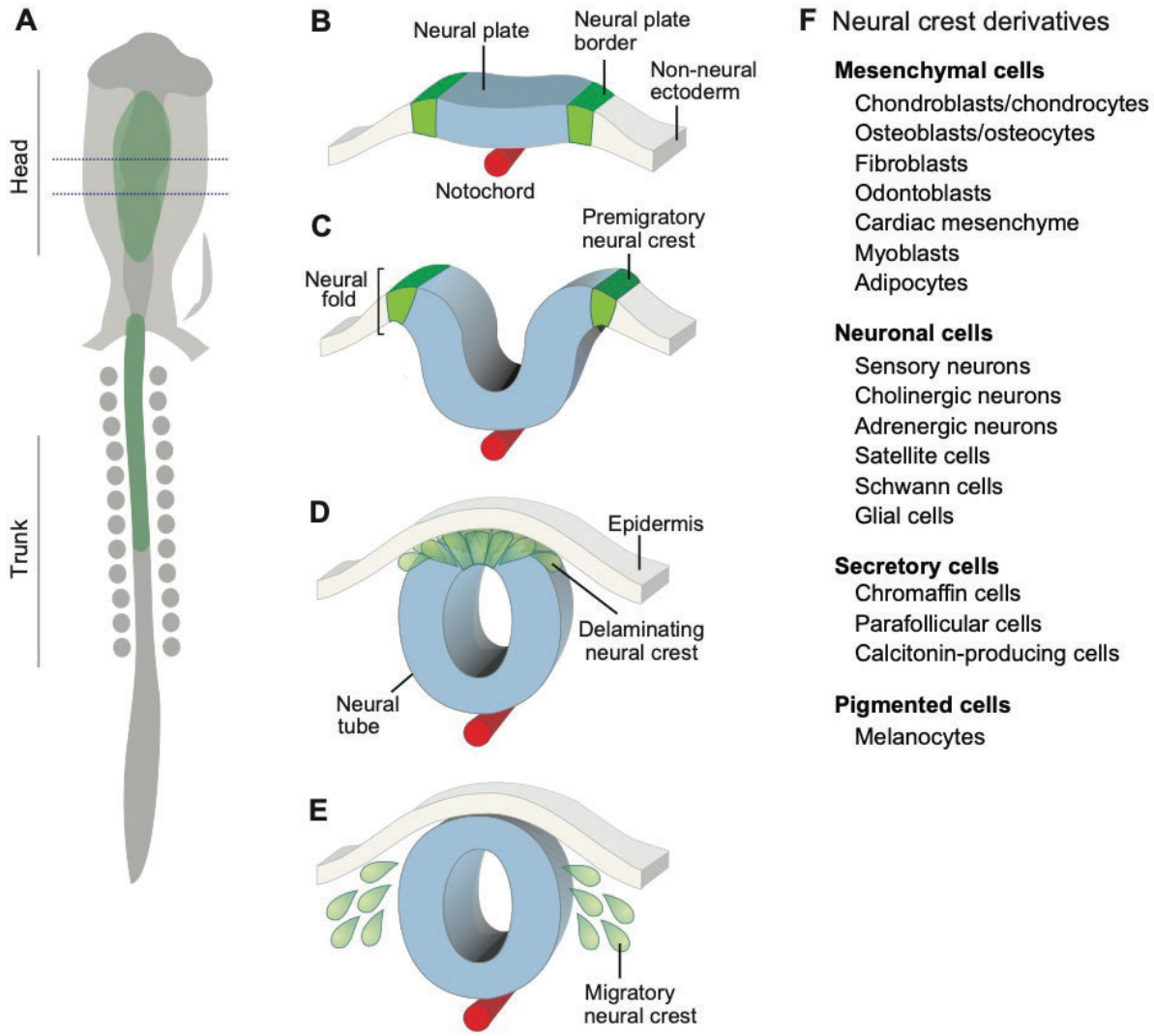

Figure 3: Neural crest cell location throughout the process of neurulation and migration. (A) A cartoon of a chick embryo shows the location of premigratory neural crest cells (green). (B-D) Cartoon transverse sections depicting the process of neurulation, highlighting, in green, the respective location of neural crest cells during induction (B), specification (C), and delamination (D). Originating in the neural plate border (B, green), neural crest cells become localized to the dorsal neural tube (D), after which they undergo EMT to become motile. Neural crest cell migration (E) occurs after neurulation is complete, leading to the derivatives shown in (F). Adapted from Simoes-Costa and Bronner 2015.

1.3 Cranial Placodes

Like neural crest cells, cranial placode cells are a migratory embryonic cell population unique to vertebrates. The term placode refers to focal thickenings of non-neural ectoderm (or future skin) on the surface of the embryo, which generates clusters of cells with similar fates (Figure 1) (Baker & Bronner-Fraser, 2001; Park & Saint-Jeannet, 2010). These cells also originate in the neural plate border, sharing an origin with neural crest cells. However, unlike neural crest cells, cranial placodes only contribute to the formation of neurosecretory cells, sensory neurons, and cranial sensory organs (Saint-Jeannet & Moody, 2014). Placode cells become migratory through invagination or delamination (Figure 4). Invagination occurs when the epithelium bends and forms a groove or vesicle and separates from the surface ectoderm (Figure 4A). Conversely, delamination happens when the cell breaks through the underlying protein-rich basement membrane (Figure 4B) (Breau & Schneider-Maunoury, 2015; Park & Saint-Jeannet, 2010).

The cranial placodes are involved in the formation of the paired sense organs (eye, nose, ear) and cranial sensory ganglia (Park & Saint-Jeannet, 2010). These placodes are defined as the adenohypophyseal, olfactory, lens, trigeminal, epibranchial, otic, and lateral line (specific to amphibians) placodes (Baker & Bronner-Fraser, 2001; Park & Saint-Jeannet, 2010). The olfactory and lens placodes give rise to the olfactory epithelium of the nose and lens of the eye, respectively. The trigeminal, otic, epibranchial (geniculate, petrosal, and nodose), and lateral line placodes are described as "neurogenic" and contribute to the sensory ganglia of the head. Each placode originates in a distinct region within the head, with location and surrounding environment contributing to their fates (Figure 1). The "neurogenic" placodes can be grouped based on their axial level of origin with the trigeminal, otic, and lateral line placodes described as "dorsolateral placodes" due to their dorsal positioning next to the hindbrain. However, the

“epibranchial placodes” (geniculate, petrosal, and nodose) are more ventral, close to the pharyngeal arches (Begbie et al., 2002; Park & Saint-Jeannet, 2010).

While often referred to as one structure, the trigeminal placode is made up of two distinct placodes, the ophthalmic and maxillomandibular (Baker & Bronner-Fraser, 2001; D’Amico-Martel & Noden, 1983), each contributing to a specific lobe of the trigeminal ganglion. Induction of these placodes occurs by factors expressed in the mid-hindbrain region such as Wnt, FGF, PDGF, and Notch (Baker et al., 1999; Begbie et al., 2002; Singh & Groves, 2016).

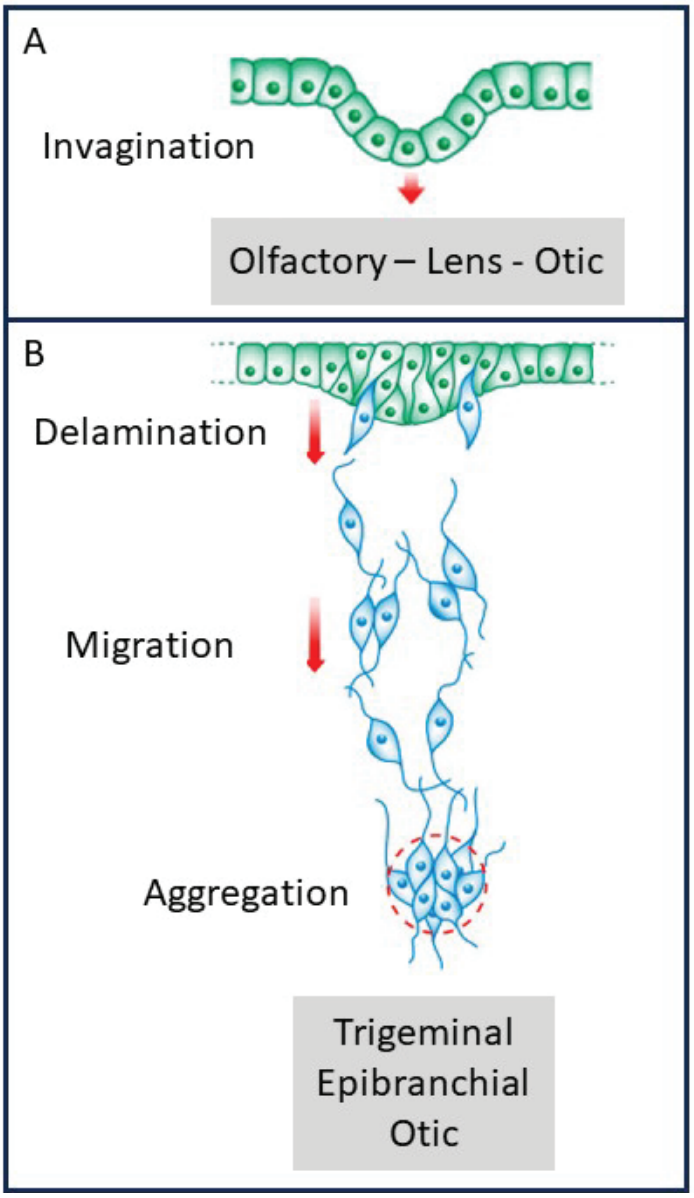

Figure 4: Placode cell development occurs in diverse ways in the vertebrate embryo. Cartoon illustrating placode cell invagination (A) and delamination (B). After emerging from the ectoderm, these cells become migratory and travel to their destinations where they aggregate to form their respective structures (Modified from Breau and Schneider-Maunoury 2015).

1.4 Formation of the Cranial Sensory Ganglia

Neural crest cells and neurogenic placode cells work together through reciprocal interactions to form the cranial sensory ganglia. During this developmental process, neural crest cells arrive at the ganglionic anlage prior to the placode cells. However, neural crest cell differentiation does not occur until after the arrival of the placode cells (Méndez-Maldonado et al., 2020). Neural crest cells form "corridors," providing a more permissive environment for placode cells to migrate and differentiate (Freter et al., 2013). Much of the research examining these reciprocal interactions has been carried out in the chick trigeminal ganglion. Studies examining trigeminal ganglion development after ablation of either neural crest cells or placode cells report defects in trigeminal ganglion formation, such as dispersal of placodal cells, smaller ganglia, and disrupted axonal trajectories (Hamburger, 1961; Lwigale, 2001; Shiau et al., 2008).

Molecules mediating neural crest-placode cell interactions have been the subject of multiple studies over the years. While placode cells express N-cadherin both prior to and during their migration and differentiation, neural crest cells do not express N-cadherin until after they differentiate into neurons (Hatta et al., 1987; Shiau & Bronner-Fraser, 2009). Interestingly, Cadherin-7-expressing neural crest cells and N-cadherin-expressing placode cells/neurons physically interact with one another to mediate initial trigeminal ganglion formation (Halmi et al., 2022). Without either one of these cadherins, the distribution and condensation of neural crest cells and placodal neurons in the trigeminal ganglion is disrupted, showing they are required for proper trigeminal ganglion assembly (Shiau & Bronner-Fraser, 2009; Wu & Taneyhill, 2019). Additionally, placodal neurons express the cell surface receptor Robo2 while neural crest cells express and secrete the Robo2 ligand, Slit1 (Shiau et al., 2008). When either Slit1 or Robo2 is inhibited, the organization of the trigeminal ganglion is lost. Additionally, the

Slit1-Robo2 complex is shown to influence subcellular localization of N-cadherin in placode cell-derived neurons (Shiau & Bronner-Fraser, 2009). These studies all corroborate the notion that neural crest cells and placode cells form reciprocal interactions during the formation of the trigeminal ganglia.

1.5 Neurogenesis

An important step in ganglion formation is the process by which progenitor cells differentiate into neurons, referred to as neurogenesis. In the chick, trigeminal neurogenesis first occurs in placode cell-derived neurons, starting as early as embryonic day (E)1 (Hamburger and Hamilton (HH) 10) in ophthalmic placode cells (Begbie et al., 2002; Hamburger & Hamilton, 1992; McCabe et al., 2009). Unlike other placode cell-derived neuron progenitors, these cells differentiate prior to delamination from the ectoderm (Begbie et al., 2002). Maxillomandibular placode cells undergo neurogenesis during migration, starting around E1.5 (HH11), completing this process before reaching the ganglion (Begbie et al., 2002; McCabe et al., 2009). Neural crest cells, however, do not start contributing neurons to the trigeminal ganglion until approximately E4 (HH24) (Shiau et al., 2008).

Proneural genes are one class of genes that are important for controlling neurogenesis, including in neurogenic placode cells, and these encode basic Helix-Loop-Helix (bHLH) transcription factors. One bHLH family involved in trigeminal neurogenesis is the Neurogenins (Neurogs). In the chick, Neurogenin1 (Neurog1) is observed in the maxillomandibular placode, while Neurogenin2 (Neurog2) is noted in the ophthalmic placode until E2.5 (HH15-17) and later in maxillomandibular neurons starting at E3 (HH18) (Begbie et al., 2002). Expression of *Neurog2* is regulated by the direct binding of Pax3 to the *Neurog2* promoter (Nakazaki et al., 2008; Perez et al., 1999). Pax3 is one of the earliest markers of the ophthalmic placode in the

chick, coinciding with ophthalmic placode cell specification, and is an essential player in neurogenesis (Baker et al., 1999; Dude et al., 2009; Stark et al., 1997). Neurogs additionally play a key role in the activation of downstream bHLH factors (Figure 5) including *Neuronal Differentiation Factor 1* (*NeuroD1*), which is expressed in chick trigeminal placode cells prior to delamination and in their neuronal derivatives up to E8 (HH34) (Abu-Elmagd et al., 2001; Dude et al., 2009). Despite what has been shown in the literature thus far, little is known about Neurog2 and NeuroD1 function in the chick trigeminal ganglion.

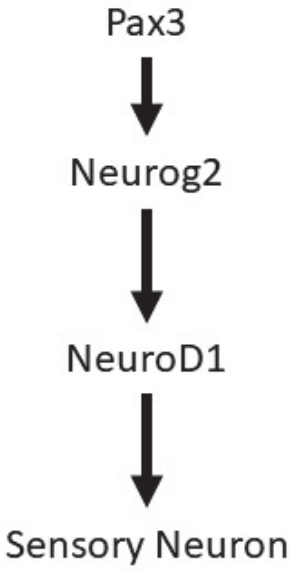

Figure 5: Summary of the regulatory interactions of neurogenesis in the ophthalmic placode. Pax3 activates *Neurog2* by binding its promoter, triggering expression of a cascade of bHLH factors such as *NeuroD1* and leading to the differentiation of a placode cell into a sensory neuron.

1.6 Elongator acetyltransferase complex subunit 1 (Elp1)

Elp1 is the largest protein of the dimeric six-subunit Elongator complex and serves as the scaffolding protein for this complex. The Elongator complex was originally identified to function in transcriptional elongation by association with RNA polymerase II (Kojic & Wainwright, 2016; Xu et al., 2015). Since this initial discovery, however, many additional functions of Elp1 have been identified, either on its own or in association with the Elongator complex (Table 1, Figure 6) (Kojic & Wainwright, 2016). Often the function of the Elongator complex is studied by knocking down/knocking out one of the Elp proteins, making it difficult to determine if the reported functions are for the complex or unique to the disrupted protein. For example, in the study of tRNA wobble uridine function, Elp1 was targeted to disrupt the Elongator complex (Goffena et al., 2018). However, mutations in different Elp proteins are associated with diseases each with unique phenotypes such as Amyotrophic lateral sclerosis(ALS), Rolandic epilepsy, Intellectual disability (IL), and familial dysautonomia (FD) (Table 2), implying that each protein may have individual roles outside of the complex (Kojic & Wainwright, 2016). This is important to keep in mind when trying to distinguish the function of the Elongator complex from that of individual Elp proteins. By comparing Elongator complex functions in Figure 5 with those reported for Elp1 in Table 1, overlap between the two can be appreciated, including tRNA modification, transcriptional elongation, regulation of actin cytoskeleton, and exocytosis. While many roles for Elp1 have been described, little is known molecularly about how these functions are carried out.

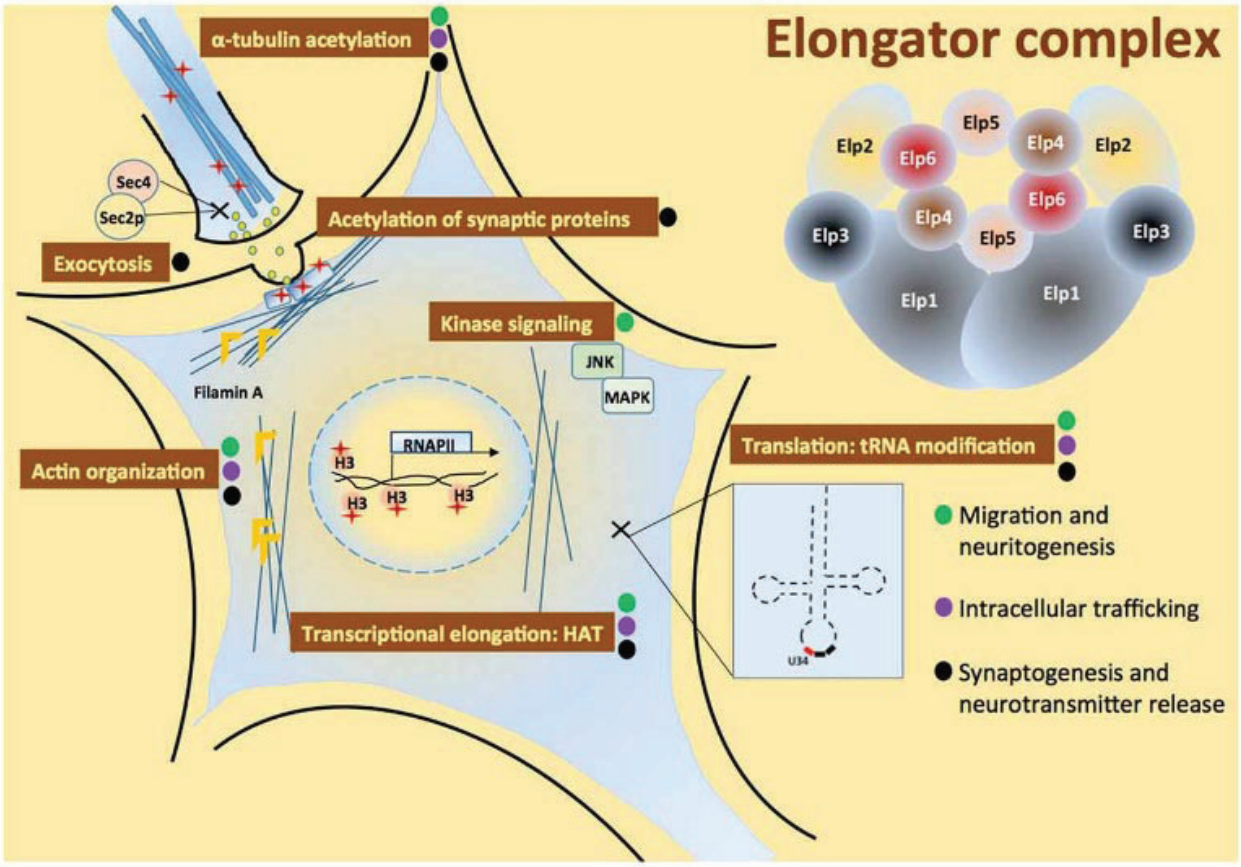

Figure 6: The Elongator complex has many proposed cellular functions. This schematic summarizes the diverse roles for the Elongator complex. The main categories include functions in migration and neuritogenesis (green dot), intracellular trafficking (purple dot), and synaptogenesis and neurotransmitter release (black dot) (Kojic & Wainwright, 2016).

Table 1: Elp1 functions in various cellular processes.

Function	References
Transcriptional elongation through interactions with RNA polymerase II	Close et al., 2006; Svejstrup, 2007; Otero et al., 1999; Hawkes et al., 2002
tRNA wobble uridine modification	Goffena et al., 2018; Huang et al., 2005; Huang et al., 2008; Bauer et al., 2012; Karlsborn et al., 2014
Neuronal differentiation	Hunnicutt et al., 2012; George et al., 2013; Abashidze et al., 2014; Leonard et al., 2022
Cell migration	Johansen et al., 2008; Close et al., 2006; Cheishvili et al., 2010; Naumanen et al., 2008
Regulation of cytoskeleton organization	Johansen et al., 2008; Abashidze et al., 2014; Cheishvili et al., 2010; Solinger et al., 2010; Planelles-Herrero et al., 2022
Vesicular trafficking; exocytosis in yeast	Li et al., 2020; Naftelberg et al., 2016; Rahl et al., 2005; Planelles-Herrero et al., 2022

Table 2: Elp protein-specific defects in neurological disorders (Adapted from Kojic and Wainwright, 2016).

Neurological Disorder	Affected Elp	Mutation	Type of disorder	Reference
Familial dysautonomia (FD)	Elp1	Mutation in the donor splice site of intron 20	Neurodevelopment abnormalities and neurodegeneration of autonomic and sensory neurons	Anderson et al., 2001; Slaugenhaupt et al., 2001; and Cuajungco et al., 2003
Intellectual disability (IL)	Elp2	Missense mutation	Neurocognitive; limitations in cognitive functioning and other skills	Najmabadi et al., 2011 and Cohen et al., 2015
Amyotrophic lateral sclerosis (ALS)	Elp3	Association with specific haplotype	Neurodegeneration of motor neurons	Simpson et al., 2009
Rolandic epilepsy	Elp4	Non-coding mutations	Neurocognitive causing seizures	Strug et al., 2009

1.7 Familial dysautonomia (FD)

FD, also referred to as "Riley-Day syndrome" or "hereditary sensory and autonomic neuropathy type III" [MIM 223900], is a neurodevelopmental and neurodegenerative disease affecting the development and survival of neurons (Norcliffe-Kaufmann et al., 2017). This disease is autosomal recessive and primarily affects the Ashkenazi Jewish population. Characterized, in part, by progressive neurodegeneration and neurodevelopmental defects (Norcliffe-Kaufmann et al., 2017), FD results in substantial neuronal dysfunction and is ultimately fatal, with only 50% of patients reaching age 40 (Axelrod, 2002; Gold-von Simson & Axelrod, 2006). In >99.5% of FD cases, a point mutation at the splice site in intron 20 of *ELP1* causes variable, tissue-specific mis-splicing of *ELP1*, leading to a decrease in ELP1 protein levels primarily in neurons (Figure 7) (Anderson et al., 2001; Slaugenhaupt et al., 2001).

Symptoms of FD include disruption of involuntary functions like digestion, breathing, and regulation of blood pressure, as well as sensory deficits (Dietrich & Dragatsis, 2016; Gold-von Simson & Axelrod, 2006). Notably, the trigeminal ganglion and trigeminal nerves of FD patients are smaller in size compared to healthy controls, indicating that the disease is not just neurodegenerative, as there is no correlation between the size of the trigeminal ganglion/nerves

and age of the patients (Gutiérrez et al., 2015; Won et al., 2019). Additionally, patients have decreased pain and temperature sensation in their face leading to self-mutilation over the course of their lifetime, suggesting dysfunction of the trigeminal ganglion/nerves (Mass & Gadoth, 1994; Norcliffe-Kaufmann et al., 2017). While the mutation causing FD is known, the mechanisms by which ELP1 controls peripheral nervous system formation and function remain obscure.

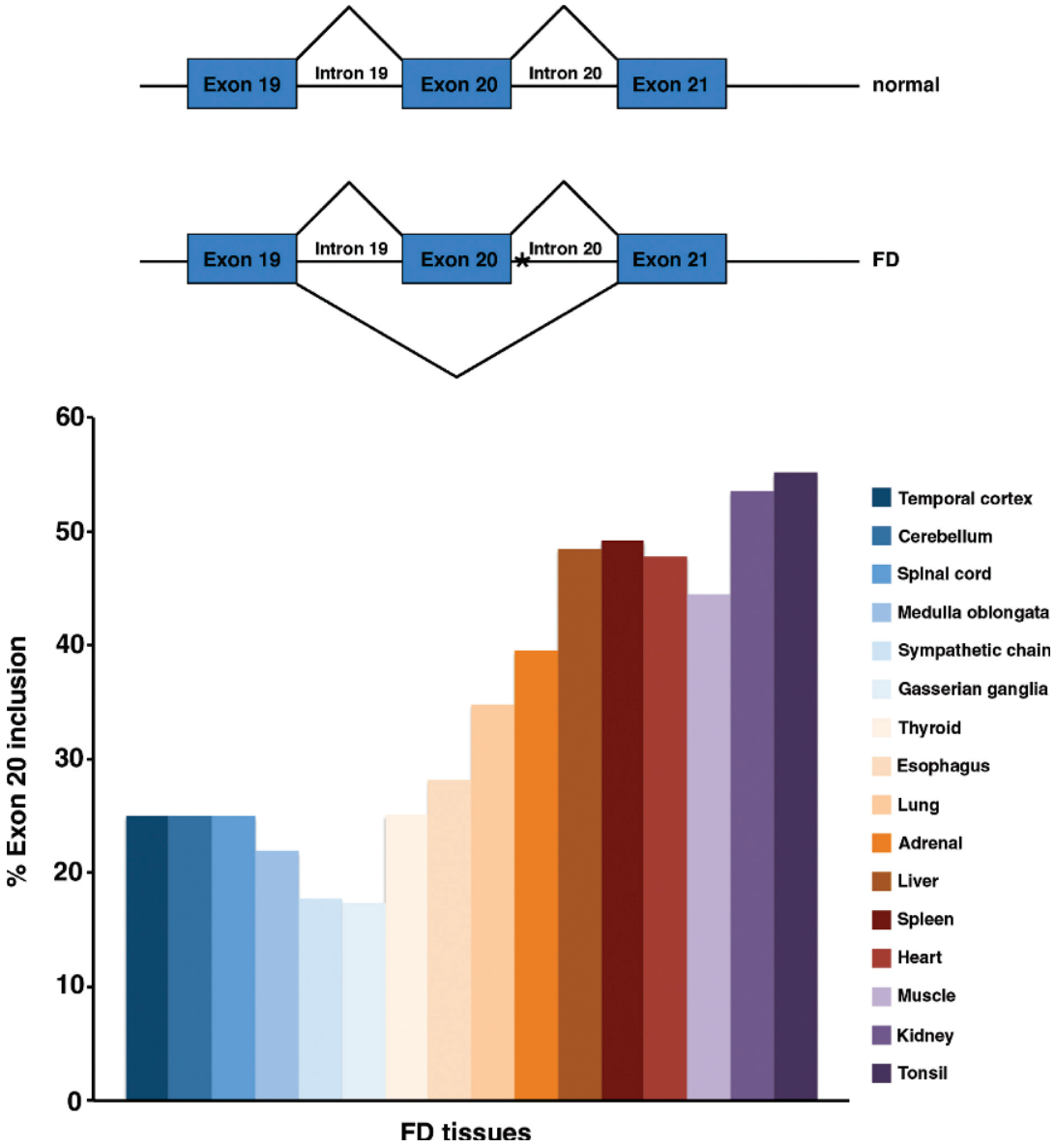

Figure 7: Tissue-specific mis-splicing of *ELP1* occurs in FD. A point mutation in the splice site of intron 20 in *ELP1* leads to the removal of exon 20 at varying rates of occurrence in patients with FD. The graph shows the percentage of correct splicing in a variety of tissues from FD patients. In shades of blue are the neuronal tissues, which have the lowest percentage of normal splicing occurrence, with the gasserian (trigeminal) ganglion being the lowest (Dietrich & Dragatsis, 2016).

1.8 Models of FD

Initial studies of Elp1 revealed the *Elp1* knockout mouse is embryonic lethal at E9, highlighting the importance of Elp1 in development (Chen et al., 2009). Given this limitation, a conditional knockout mouse model where *Elp1* was deleted from only neural crest cells, using a Wnt1-Cre based approach, has been used to study FD (known as the Elp1 CKO) (George et al., 2013; Goffena et al., 2018; Leonard et al., 2022). Many neurons, especially in the trunk, are neural crest-derived, making the Elp1 CKO a good model to investigate Elp1 function in the context of neural crest-derived sensory neurons. Examination of trunk neural crest-derived dorsal root ganglia in this model revealed that Elp1 deletion caused second wave neuronal progenitors to differentiate early or undergo cell death, failing to generate the full complement of TrkA nociceptive neurons (George et al., 2013). The TrkA population is responsible for the subset of neurons sensing pain and temperature, further suggesting a role for Elp1 in nociceptors (Reichardt, 2006).

A report examining Elp1 function in the trigeminal ganglion of this same Elp1 CKO revealed Elp1 is critical for trigeminal ganglion development. While initial formation of the trigeminal ganglion is not affected, disorganization and straying of axons is observed (Figure 8), corresponding to stages when neural crest cells begin differentiating into trigeminal neurons (E11.5-E13.5) (Leonard et al., 2022). During this developmental window, target innervation by the ophthalmic, maxillary, and mandibular nerves is also disrupted. In the frontal nerve (a division of the ophthalmic branch), initial innervation is observed, followed by a reduction of innervation and an increase in cell death. In contrast, the medial and lateral nasal nerves, also part of the ophthalmic branch, fail to form at all. The maxillary and mandibular nerves present with disorganized and defasciculated axons with a reduction of infraorbital nerve innervation

(Leonard et al., 2022). Additionally, this study showed a statistically significant decrease in TrkA immunostaining and neuron number in the Elp1 CKO, aligning with the data seen in the trunk dorsal root ganglion (George et al., 2013).

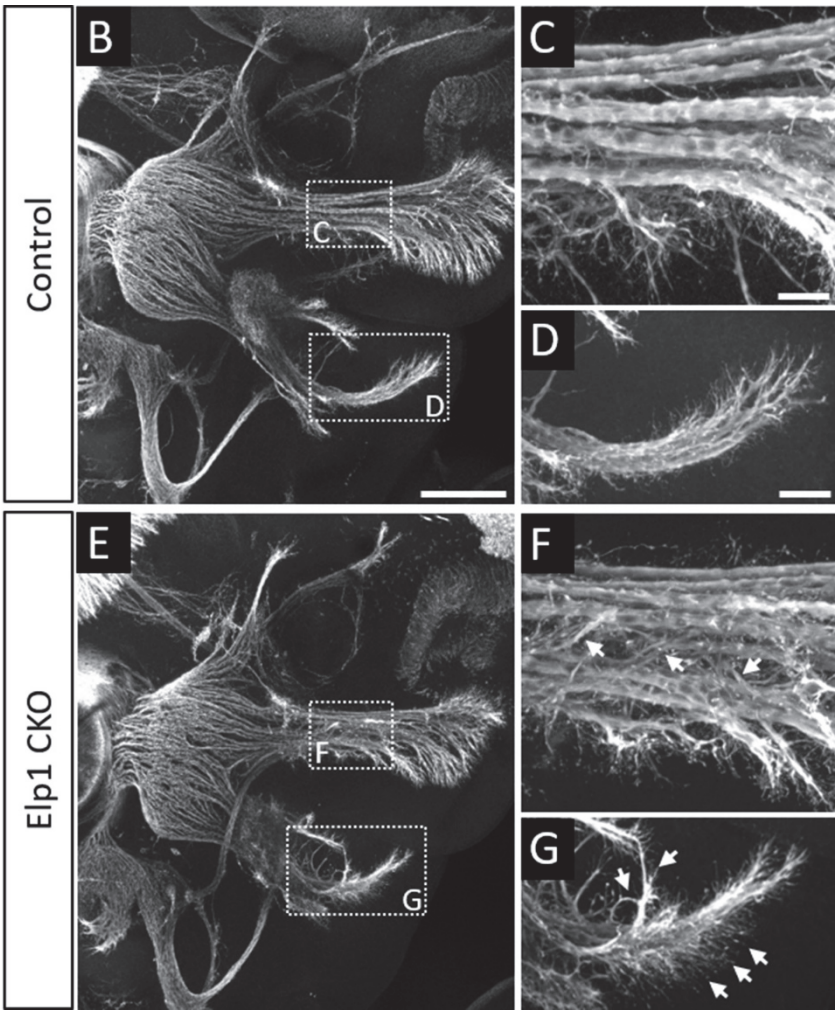

Figure 8: Loss of Elp1 in neural crest cells leads to trigeminal ganglion deficits in the mouse. Whole-mount immunohistochemistry for Beta tubulin III (Tubb3, staining all neurons) at E11.5 was performed followed by FRUIT clearing and max intensity projections of confocal Z-stacks. Although the general structure of the trigeminal ganglion and developing nerves is initially present in the CKO embryos (E), disorganization of the nerves is observed with decreased fasciculation and misguided axons (E-G). Modified from Leonard et al. 2022.

A different conditional knockout mouse model of FD was generated by Wnt1-Cre-mediated deletion of exon 20 (the exon spliced out in FD) in *Elp1* in the neural crest cell population (Jackson et al., 2014). In this model, pups at birth had a decrease in trigeminal ganglion size, further suggesting Elp1 affects trigeminal ganglion development. This same group then isolated neural crest-derived sympathetic neurons from a mouse strain possessing exon 20 of *Elp1* flanked by *loxP* sites and a tamoxifen-inducible Cre driver (Li et al., 2020). These neurons were then made "null" for Elp1 through the addition of tamoxifen for 24 hours. Interestingly, these studies revealed that Elp1 plays an important role in protein trafficking, including localizing to Rab7-positive late endosomes that function, in part, in TrkA retrograde trafficking and signaling. Importantly, loss of Elp1 led to a reduction in sympathetic neurons. This phenotype could be rescued by using an inhibitor of (or knocking down) Shp1 (protein tyrosine phosphatase non-receptor type 6), which becomes hyperactive and dephosphorylates TrkA in this Elp1 CKO model, leading to a loss of TrkA signaling and affecting sympathetic neuron survival (Li et al., 2020). Intriguingly, half of the Elp1-positive recycling endosomes were not immunoreactive for TrkA, suggesting Elp1 could be involved in the trafficking of other proteins, as hinted at previously in a prior report that identified trafficking defects when Elp1 levels were reduced (Naftelberg et al., 2016).

Studies on Elp1 have also been performed in the chick embryo, examining effects on neural crest-derived dorsal root ganglia (Abashidze et al., 2014; Hunnicutt et al., 2012). The chick embryo is a very useful model to study early embryonic development due to its accessibility, external growth outside of the mother, and the ability to perform molecular perturbation experiments and allow the embryo to continue to grow to desired developmental timepoints. Additionally, chicken embryos are relatively large and develop rapidly with

similarities to mammals at the molecular, cellular, and anatomical levels, making them an ideal model to study embryonic development.

In these reports, RNAi- and shRNA-mediated knockdown of Elp1 in neural crest cells provided a biologically relevant model for studying FD because patients do not have a complete loss of ELP1 protein. In these studies, reduction of Elp1 led to premature neuronal differentiation, increased neuron branching, and premature cell death (Hunnicutt et al., 2012). Another group used siRNA in a similar manner and observed abnormal axonal or neurite branching, including an increase in branching points and neuron guidance abnormalities, and identified roles for Elp1 in axonal transport (Abashidze et al., 2014). These studies add to the data from mouse models and strongly suggest functions for Elp1 in nerve outgrowth and/or target tissue innervation, neuron survival, and protein trafficking (George et al., 2013; Goffena et al., 2018; Li et al., 2020; Naftelberg et al., 2016).

1.9 Conclusions

Development of the cranial sensory ganglia is a very complex and diverse process. The goal of this research is to identify molecules involved in the development of the trigeminal ganglion and to elucidate their function. Our lab performed a bulk RNAsequencing experiment on trigeminal ganglia at various stages of chick development when only placode cell-derived neurons were present. Through this experiment and evidence from the literature, the molecules Neurog2, NeuroD1, and Elp1 were identified as potential regulators of trigeminal gangliogenesis. However, the role of these molecules in trigeminal placode cells had yet to be studied. This dissertation aimed to uncover novel functions for these molecules in chick trigeminal placode cells and their neuronal derivatives. We chose the chick as a model system because currently there are no known Cre drivers that allow for targeting of specifically trigeminal placode cells in

the mouse. Moreover, the location of trigeminal placode cells in the surface ectoderm, and the ease with which molecular perturbation experiments can be performed, make the chick embryo an outstanding model to study gene function in trigeminal placode cells. The results of this dissertation show that knockdown of Neurog2, NeuroD1, or Elp1 in trigeminal placode cells leads to disruption of trigeminal ganglion development in specific ways.

Chapter 2: Materials and Methods

2.1 Chicken embryos

Fertilized chicken eggs (*Gallus gallus*) were obtained from the University of Maryland (College Park, MD) and/or outside vendors (e.g., Centurion, GA). The eggs were incubated at 37°C in a humidified incubator to desired developmental timepoints. After incubation, eggs were windowed to gain access to the embryo. India ink (Pelikan) diluted in Ringer's solution (123mM NaCl, 1.5mM $CaCl_2$, 4.96mM KCl, 0.81mM Na_2HPO_4, 0.147mM KH_2PO_4, pH 7.4) was injected under the embryo using a 1 mL syringe with an 18-gauge needle to provide contrast when viewing the embryo under a dissecting microscope. Staging of embryos was then conducted according to the HH staging guide (Hamburger & Hamilton, 1992).

2.2 Morpholinos

A 3' lissamine-tagged translation-blocking Neurog2 morpholino antisense oligonucleotide (MO) (5'–CTCCGCCTTCACCGGCATCC–3') and NeuroD1 MO (5'–CGGTGACGGTCGCATAACCCCG–3′) were designed to inhibit translation of either transcript according to the manufacturer's criteria (GeneTools, LLC). A standard scrambled Control MO (5'–CCTCTTACCTCAGTTACAATTTATA–3') prepared by the manufacturer served as a control. These MOs were used at a concentration of 500 μM.

For the Elp1 experiments, a 3' lissamine-tagged Elp1 translation-blocking MO (5'–CAGCAGCCGCAGATTCCTCATGG–3') and Elp1 splice-blocking MO (5'–CCTGACAGACGCCTCACCGACTG–3') were designed according to the manufacturer's criteria (GeneTools, LLC). These MOs were mixed and used at a 1:1 ratio (2 mM total

concentration). The same standard scrambled Control MO described above was used but at a concentration of 2 mM.

The specificity of all MO sequences was verified using the NCBI Nucleotide BLAST tool. According to directions from the manufacturer, the inverse complement of the MO sequence was compared with the chicken (*Gallus Gallus*) transcriptome to ensure homology was specific to desired targets, thereby mitigating the possibility of off-target effects.

2.3 5' Rapid Amplification of cDNA Ends (RACE)

Total RNA was isolated from trigeminal ganglia tissue collected from chick embryos at E3-3.5 (HH18-20) using RNeasy Mini kit (Qiagen, 74104). 5' RACE was then performed using the SMARTer RACE 5'/3' Kit according to the manufacturer's instructions (Takara Bio, 634858). Gene-specific primers (GSP) to each of the *Elp1* splice variants, *Elp1201* (GSP1 5'–CTTTGACTGCGGAGGGTTTTATGCCA–3') and *Elp1202* (GSP2 5'–GGTGCTCGAAAGGTTCGAGTATGGAGC–3'), were designed based on kit specifications and used to amplify the 5' ends from 5' RACE-ready cDNA. 5' RACE clones were then sent for sequencing (Genewiz, from Azenta Life Sciences).

2.4 In ovo ectodermal electroporation

Electroporation of the embryo ectoderm to target forming placode cells was performed as previously described (Shah et al., 2017). Briefly, a 27 1/2-gauge needle was used to make a hole above the embryo head, in line with the ectodermal edge, just outside the area opaca. A 1 mm x 0.75 mm 4-inch glass needle was inserted through the vitelline membrane into the space where the embryo is housed. MOs were then overlaid on top of the ectoderm at E1.5 (HH10-11; prior to placode cell delamination) to target forming trigeminal placode cells and their neuronal

derivatives. Platinum electrodes (0.5 mm thick) were placed with the positive electrode on top of the chick embryo and the negative electrode beneath. The lissamine tag imparts the MO with a slightly positive charge. With the negative electrode under the embryo, the MO is thus pulled down into the ectodermal cells. Three pulses of 9V lasting 50 milliseconds with intervals of 200 milliseconds were then applied using an electroporator (California Institute of Technology). Eggs were then re-sealed using packing tape followed by parafilm and re-incubated for the desired amount of time depending on the experiment.

2.5 Embryo collection, embedding, and sectioning

Embryos were dissected off the yolk at specific stages using the Hamburger and Hamilton staging guide then rinsed in Ringer's solution and extra tissue surrounding the embryo was trimmed away. Embryos were then fixed in 4% paraformaldehyde (PFA) via submersion and gentle agitation at 4°C overnight (or 45 minutes at room temperature for wildtype immunohistochemistry). After fixation, embryos were permeabilized and washed three times in 1X phosphate-buffered saline (PBS) with 0.1% Triton X-100 (PBS-Tx) for 10 minutes each. Embryos used for whole-mount immunohistochemistry were stored in 1X PBS until ready for processing.

All other embryos were put through a sucrose gradient, 5% sucrose (w/v) in 1X PBS at room temperature until embryos sank (~5-10 minutes), followed by 15% sucrose (w/v) in PBS at 4°C overnight. Embryos were then equilibrated into gelatin by submerging them in 7.5% gelatin (made in 15% sucrose) at 37°C for 8 hours and then transitioning into 20% gelatin (made in 1X PBS) at 37°C overnight. After these equilibration steps, embryos were positioned into molds containing 20% gelatin. The gelatin was allowed to solidify and then the entire mold was set on ice for 10 minutes. Next, the molds containing the embedded embryos were frozen in liquid

nitrogen vapor and each embedded embryo was stored at -80°C until further processing. Embryos were sectioned using a cryostat (Leica) at 12-14µm, and sections were collected on Superfrost Plus charged slides (VWR, 48311-703). Sectioned tissue was used immediately or stored at -20°C until processed for immunohistochemistry.

2.6 Immunohistochemistry and tissue clearing

2.6.1 Tissue sections

Slides containing sectioned tissue were either used immediately or removed from storage at -20°C and brought to room temperature. All slides were degelatinized in 1X PBS at 42°C for 20 minutes. After degelatinization, slides were placed in PBS-Tx for 30 minutes. Tissue was permeabilized in 1X PBS/0.5% TritonX-100 for 5 minutes and then blocked in 10% heat-treated sheep serum (HTSS) diluted in PBS-Tx for 1 hour. Primary antibodies were diluted in PBS-Tx + 5% HTSS, according to individual antibody dilutions (Table 3) and incubated in a humidified chamber overnight at 4°C. Slides were then washed four times for 30 minutes each at room temperature in PBS-Tx to remove any unbound primary antibodies. Sections were then incubated with secondary antibodies, diluted at 1:500 in PBS-Tx + 5% HTSS, in a humidified chamber for 1 hour at room temperature. Slides were then washed four times for 30 minutes each at room temperature in PBS-Tx to remove unbound secondary antibodies, followed by two rinses in 1X PBS for 5 minutes each, all at room temperature. Coverslips were mounted with DAPI Fluoromount-G Mounting Medium (Southern Biotech, 0100-20) and dried in the dark at room temperature overnight prior to imaging. After drying overnight, slides were stored at 4°C when not being imaged.

Table 3: Antibodies used for immunohistochemistry (IHC) and immunoblotting (WB).

Antibody	Source	Catalog Number	Use/Dilution
Elp1 (IKBKAP): mouse monoclonal)	Sigma	WH0008518M3	IHC (1:50)
Tubb3 (β-tubulin III): mouse monoclonal	Abcam	ab78078	IHC (1:500 for sections; 1:250 for whole-mount)
Sox10: rabbit polyclonal	GeneTex	GTX128374	IHC (1:500)
E-Cadherin: mouse monoclonal	BD Transduction Labratories	610182	IHC (1:500)
Elp1 (IKBKAP/IKAP): rabbit polyclonal	LifeSpan BioSciences	LS-B571	WB (1:10,000)
Neurog2: mouse monoclonal	Santa Cruz	sc-293430	WB (1:200)
NeuroD1: rabbit polyclonal	LifeSpan Biosciences	LS-C331294	WB (1:1000)
Beta-actin: mouse monoclonal	Santa Cruz	sc-47778	WB (1:10,000)
HRP-conjugated anti-rabbit IgG	Rockland	611-1302	WB (1:15,000)
HRP-conjugated anti-mouse IgG1	Jackson Immunoresearch	115-035-205	WB (1:15,000)

2.6.2 Whole-mount

Embryos set aside for whole-mount immunohistochemistry (stored in 1X PBS at 4˚C) were blocked in PBS-Tx + 10% HTSS for up to two hours at room temperature with gentle agitation. Embryos were then incubated with primary antibody (Table 3) diluted in PBS-Tx + 5% HTSS for up to 2 days at 4°C with gentle agitation. Embryos were then washed four times for 30 minutes each in PBS-Tx at room temperature, then incubated with secondary antibody diluted at 1:500 in PBS-Tx + 5% HTSS overnight at 4°C with gentle agitation. After secondary incubation, embryos were washed four times for 30 minutes each in PBS-Tx, followed by two washes with 1X PBS for 20 minutes each, all at room temperature. E2.5 (HH15-17) embryos were imaged at this step, while E3.5 (HH19-20) embryos were cleared before imaging, as described below.

2.6.3 Fructose and urea solution (FRUIT) clearing

After whole-mount immunohistochemistry, embryos were cleared using the FRUIT clearing method to better visualize the forming trigeminal ganglion (Hou et al., 2015). Embryos were moved through a series of FRUIT buffers containing 8M urea (Sigma, U5378), 0.5% (v/v) α-thioglycerol (Thermo Fisher, T090525G), with increasing concentrations of fructose (Sigma, F3510). Embryos were incubated in 35% FRUIT for 6 hours, 40% FRUIT overnight, 60% FRUIT for 8 hours, followed by 80% FRUIT overnight. All incubations were performed at room temperature with gentle rocking. Embryos were stored and imaged in 80% FRUIT buffer. Embryos were not stored in 80% FRUIT for more than 2 days prior to imaging due to crystallization occurring if embryos are left for too long.

2.7 TUNEL staining

After immunohistochemistry, TUNEL staining was performed on tissue sections using the *In Situ* Cell Death Detection Kit, Fluorescein (Roche, 11684795910) as per the manufacturer's instructions. After washing off secondary antibodies, tissue was post-fixed with 4% PFA at room temperature for 20 minutes and then washed three times for five minutes each in 1X PBS at room temperature. Sections were then incubated with TUNEL solution for one hour at 37°C, followed by two washes with 1X PBS for 10 minutes each at room temperature. Coverslips were mounted with DAPI Fluoromount-G Mounting Medium and dried in the dark at room temperature overnight prior to imaging. After drying overnight, slides were stored at 4°C when not being imaged.

2.8 Confocal imaging

All imaging was performed on a Zeiss LSM 800 confocal microscope. Tissue sections were imaged using 5X, 10X, or 20X air objectives, or the 63X oil objective. Embryos processed for whole-mount immunohistochemistry were imaged in either 1X PBS (Elp1 MO, E2.5 (HH15-17) or 80% FRUIT. Z-stack images were taken at 5 μm intervals using 5X and 10X air objectives. For all applications, laser power, gain, offset, and digital zoom remained the same for Contralateral vs. MO-treated tissue. CZI files were processed using Zen software (Blue edition 2.0, Zeiss) while Z-stack CZI files were processed in ImageJ using the Z-project function (Hyperstack mode) to create maximum intensity projections.

2.9 Measurements and Statistical Analysis

Measurements were conducted using the open-source image processing program FIJI (Schindelin et al., 2012), which is based on ImageJ software (Collins, 2007).

2.9.1 Neurog2 and NeuroD1 knockdown

The width of the ophthalmic lobe was measured on the electroporated, and contralateral control sides of embryos treated with the Neurog2 MO (E3-3.5, HH18-20) and NeuroD1 MO (E2.5 (HH15-17) and E3-3.5 (HH18-20)) using 5X and 10X maximum intensity Z-stack projections, respectively, at a distance of 100 μm from the point where the ophthalmic and maxillomandibular lobes separate. A spatial calibration of the images was performed using FIJI based on the scale bar so that the distances were measured in microns. Data associated with the width of the trigeminal ganglion ophthalmic branch are presented as boxplots. Boxes represent interquartile range, with the median value indicated as a line and whiskers representing the range. The Shapiro–Wilk test was used to assess distribution. Group differences were analyzed

by the paired sample t-test, with *p* values equal to or below 0.05 deemed significant. All statistical analyses and boxplots were produced in R studio on R software (version 4.0.3).

2.9.2 Elp1 knockdown

Measurements were performed on Tubb3-labeled maximum intensity Z-projections described above. To measure area, the boundary of the trigeminal ganglion was determined by Tubb3 staining and outlined using the freehand sections tool then measured. Ectodermal Tubb3 staining was cropped out to better visualize the trigeminal ganglion, as it merges with maxillomandibular branching of the trigeminal ganglion when creating maximum intensity Z-projections.

Similarly, measurements of the area occupied by axon projections from the ophthalmic branch that innervate the eye were obtained by outlining the nerve innervation starting at the point at which additional branches break away from the main ophthalmic branch. Contralateral and MO-treated trigeminal ganglia were compared using paired t-tests in Graphpad Prism, with *p* values less than or equal to 0.05 were considered significant.

2.10 Tissue collection

Embryos electroporated with Elp1 MO or the standard Control MO (described above in 2.2), were collected 48 hours post-electroporation. Successfully electroporated trigeminal ganglia were dissected in 1X PBS under a Zeiss SteREO Discovery V8 Pentafluor fluorescent microscope to visualize MO-positive fluorescent tissue and then pooled for immunoblotting (n = 18 Control MO, n = 21 Elp1 MOs). The tissue was pelleted by centrifuging at 500 x g for 5 minutes at 4°C and excess buffer was removed, followed by flash-freezing of tissue in liquid nitrogen, and storage at -80°C until ready for immunoblotting.

2.11 Immunoblotting

Tissue pellets were thawed on ice and lysed in lysis buffer (50mM Tris pH 8.0, 150mM NaCl, 1% IGEPAL CA-630) supplemented with 1X cOmplete protease inhibitor cocktail (Roche, 04693124001) and 1mM PMSF (Roche, 54561623) for 30 minutes on ice, gently vortexing every 10 minutes. Samples were then centrifuged at max g for 15 minutes at 4°C and the solubilized protein fraction was collected. Protein concentration was determined using a Bradford assay (Thermo, 1857210) and equivalent amounts of protein per sample were boiled in 1X Laemmli sample buffer at 99°C for 5 minutes, followed by cooling to room temperature. Prepared samples were loaded onto a 10% (Neurog2, NeuroD1) or 7.5% (Elp1) Sodium dodecyl sulfate–polyacrylamide gel electrophoresis (SDS-PAGE) (Biorad 4561033, 4561024 respectively) and separated by electrophoresis at 70V for approximately 2.5 hours in 1X running buffer (diluted from 10X running buffer (25mM Tris base, 1.92M Glycine, 3.5mM SDS)). To transfer proteins from the gel, 0.2 μm PVDF membrane (Thermo Fisher, 88520) was first equilibrated for 30 seconds in methanol followed by a 20-minute equilibration in 1X transfer buffer (100mL 10X running buffer, 200 mL methanol, 700 mL ddH_2O). After protein separation, the SDS-PAGE gel was incubated in 1X transfer buffer for 20 minutes for equilibration. Proteins were then transferred to PVDF membrane using the Mini Trans-Blot ® Cell (Bio-Rad) wet transfer system running at 70V for 2 hours at 4°C. Membranes were incubated in a blocking solution (1X PBS + 0.1% Tween-20 (PTW) + 5% milk) for 45 minutes at room temperature followed by primary antibody incubation overnight at 4°C, also diluted in blocking solution (Table 3). After primary antibody incubation, membranes were washed in PTW three times for 10 minutes each. Secondary antibodies (Table 3) were diluted in blocking solution for one hour at room temperature followed by three additional washes in PTW for 10 minutes each.

Membranes were incubated with chemiluminescent substrates (Supersignal West Pico PLUS (Thermo Fisher, 34580) and/or Supersignal West Femto (Thermo Fisher, 34095)), and developed using a ChemiDoc XRS system (Bio-Rad). Blots were then stripped using Restore Plus Western Blot Stripping Buffer (Thermo Fisher, 46430) for 15 minutes, rinsed two times in PTW, and re-blocked for 45 minutes in blocking solution. Membranes were then re-probed using Beta-actin (Table 3) as a loading control antibody following the above procedures. Immunoblot analysis was performed using Image Lab software (Bio-Rad) to determine band size and volume. Relative protein levels were calculated by normalizing to loading control band volumes. Differences in amounts of protein were determined by comparing normalized ratios between Control MO- and experimental MO-treated samples, with Control MO-treated samples set to one.

Chapter 3: Neurogenin 2 and Neuronal Differentiation 1 Control Proper Development of the Chick Trigeminal Ganglion and Its Nerve Branches

Adapted from the following article published in

Journal of Developmental Biology

Bina P, **Hines MA**, Sanyal J, Taneyhill LA. (2023). Neurogenin2 and Neuronal Differentiation 1 Control Proper Development of the Chick Trigeminal Ganglion and Its Nerve Branches. *Journal of Developmental Biology, 11*(1), 8. https://doi.org/10.3390/jdb11010008

3.1 Summary

Vertebrate neurogenesis is controlled, in part, by proneural genes encoding basic Helix-Loop-Helix (bHLH) transcription factors (Hardwick & Philpott, 2015) that also regulate cell type determination and terminal differentiation (Lee et al., 1995). One family of bHLH proteins is the Neurogenins (Neurogs), which consists of Neurogs1–3 (Huang et al., 2014). In the chick, *Neurog1* is observed in the maxillomandibular trigeminal placode, the vestibulo-acoustic otic vesicle, and the epibranchial placodes (Xu et al., 2008). *Neurog2* is a chick ophthalmic placode specific marker until E2.5 (HH15-17) (Xu et al., 2008), after which it is considered a marker for all placode-derived neurons since its expression is detected in other placodes at E2.5 and in the maxillomandibular neurons of the trigeminal ganglion at E3 (HH18) (Xu et al., 2008). *Neurog2* is also expressed transiently in a subset of neural crest cells (Xu et al., 2008). *Neurog3* is not expressed in the chick trigeminal ganglion but is detected in the developing retina and in some cells of the non-neural retinal pigment epithelium (Ma et al., 2009). Interestingly, the converse expression pattern is observed for mouse *Neurog1* and *Neurog2*, with *Neurog1* noted in the trigeminal and vestibulo-acoustic placodes (Ma et al., 2009), while *Neurog2* is primarily expressed in the epibranchial placodes (Fode et al., 1998). Additionally, Neurogs play a key role

in activating downstream bHLH factors such as *NeuroD1* which is expressed in chick trigeminal placode cells prior to delamination and in their neuronal derivatives up to E8 (HH34) (Abu-Elmagd et al., 2001). Notably, Neurogs also regulate downstream signaling pathways controlling the neuronal cytoskeleton and subsequent neuron morphology.

Despite our understanding of *Neurog2* and *NeuroD1* expression, little is known about Neurog2 and NeuroD1 function in the chick embryo, particularly with respect to the trigeminal ganglion. To this end, we depleted Neurog2 or NeuroD1 from chick trigeminal placode cells using validated MOs and evaluated trigeminal ganglion development. Our studies reveal, for the first time, a role for Neurog2 and NeuroD1 in chick trigeminal placode cells and shed light on mechanisms underlying trigeminal ganglion development.

3.2 Results

3.2.1 Neurog2 controls the proper formation of the trigeminal ganglion and its nerve branches.

To examine the function of Neurog2 during trigeminal ganglion neurodevelopment, Neurog2 knockdown experiments were carried out in trigeminal placode cells followed by immunohistochemistry on whole embryos to examine the forming trigeminal ganglion. To knockdown Neurog2 expression, a MO was designed to target the sequence surrounding the translational start site of the *Neurog2* transcript. The Neurog2 MO was unilaterally electroporated into the chick trigeminal placode ectoderm. Successfully electroporated embryos were re-incubated for specific periods of time and then processed for further experimentation, as described below.

The efficacy of the Neurog2 MO was first tested by electroporating either a standard scrambled Control MO (hereafter referred to as Control MO) or the Neurog2 MO, followed by collection of electroporated trigeminal ganglia at E2-3 (HH16-18) to examine Neurog2 protein

levels by immunoblotting (Shah et al., 2017). Analysis of Neurog2 protein levels revealed a 28.1% and 28.7% reduction in the presence of the Neurog2 MO compared to the Control MO for Neurog2 immunoreactive bands at 150 kDa and 23 kDa, respectively (Figure 9).

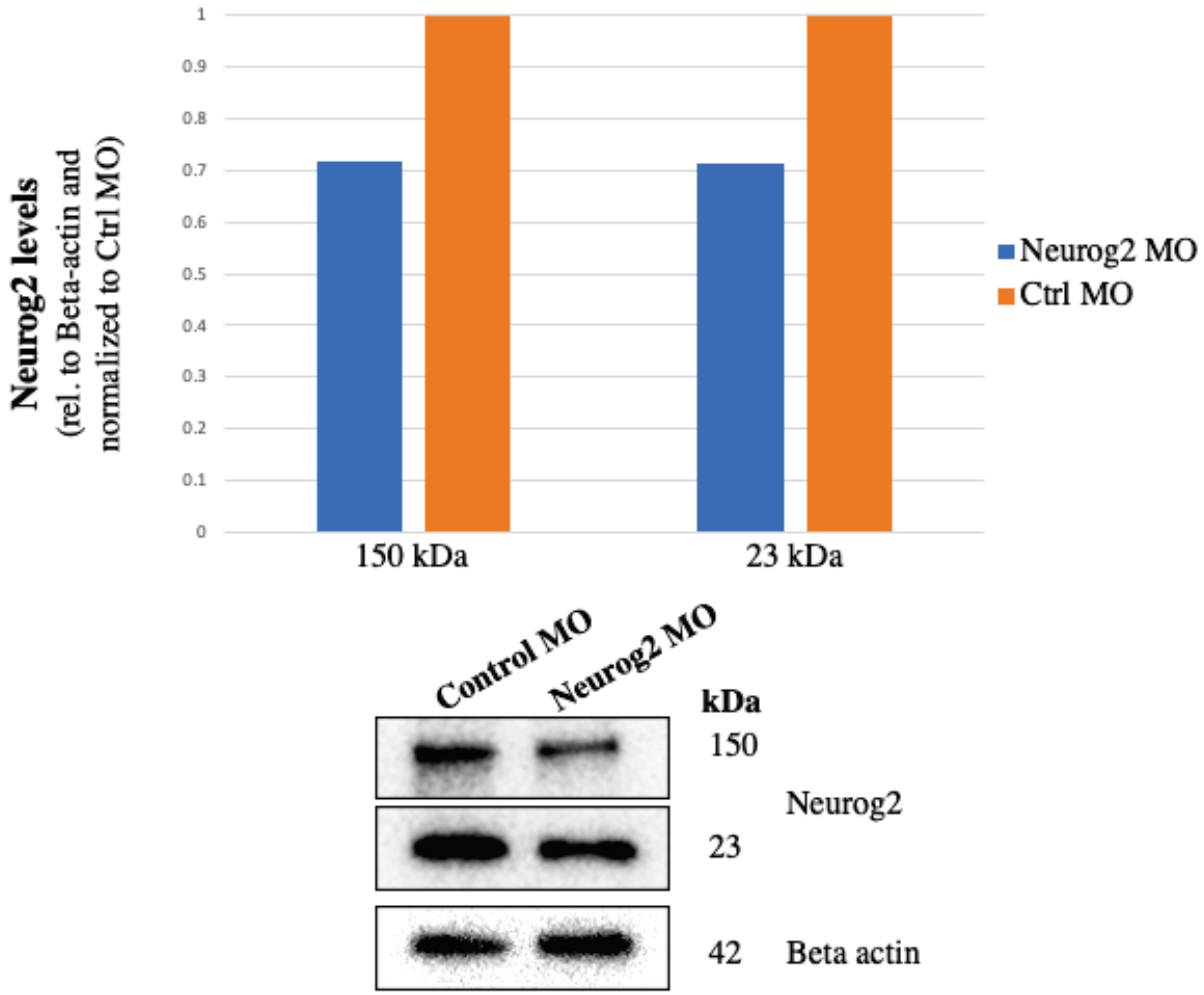

Figure 9: The Neurog2 MO reduces Neurog2 protein levels. At ~E1.5 (HH9^{+} to 10), placode cells were unilaterally electroporated either with a Neurog2 or Control (Ctrl) MO. After re-incubation to E2.5–3 (HH15–18), the forming trigeminal ganglion on the electroporated side was dissected and pooled from multiple embryos. Lysates were prepared, and equivalent amounts of protein per sample were separated on a 10% SDS-PAGE gel. Immunoblotting for Neurog2 and Beta-actin (control) was then performed, and band intensity was calculated from unmodified immunoblot images using Image Lab software (Bio-Rad). Relative protein levels were ascertained by normalizing Neurog2 volumes to Beta actin volumes. Knockdown amount was determined by comparing normalized ratios between Ctrl MO and Neurog2 MO samples, with the Ctrl MO sample set as one.

To assess effects on trigeminal ganglion formation, successfully electroporated embryos were re-incubated to E3-5 (HH18-26), collected, fixed, and processed for whole-mount immunohistochemistry to detect Tubb3, which labels differentiated neurons in the developing ganglion. At E2.5-3.5 (HH15-20), neuronal differentiation is occurring in the placodal population as neural crest cells will not begin differentiating into neurons until E4 (HH22-24) (D'Amico-Martel & Noden, 1983; Hamburger, 1961; Shiau et al., 2008); therefore, only placode cell-derived neurons will be identified. Confocal images of whole embryo heads were obtained to examine gross trigeminal ganglion morphology on the electroporated and contralateral control side, which possessed no MO.

At E3 (HH18), drastic changes in the trigeminal ganglion following Neurog2 depletion were already apparent. In contrast to the trigeminal ganglion on the contralateral control side (Figure 10A), the entire trigeminal ganglion and associated nerve structures were diminished in size on the Neurog2-depleted side (Figure 10B), which possessed many MO-positive cells (Figure 10C,F, arrows). Moreover, fewer axons were present in the ophthalmic branch, resulting in improper innervation of the eye region (Figure 10B, arrowheads). In addition, knockdown of Neurog2 appeared to alter the ability of the maxillomandibular branch to separate into definitive maxillary and mandibular branches, as shown by neurons deviating from the established maxillary branch (Figure 10A,B,D,E, carets). Besides these observations, however, the general morphology of the ganglion appeared similar: a bilobed structure possessing ophthalmic and maxillomandibular lobes and branches.

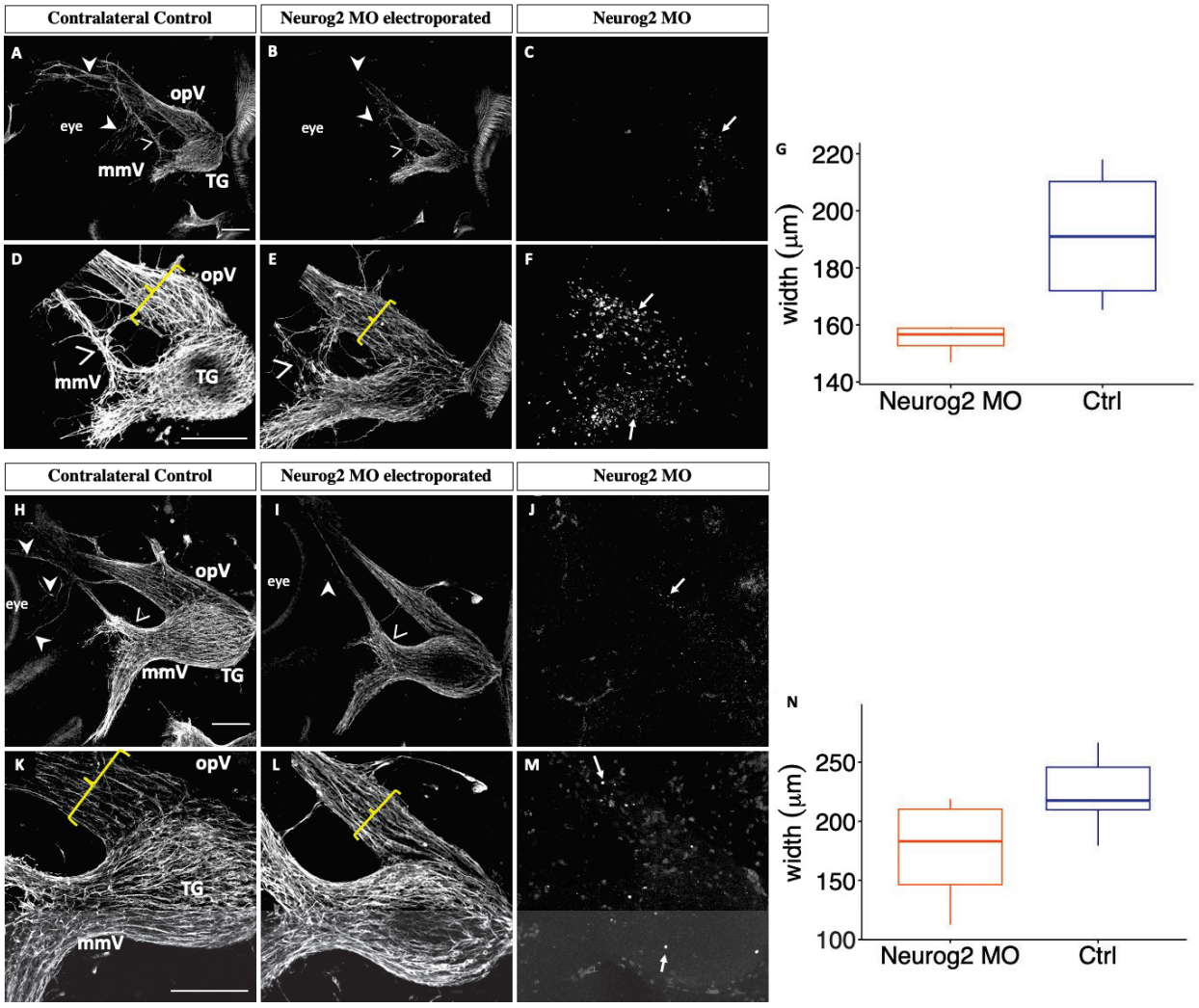

Figure 10: Depletion of Neurog2 in trigeminal placode cells impairs trigeminal ganglion development. Lateral view of the trigeminal ganglion in a chick head (E3 (HH18), n = 4, (A-F) and E3-3.5 (HH20), n = 6, (H-M)). Representative images are maximum intensity projections of confocal Z-stacks through the contralateral control (A,D,H,K) and Neurog2 MO-electroporated (B,E,I,L) sides after processing for whole-mount Tubb3 immunohistochemistry to detect placode-derived neurons (A,B,D,E,H,I,K,L, arrowheads) and tissue clearing. Bottom rows (D-F, K-M) show higher magnification images of their corresponding top rows (A-C, H-J). (C,F,J,M) MO-positive cells (arrows). Brackets indicate width of ophthalmic branch. (G,N) Quantification of the width of the ophthalmic branch on the control (blue) and Neurog2 MO-treated (orange) sides. Plots represent the median (center line), 75th percentile (top of box), and 25th percentile (bottom of box), with whiskers connecting the largest and smallest values. A paired sample t-test revealed p values of 0.05 (G) and 0.02 (N). Scale bar in (A,D) is 1 mm and applies to (B,C) and (E,F), respectively. Scale bar in (H,K) is 200 µm and applies to (I,J) and (L,M), respectively. Abbreviations: mmV, maxillomandibular lobe; opV, ophthalmic lobe; and TG, trigeminal ganglion.

Although Tubb3-positive placodal neurons were observed throughout the forming ganglion, higher magnification images (Figure 10D-F) revealed neurons that were less organized and seemed to drift away from established axon bundles upon Neurog2 knockdown. Axons of the maxillomandibular nerve traveled without direction from the established nerve on the Neurog2-depleted side (Figure 10E) compared to the contralateral control side (Figure 10D). Moreover, the ophthalmic nerve branch was smaller in width on the electroporated side compared to the control (Figure 10D,E, brackets). Quantification revealed that this size difference was in fact statistically significant ($p = 0.05$, Figure 10G).

At E3-3.5 (HH20), the trigeminal ganglion and associated nerve structures were still reduced in size after Neurog2 knockdown (Figure 10I) compared to the trigeminal ganglion on the untreated contralateral control side (Figure 10H), with many MO-positive cells scattered throughout the forming ganglion (Figure 10J,M, arrows). Furthermore, the ophthalmic nerve extended less elaborately around the eye than on the contralateral control side (Figure 10H,I, arrowheads). Maxillary neurons were arranged in bundles but appeared less compact after Neurog2 knockdown than those on the untreated side (Figure 10H,I, carets). However, the trigeminal ganglion and its nerve branches appeared to have a similar overall morphology on the electroporated and contralateral control sides of examined embryos. With higher magnification (Figure 10K-M), though, a reduction in the width of the ophthalmic branch and the presence of likely fewer placode-derived neurons were better appreciated (Figure 10K,L, brackets). This decrease in width was also statistically significant at this developmental stage ($p = 0.02$, Figure 10N). Collectively, these results reveal that Neurog2 knockdown impacts the development of the trigeminal ganglion and its nerve branches across multiple embryonic stages.

3.2.2 Neurog2 depletion does not cause apoptosis of trigeminal placode cells or their neuronal derivatives during trigeminal ganglion assembly.

Next, we investigated whether the smaller trigeminal ganglion phenotype observed upon Neurog2 knockdown was due to increased cell death. To this end, we performed TUNEL analyses at E3-3.5 (HH19) to detect apoptotic cells after unilateral electroporation of trigeminal placode cells with Neurog2 MO. Neurog2 knockdown (Figure 11D-F) did not cause apoptosis of MO-positive cells, or other cells within the forming trigeminal ganglion, compared to the contralateral control side (Figure 11A-C). These results indicate that depletion of Neurog2 from placode cells does not lead to increased cell death in the trigeminal ganglion at this developmental stage.

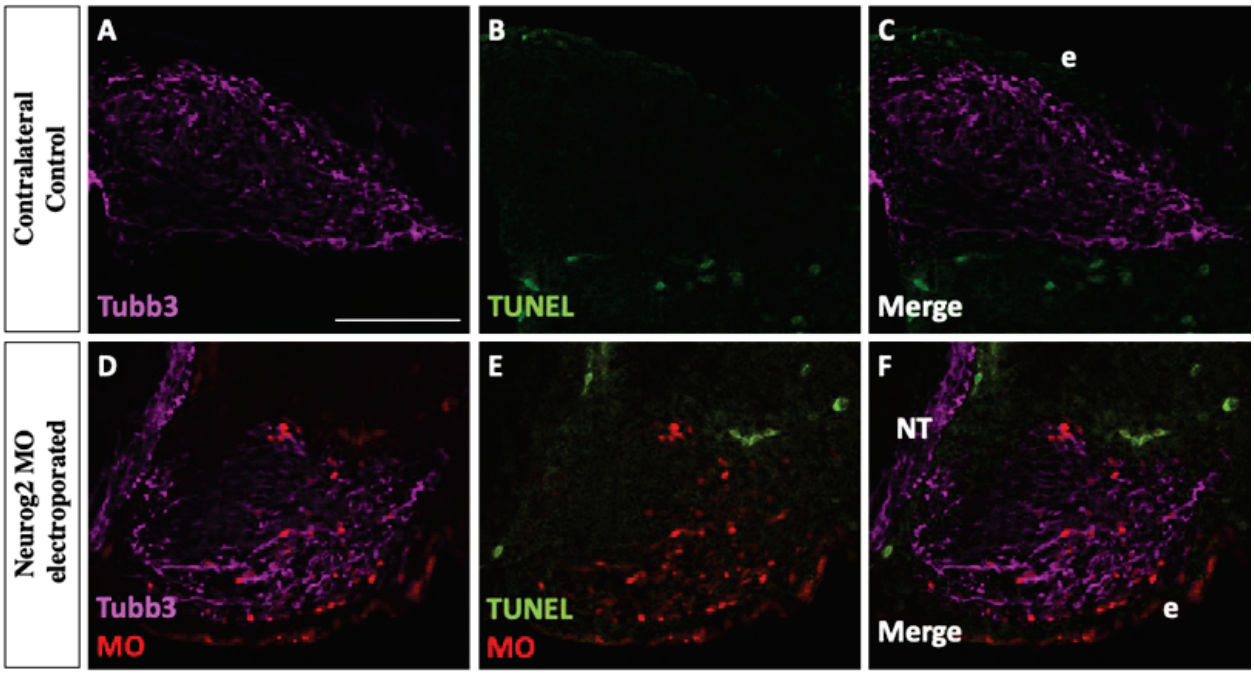

Figure 11: Depletion of Neurog2 in trigeminal placode cells does not cause increased cell death. Representative transverse section through the forming trigeminal ganglion (E3-3.5 (HH19), n = 5) after Neurog2 MO unilateral electroporation (D-F, red) followed by Tubb3 immunohistochemistry to detect placode cell-derived neurons (A,C,D,F, purple) and TUNEL staining to identify apoptotic cells (B,C,E,F, green). Scale bar in (A) is 100 μm and applies to all images. Abbreviations: e, ectoderm and NT, neural tube.

3.2.3 NeuroD1 regulates early chick trigeminal ganglion assembly.

To further understand the function of bHLH factors in trigeminal ganglion development, we examined the role of NeuroD1 through knockdown experiments in trigeminal placode cells followed by immunohistochemistry on whole embryos. The NeuroD1 MO was designed to target the sequence surrounding the translational start site of the *NeuroD1* transcript. Successfully electroporated embryos were re-incubated to various developmental stages, and then processed for either immunoblotting or Tubb3 whole-mount immunohistochemistry, as described below. We first tested the efficacy of the NeuroD1 MO by evaluating NeuroD1 protein levels through immunoblotting as we did previously for the Neurog2 MO. After electroporation, trigeminal ganglia at E2.5-3 (HH15-18) were then dissected and pooled for immunoblotting, which revealed five different bands immunoreactive with the NeuroD1 antibody, four of which are reduced in intensity after MO-mediated knockdown of NeuroD1 (Figure 12). The 25 kDa band is likely a background band since its intensity is not changed in the presence of the NeuroD1 MO (Figure 12). Compared to NeuroD1 protein levels in the Control MO sample, knockdown of NeuroD1 via the MO resulted in a 44%, 39%, 37%, and 29% decrease in the 200 kDa, 75 kDa, 50 kDa, and 35 kDa NeuroD1 protein bands, respectively.

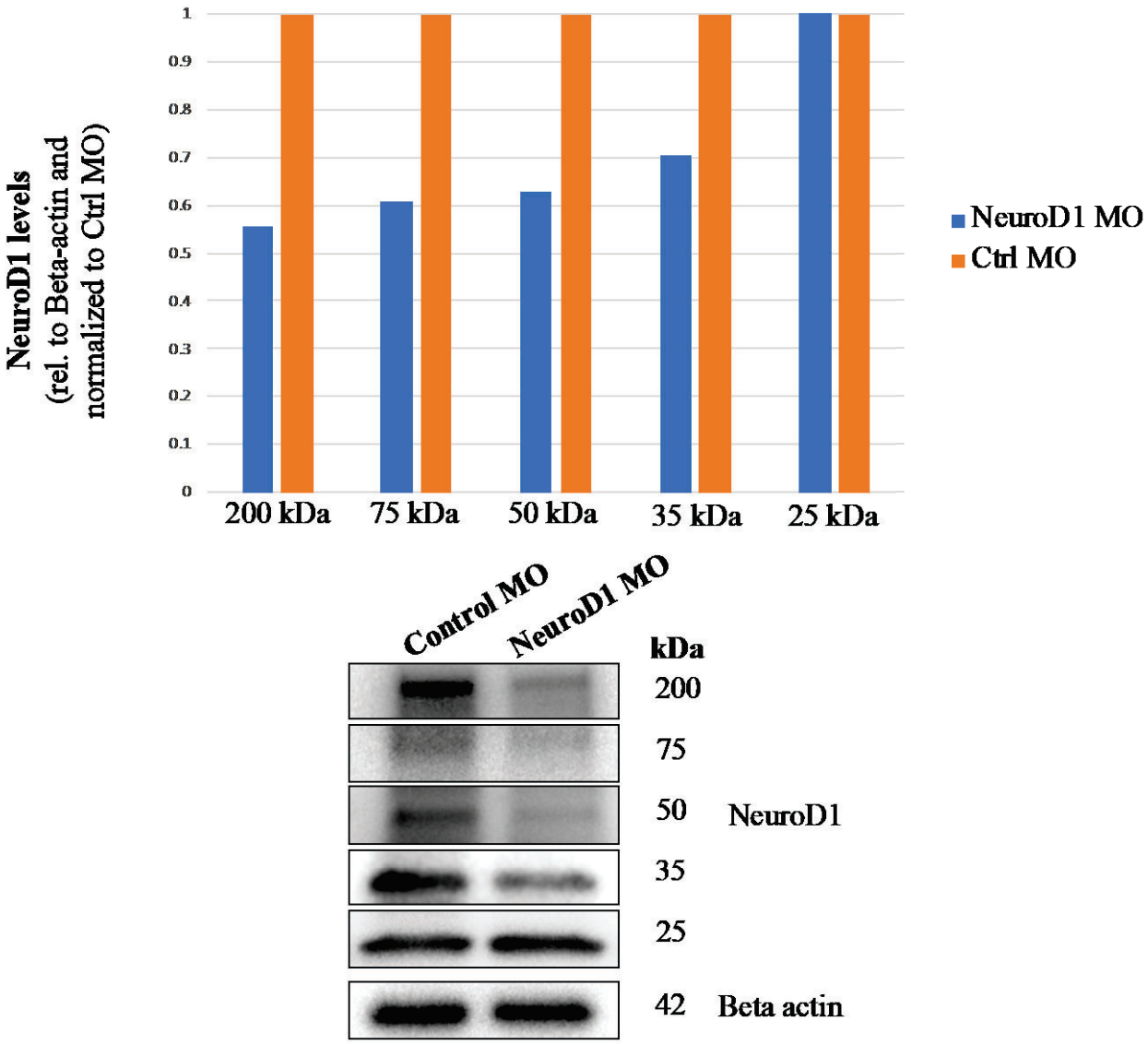

Figure 12: The NeuroD1 MO reduces NeuroD1 protein levels. At ~E1.5 (HH9+ to 10), placode cells were unilaterally electroporated either with a NeuroD1 or control (Ctrl) MO. After re-incubation to E2.5-3 (HH15-18), the forming trigeminal ganglion on the electroporated side was dissected and pooled from multiple embryos. Lysates were prepared, and equivalent amounts of protein per sample were separated on a 10% SDS-PAGE gel. Immunoblotting for NeuroD1 and Beta actin (control) was then performed, and band intensity was calculated from unmodified immunoblot images using Image Lab software (Bio-Rad). Relative protein levels were ascertained by normalizing NeuroD1 volumes to Beta actin volumes. Knockdown amount was determined by comparing normalized ratios between Ctrl MO and NeuroD1 MO samples, with the Ctrl MO sample set as one. The 25 kDa band is a background band given that the level of NeuroD1 protein was not changed between the control and NeuroD1 MO-treated samples.

To evaluate effects on trigeminal ganglion development, unilateral electroporation of NeuroD1 MO was conducted, followed by incubation of embryos to E2-2.5 (HH14-16), Tubb3 whole-mount immunohistochemistry and confocal image acquisition was carried out in our Neurog2 MO analyses. At E2 (HH14), changes in the trigeminal ganglion were already evident. In contrast to the trigeminal ganglion on the contralateral control side (Figure 13A, arrowhead), the forming trigeminal ganglion on the NeuroD1-depleted side was diminished in size and there appeared to be fewer neurons present (Figure 13B, arrowhead). Many MO-positive cells were also found in the electroporated ganglion (Figure 13C,F, arrows), and Tubb3-positive placodal neurons were observed throughout the condensing ganglion. Higher magnification images (Figure 13D-F) revealed neurons that were less organized. Accordingly, trigeminal sensory neurons on the electroporated side were widely dispersed (Figure 13E), whereas those on the control side were more densely packed (Figure 13D).

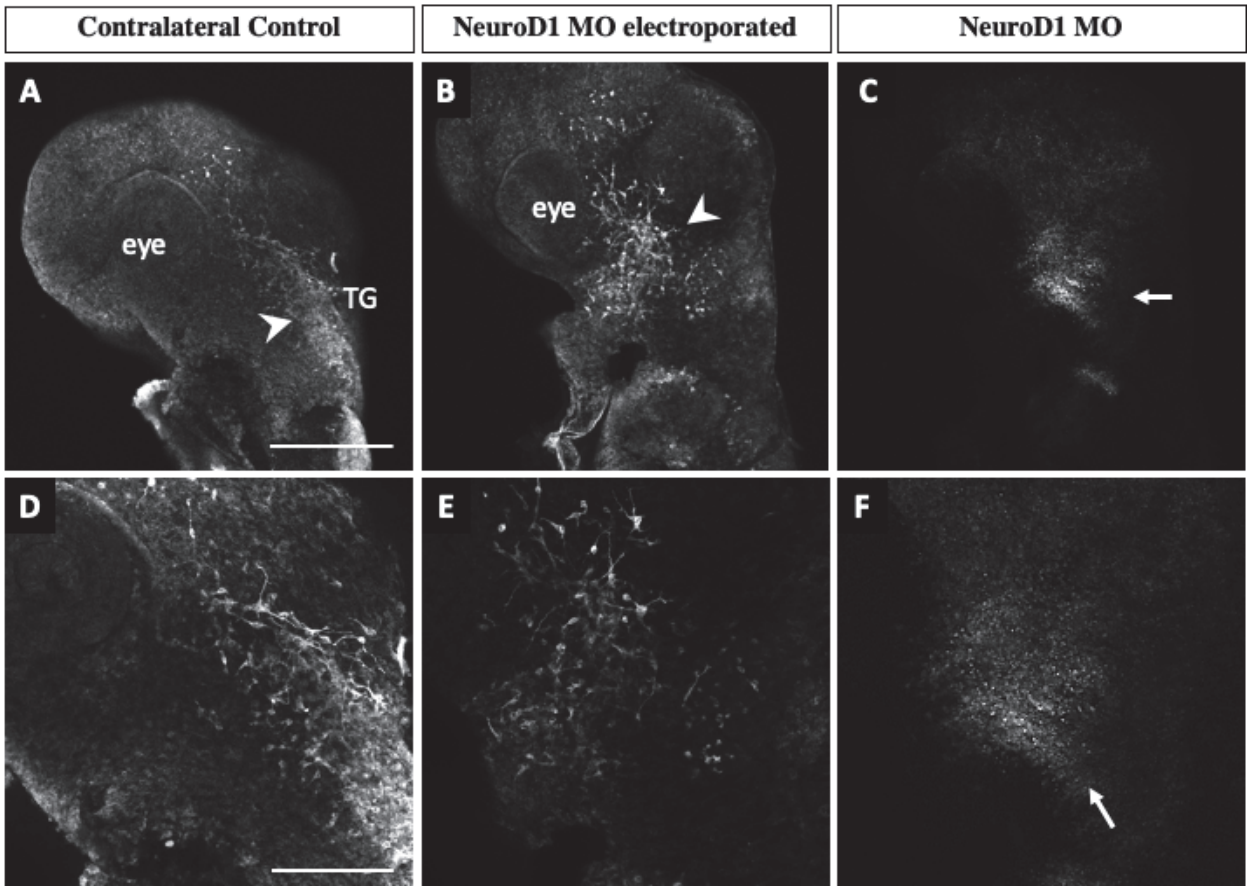

Figure 13: Depletion of NeuroD1 in trigeminal placode cells impairs trigeminal ganglion development. Lateral view of the trigeminal ganglion in a chick head (E2 (HH14), n = 3). Representative images are maximum intensity projections of confocal Z-stacks through the contralateral control (A,D) and NeuroD1 MO-electroporated (B,E) sides after processing for whole-mount Tubb3 immunohistochemistry to detect placode-derived neurons (A,B,D,E, arrowheads) and tissue clearing. Bottom row shows higher magnification images of the top row. (C,F) MO-positive cells (arrows). Scale bar in (A) is 500 μm and applies to (B,C), and 200 μm in (D) and applies to (E,F). Abbreviations: TG, trigeminal ganglion.

At E2.5 (HH15-17) and E3-3.5 (HH18-20), both electroporated and control trigeminal ganglia possessed Tubb3-positive placodal neurons (Figure 14A,B,H,I, arrowheads), and MO-positive neurons were also observed in the electroporated ganglion (Figure 14C,F,J,M, arrows). However, there were differences in the way the neurites, and eventual axons, developed upon NeuroD1 knockdown (Figure 14A,B,H,I, arrowheads). Trigeminal sensory neurons on the contralateral control side extended axons into the eye area (Figure 14A,D), whereas those axons from NeuroD1 MO-electroporated trigeminal sensory neurons did not readily reach the eye (Figure 14B,E). Moreover, neurons within both lobes on the NeuroD1 MO-treated side exhibited an aberrant morphology (Figure 14E,L) compared to those on the contralateral side (Figure 14D,K). Additionally, trigeminal sensory neurons were more dispersed within the ophthalmic branch on the electroporated side compared to the control (Figure 14D,E,K,L, brackets). This increase in width upon NeuroD1 depletion was statistically significant at these developmental stages ($p = 0.03$, Figure 14G,N). Taken together, these results highlight a role for NeuroD1 in controlling the condensation of placodal neurons within the forming trigeminal ganglion.

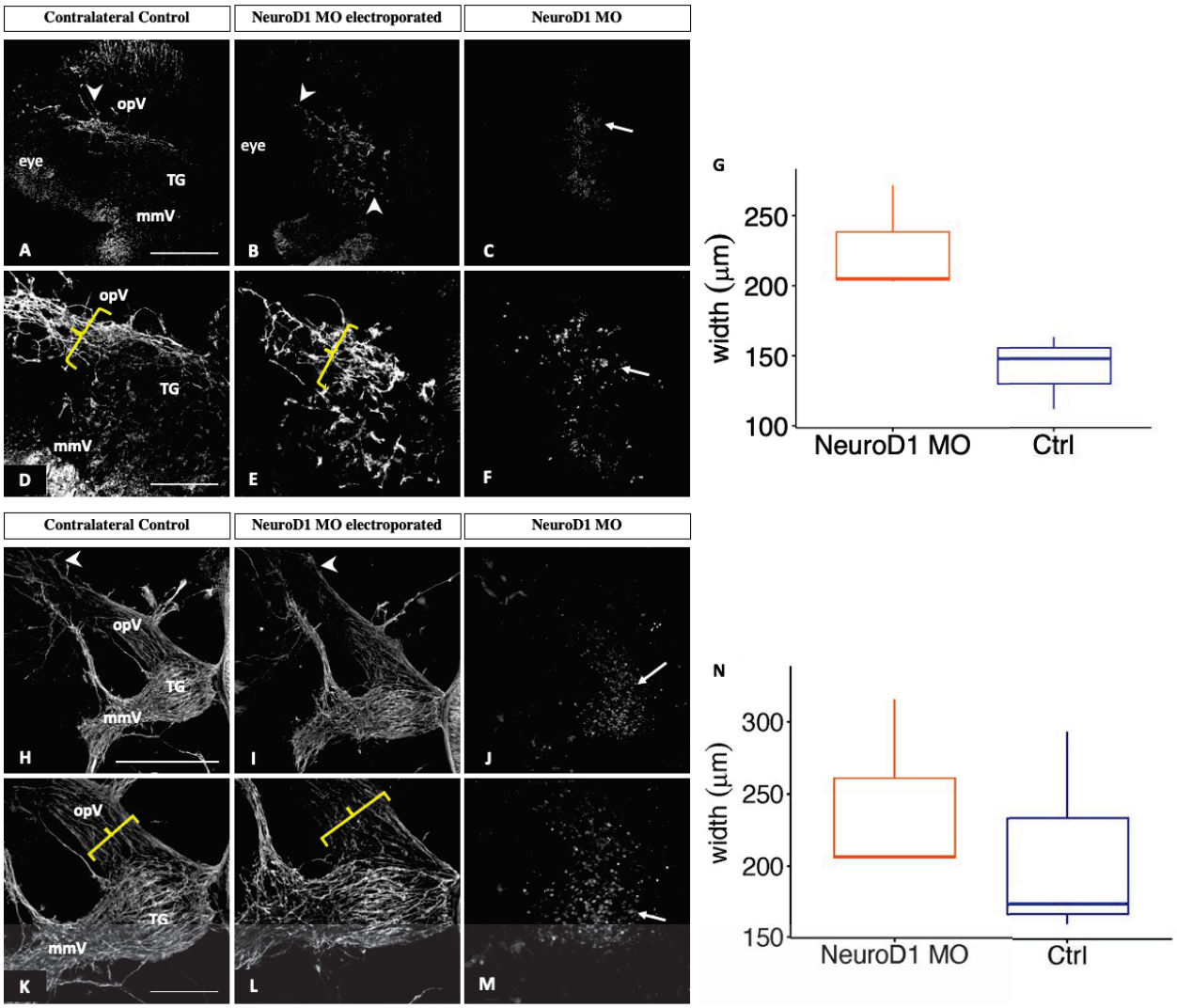

Figure 14: NeuroD1 depletion in trigeminal placode cells disrupts trigeminal ganglion development. Lateral view of the trigeminal ganglion in a chick head (E2.5 (HH16), n = 3, (A-F) and E3-3.5 (HH19), n = 3, (H-M)). Representative images are maximum intensity projections of confocal Z-stacks through the contralateral control (A,D,H,K) and NeuroD1 MO-electroporated (B,E,I,L) sides after processing for whole-mount Tubb3 immunohistochemistry to detect placode-derived neurons (A,B,D,E,H,I,K,L, arrowheads) and tissue clearing. Bottom rows (D-F, K-M) show higher magnification images of their corresponding top rows (A-C, H-J). (C,F,J,M) MO-positive cells (arrows). Brackets indicate width of ophthalmic branch. (G,N) Quantification of the width of the ophthalmic branch on the control (blue) and NeuroD1 MO-treated (orange) sides. Plots represent the median (center line), 75th percentile (top of box), and 25th percentile (bottom of box), with whiskers connecting the largest and smallest values. A paired sample t-test revealed p values of 0.03 at both developmental stages (G,N). Scale bar in (A,D) is 500 µm and applies to (B,C) and (E,F), respectively. Scale bar in (H,K) is 200 µm and applies to (I,J) and (L,M), respectively. Abbreviations: mmV, maxillomandibular lobe; opV, ophthalmic lobe; and TG, trigeminal ganglion.

3.3 Conclusions

To address the function of Neurog2 in chick trigeminal gangliogenesis, MO-mediated knockdown of Neurog2 was carried out in trigeminal placode cells. Despite achieving only 28.1% and 28.7% reduction in Neurog2 protein levels (Figure 9), Neurog2 MO treatment clearly caused dramatic effects on trigeminal gangliogenesis (Figure 10), providing evidence that this protein is important for trigeminal ganglion development. Compared to the contralateral control side trigeminal ganglion, the ophthalmic branch of the Neurog2-depleted trigeminal ganglion extended less elaborately around the eye (Figure 10). Further, Neurog2 knockdown resulted in a statistically significant decrease in the size of the ophthalmic branch compared to this branch of the trigeminal ganglion on the contralateral control side (Figure 10G,N). Additionally, Neurog2 depletion appeared to impair the segregation of the maxillomandibular branch into definitive maxillary and mandibular branches in the E3 trigeminal ganglion (HH18, Figure 10A-F). Axons of the maxillomandibular branch on the Neurog2-depleted side also seemed less compact compared to those on the contralateral control side at E3-3.5 (HH20, Figure 10H-M).

Since ophthalmic branch width is reduced upon Neurog2 knockdown, ophthalmic placodal neurons are born early and exit the cell cycle prior to delamination (McCabe et al., 2009), and the Neurog2 MO was introduced into ophthalmic placode cells just prior to their delamination, these results suggest that Neurog2 knockdown may in fact be altering the number of ophthalmic placode precursor cells available to differentiate and/or the ability of these precursors to become neurons. Future experiments designed to address Neurog2 function earlier in placode cell development would address this possibility.

To ascertain the function of NeuroD1 in chick trigeminal ganglion development, MO-mediated knockdown of NeuroD1 was performed in trigeminal placode cells. Upon

electroporation with NeuroD1 and Control MOs, immunoblotting for NeuroD1 protein revealed five distinct bands (Figure 12). NeuroD1 protein has a predicted molecular weight of approximately 39 kDa in chicks (Uniprot); however, immunoblot data have shown bands of various molecular weights (e.g., antibody websites), with a predominant band at 50 kDa (Lee et al., 2020; Li et al., 2019; Morimoto et al., 2022; Sato et al., 2020; Singh et al., 2022). Given that four of the five bands showed a reduction after knockdown, we conclude that these four bands represent NeuroD1 protein, while the last band (25 kDa) is a background band. The presence of bands at higher molecular weights than the predicted NeuroD1 protein product could be caused by post-translational modifications, such as phosphorylation of NeuroD1, leading to a shift in electrophoretic mobility. This type of modification is not without precedence, as phosphorylation of Ser336 in NeuroD1 is essential for certain developmental processes, including dendrite growth and formation (Gaudillière et al., 2004). Additionally, NeuroD1 protein stability is regulated by ERK-dependent phosphorylation which, in this instance, leads to ubiquitination and NeuroD1 degradation by the proteasome (Lee et al., 2020). As such, the 35 kDa band could be a degradation product. Accordingly, a 44%, 39%, 37%, and 29% reduction in NeuroD1 protein levels impaired trigeminal gangliogenesis, indicating that this protein is critical for trigeminal ganglion development.

Depletion of NeuroD1 from trigeminal placode cells negatively affected trigeminal ganglion development. Axons from the ophthalmic branch of the trigeminal ganglion did not properly innervate the eye region and maxillomandibular neurons also possessed an abnormal morphology (Figures 13 and 14). Notably, ophthalmic and maxillomandibular neurons appeared to be dispersed and less compact after NeuroD1 knockdown compared to those on the contralateral control side of the embryo (Figures 13 and 14). These findings for the ophthalmic

branch were statistically significant at later developmental stages (Figure 14 G,N). As with Neurog2 MO treatment, we noted NeuroD1 MO-positive cells in the trigeminal ganglion in tissue sections (not shown), suggesting that effects on delamination are not necessarily substantial, at least at the stages we examined, suggesting that this dispersed, less-compact phenotype likely reflects mechanisms related to nerve outgrowth and/or axon bundling.

Our studies herein reveal that Neurog2 and NeuroD1 are critical to the successful development of the trigeminal ganglion and its nerve branches. Through knockdown experiments, we demonstrated that Neurog2 and NeuroD1 are important for precise axon outgrowth and innervation of target tissues as well as neuron morphology. Altogether, our results provide new insight into molecules important for the proper formation of trigeminal placode cell-derived neurons and have advanced our understanding of trigeminal gangliogenesis in the chick embryo.

Chapter 4: Spatio-temporal expression characterization of Elp1 in chick trigeminal ganglion

4.1 Summary

Elp1 was identified by RNAsequencing to be expressed during chick trigeminal ganglion development. Interestingly, mutations in human *ELP1* cause FD, a neurodevelopmental and neurodegenerative disease. This disease is characterized by general neuronal dysfunction. Previous research in FD models looking at sensory neurons have focused on neural crest cell-derived neuronal populations in the trunk (Abashidze et al., 2014; George et al., 2013; Goffena et al., 2018; Hunnicutt et al., 2012; Jackson et al., 2014; Li et al., 2020). Evidence such as smaller trigeminal nerves in patients (and in FD mouse models), decreased sensitivity to pain and temperature in the face, absent corneal reflexes, and reduced basal lacrimation suggests there is dysfunction of the trigeminal nerve in FD patients (Jackson et al., 2014; Mass & Gadoth, 1994; Norcliffe-Kaufmann et al., 2017; Won et al., 2019). While Elp1 expression has been characterized in sensory nerves in the trunk, there are differences between the neuronal contributions to the cranial and trunk ganglia; namely, placode cells and their neuronal derivatives are only found in the head (Vermeiren et al., 2020). To ensure expression occurs at the right time and place to play a role in trigeminal ganglion development, an expression profile of Elp1 during the formation of the chick trigeminal ganglion was established. Our data show that Elp1 is expressed in migratory cranial neural crest cells and in undifferentiated neural crest cells and placode cell-derived neurons contributing to the trigeminal ganglion.

4.2 Results

Characterization of Elp1 protein expression profile was performed in stages, grouped every 12-24 hours as this correlates with the timeframe of major developmental events (e.g., neural crest cell migration, neural crest and placode cell intermixing, and neural crest and placode cell condensation). Initially, a control experiment was performed to test the specificity of the Elp1 primary antibody (Figure 15). Immunostaining for Elp1 (Figure 15A,B, white) was performed in combination with SRY-box transcription factor 10 (Sox10; Figure 15A,C, green) and Tubb3 (Figure 15A,D, purple), marking neural crest cells and placode cell-derived neurons of the trigeminal ganglion, respectively. In comparison, immunostaining conducted in the absence of Elp1 primary antibody was performed using only a secondary antibody specific for Elp1 (Figure 15E,F) accompanied by the same combination of Sox10 (Figure 15E,G, green) and Tubb3 (Figure 15E,H, purple) antibodies to mark the cells of the trigeminal ganglion. This experiment confirmed specificity of the Elp1 antibody, which was then used for subsequent characterization of the spatio-temporal expression pattern of Elp1.

4.2.1 Immunohistochemical characterization of Elp1 in chick tissue sections.

The first stage group investigated was E1.5 (HH11/12), when neural crest cells are migrating from the dorsal neural tube to their respective locations. At these timepoints, placode cells reside in the ectoderm and have yet to start their migration. Data reveals Elp1 expression is punctate in appearance with dynamic expression within cells immunoreactive for Sox10, a nuclear marker of migratory neural crest cells (Figure 16E,G, arrowhead). Furthermore, Elp1 expression is observed in the ectoderm, demonstrated by its presence in E-Cadherin-positive cells, a cell surface marker of ectodermal cells. This ectodermal expression appeared to be concentrated at the apical side of the cells (Figure 16E,F,H, arrows).

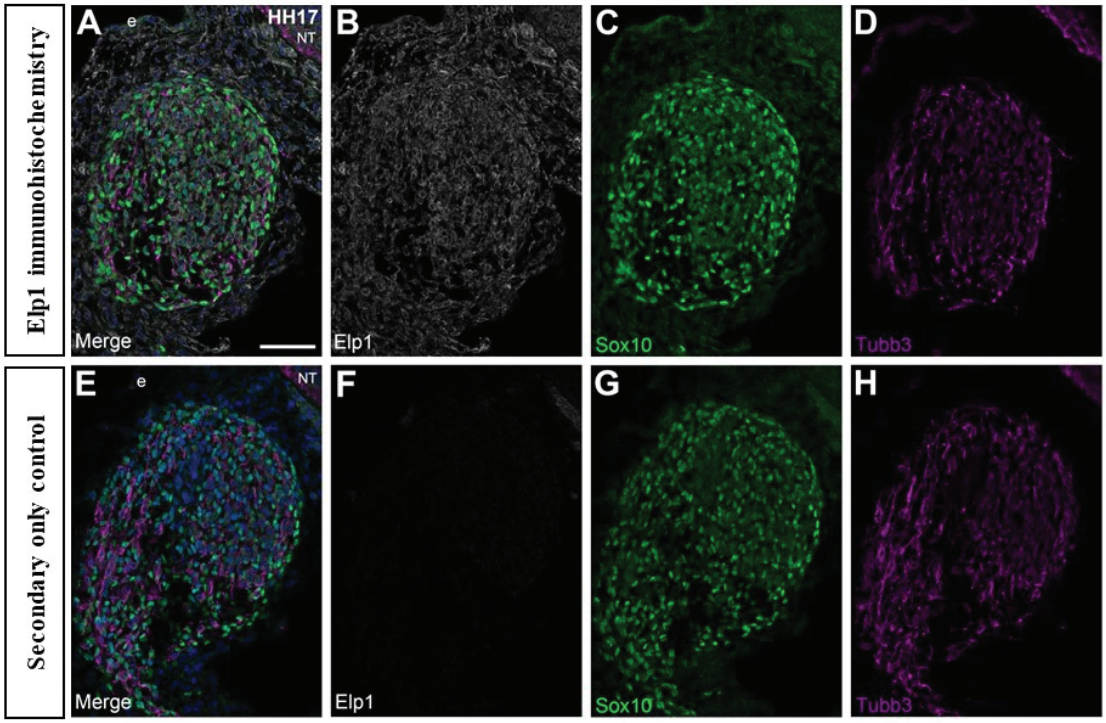

Figure 15: Secondary antibody only control for Elp1 immunohistochemistry supports specificity of Elp1 antibody. Representative transverse section through the forming trigeminal ganglion ophthalmic lobe (E2.5, HH17) followed by immunohistochemistry for Elp1 (A,B, white), Sox10 (A,C,E,G, green, labels neural crest cells), and Tubb3 (A,D,E,H, purple, labels placode cell-derived neurons) with corresponding merged images of all channels with DAPI (A,E, blue, marks all nuclei). Secondary antibody only control with absence of primary antibody for Elp1 (E,F, white) yields no detectable fluorescence (E, F). Scale bar in (A) is 50μm and applies to all images but is 10μm for (E-H). Abbreviations: e = ectoderm; NT = neural tube.

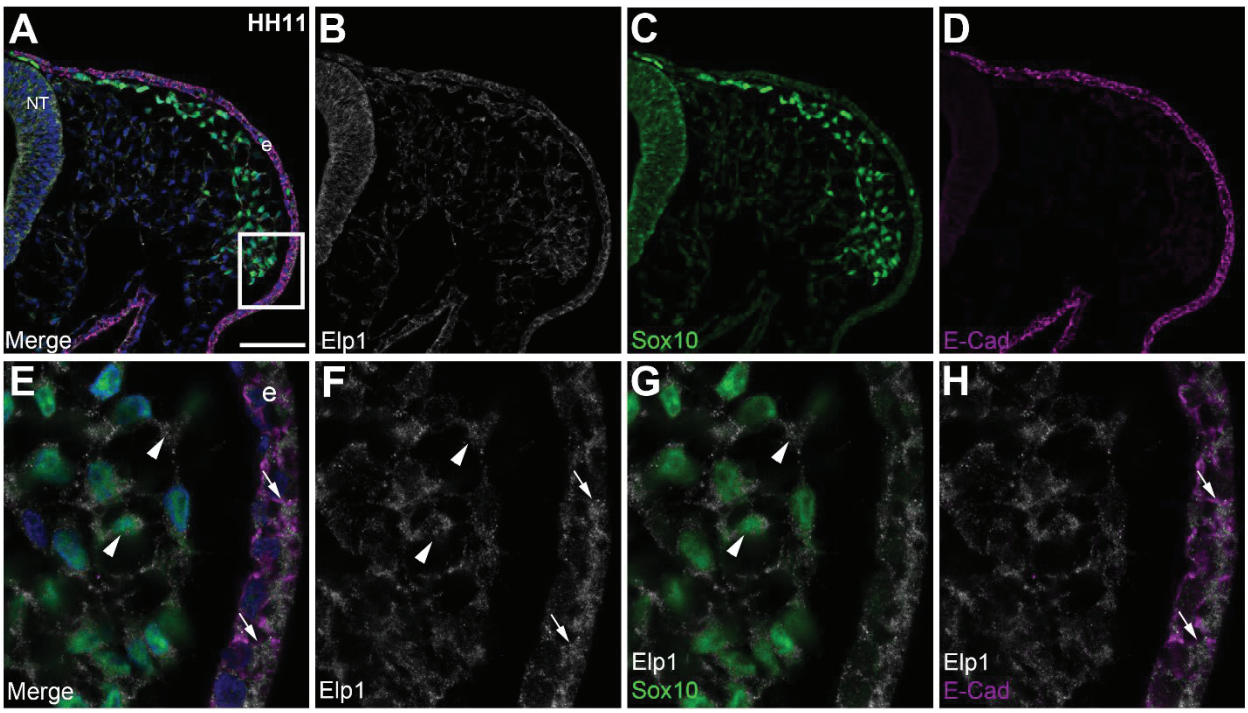

Figure 16: Elp1 is expressed in migratory neural crest cells and the surface ectoderm prior to trigeminal ganglion assembly. Representative transverse section through an (E1.5) (HH11) embryo midbrain followed by immunohistochemistry for Elp1 (A,B,E-H, white), Sox10 (A,C,E,G, green, labels migratory neural crest cells), and E-Cadherin (E-Cad, A,D,E,H, purple, labels ectoderm) with corresponding merged images of all channels with DAPI (A,E, blue, marks all nuclei). A higher magnification image of boxed region in (A) is shown in (E-H) with merge image of Elp1 and Sox10 (G, white and green, respectively) and a merge image of Elp1 and Tubb3 (H, white and purple, respectively). Arrowheads point to Elp1 in migratory neural crest cells (E-G), while arrows indicate Elp1 in the ectoderm (E,F,H). Scale bar in (A) is 50μm and applies to all images but is 10μm for (E-H). Abbreviations: NT = neural tube; e = ectoderm.

During E2 (HH13-15), placode cells start to delaminate from the ectoderm and differentiate into neurons, identified by their immunoreactivity for Tubb3 (Figure 17A,D,E,H, purple). Tubb3 is a marker for all neurons, but at the stages in this expression profile, all neurons are placode cell-derived (D'Amico-Martel & Noden, 1980). Here, Sox10 labels neural crest cells (Figure 17A,C,E,G, green). At these stages, Elp1 expression (Figure 17A,B,E,F, white) is still present in the ectoderm (Figure 17B,F). However, the apical distribution of Elp1 is decreasing, with enrichment reduced compared to the previous stage group. Here we found continued and dynamic punctate expression of Elp1 in the cytoplasm of Sox10-positive cells as well as some nuclear expression (Figure 17E,F,G, arrowheads). Additionally, at these stages, Elp1 expression is noted in the cytoplasm of Tubb3-positive neurons (Figure 17E,F,H, arrows).

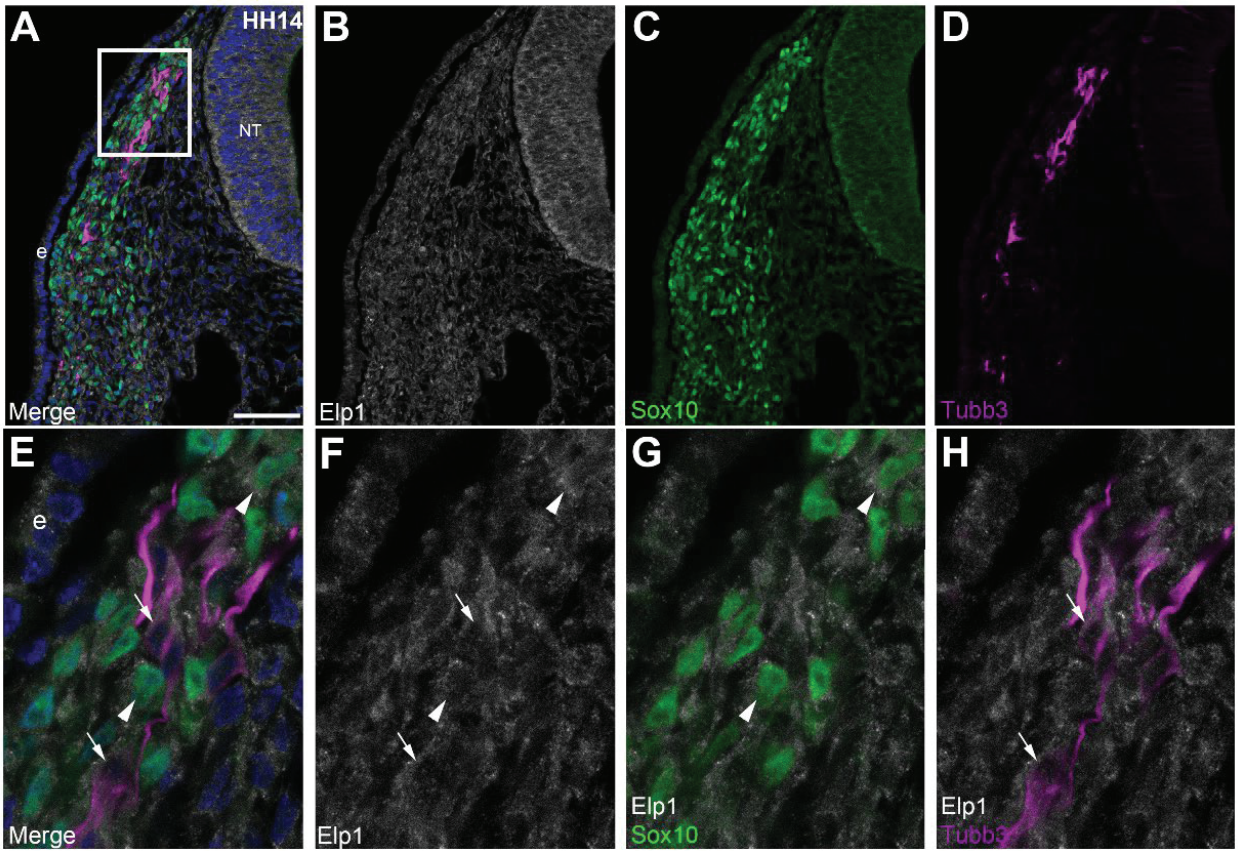

F**igure 17: Elp1 is expressed in neural crest cells and placode cell-derived neurons of the trigeminal ganglion during early placode cell delamination and migration.** Representative transverse section through the forming trigeminal ganglion ophthalmic lobe (E2, HH14) followed by immunohistochemistry for Elp1 (A,B,E-H, white), Sox10 (A,C,E,G, green, labels neural crest cells), and Tubb3 (A,D,E,H purple, labels placode cell-derived neurons) with corresponding merged images of all channels with DAPI (A,E, blue, marks all nuclei). A higher magnification image of boxed region in (A) is shown in (E-H) with merge image of Elp1 and Sox10 (G, white and green, respectively) and a merge image of Elp1 and Tubb3 (H, white and purple, respectively). Arrowheads point to Elp1 in migratory neural crest cells (E-G), while arrows indicate Elp1 in the ectoderm (E,F,H). Scale bar in (A) is 50μm and applies to all images but is 10μm for (E-H). Abbreviations: e = ectoderm.

At E2.5 (HH16-17) neural crest cells and placode cell-derived neurons have coalesced to form the trigeminal ganglion proper, where a more defined “teardrop” or “semilunar” shape is then observed in sections. At these stages, more neurons have started populating the trigeminal anlage along with the neural crest cells. In these stage groups, Sox10 remains a neural crest cell marker (Figure 18A,C,E,F, green) and Tubb3 is observed in neurons that are still solely placode cell-derived (Figure 18A,D,E,G, purple). Elp1 is expressed in the ectoderm (Figure 18A,B,E-H, white), with a loss of apical distribution (Figure 18A,B). Expression of Elp1 in Sox10-positive neural crest cells (Figure 18E-G, arrowheads) and the cytoplasm of Tubb3-positive neurons (Figure 18E,F, H, arrows) remains the same as in the previous stage grouping.

Lastly, during E3-3.5 (HH18-20), a more defined trigeminal ganglion structure is present, with more placode cell-derived neurons surrounded by undifferentiated neural crest cells. At these stages, Sox10 (Figure 19A,C,E,F, green) and Tubb3 (Figure 19A,D,E,G, purple) remain a marker for undifferentiated neural crest cells and placode cell-derived neurons, respectively. Elp1 expression (Figure 19A,B,E-H, white) remains the same as the previous stage groups, with ectodermal (Figure 19A ,B), neural crest cell (Figure 19E-G, arrowhead), and neuronal (Figure 19E,F,H, arrows) expression noted.

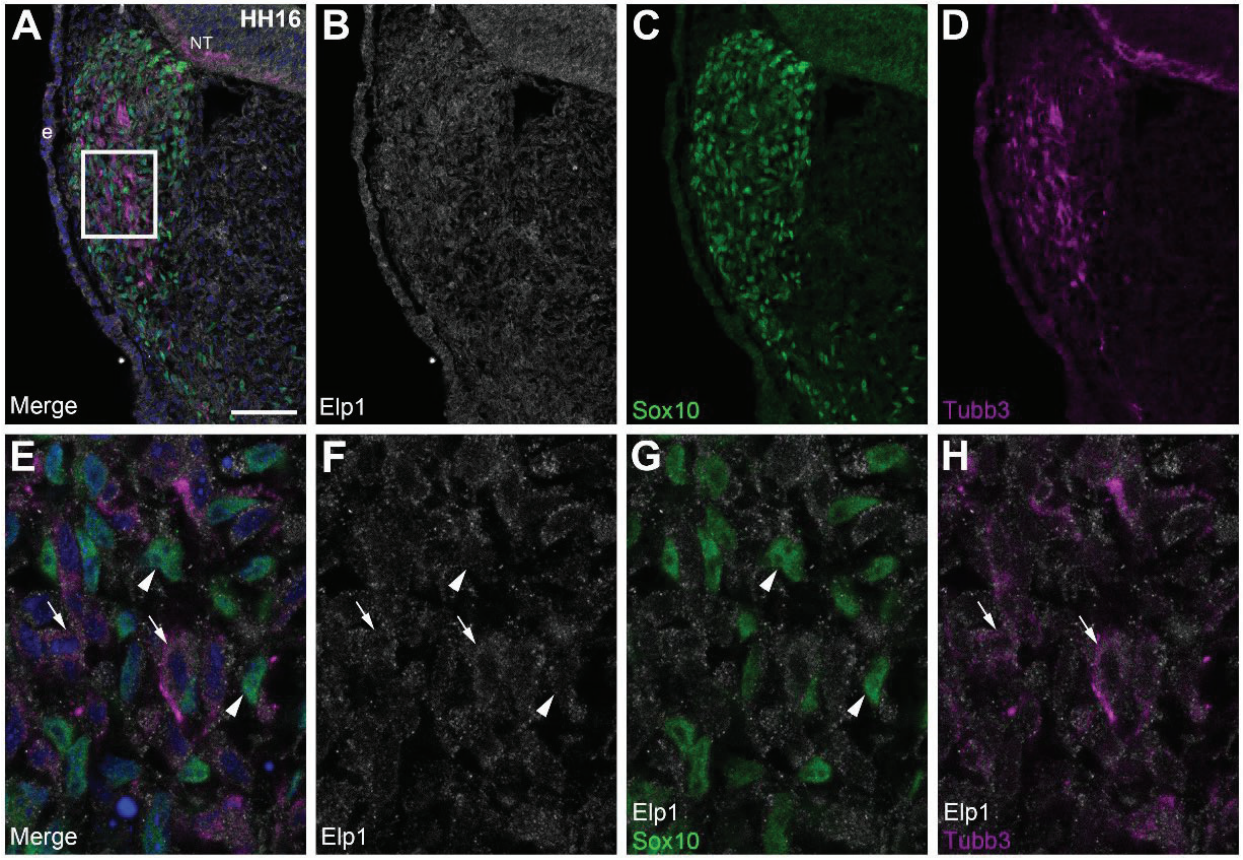

Figure 18: Elp1 is expressed in neural crest cells and placode cell-derived neurons of the trigeminal ganglion during initial coalescence and condensation. Representative transverse section through the forming trigeminal ganglion ophthalmic lobe (E2.5, HH16) followed by immunohistochemistry for Elp1 (A,B,E-H, white), Sox10 (A,C,E,G, green, labels neural crest cells), and Tubb3 (A,D,E,H purple, labels placode cell-derived neurons) with corresponding merged images of all channels with DAPI (A,E, blue, marks all nuclei). A higher magnification image of boxed region in (A) is shown in (E-H) with merge image of Elp1 and Sox10 (G, white and green, respectively) and a merge image of Elp1 and Tubb3 (H, white and purple, respectively). Arrowheads point to Elp1 in migratory neural crest cells (E-G), while arrows indicate Elp1 in the ectoderm (E,F,H). Scale bar in (A) is 50μm and applies to all images but is 10μm for (E-H). Abbreviations: e = ectoderm; NT = neural tube.

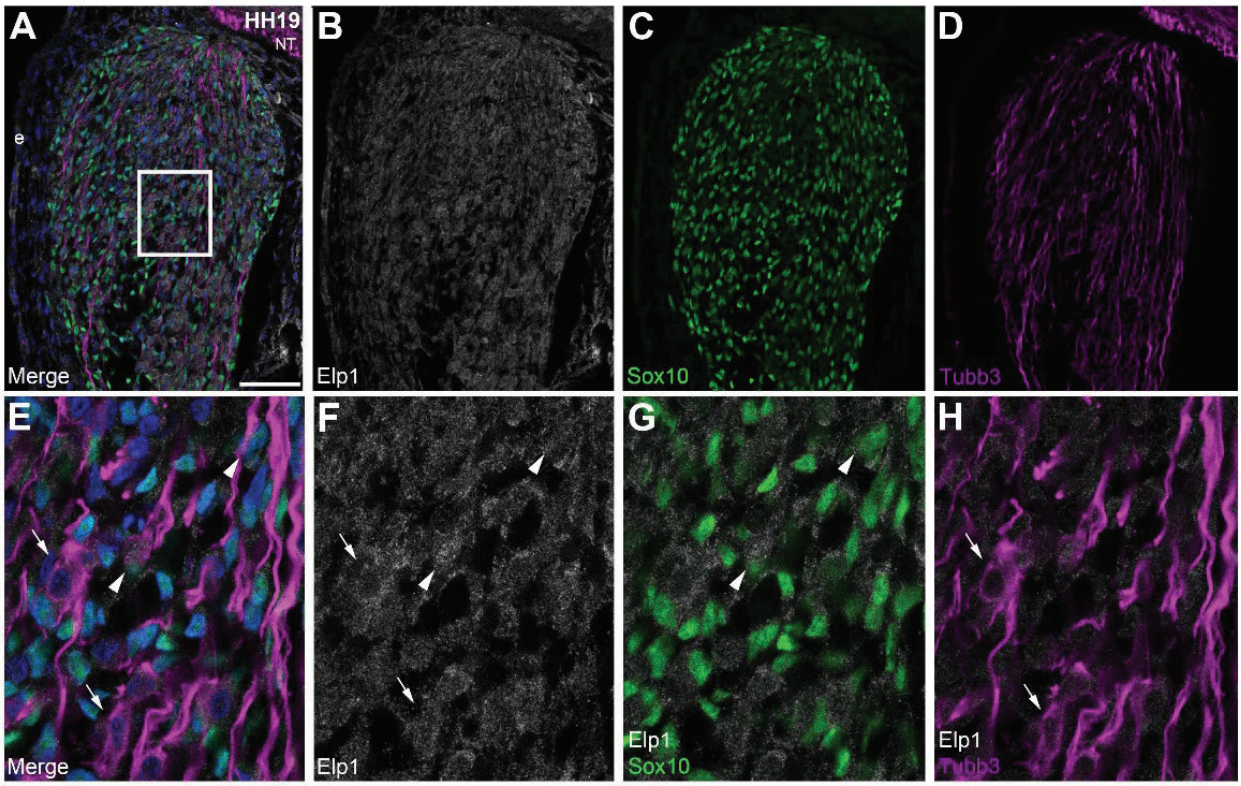

Figure 19: Elp1 is expressed in undifferentiated neural crest cells and placode cell-derived neurons of the trigeminal ganglion. Representative transverse section through the forming trigeminal ganglion ophthalmic lobe (E3, HH19) followed by immunohistochemistry for Elp1 (A,B,E-H, white), Sox10 (A,C,E,G, green, labels neural crest cells), and Tubb3 (A,D,E,H, purple, labels placode cell-derived neurons) with corresponding merged images of all channels with DAPI (A,E, blue, marks all nuclei). A higher magnification image of boxed region in (A) is shown in (E-H) with merge image of Elp1 and Sox10 (G, white and green, respectively) and a merge image of Elp1 and Tubb3 (H, white and purple, respectively). Arrowheads point to Elp1 in migratory neural crest cells (E-G), while arrows indicate Elp1 in the ectoderm (E,F,H). Scale bar in (A) is 50μm and applies to all images but is 10μm for (E-H). Abbreviations: e = ectoderm.

4.2.2 Immunoblot characterization of Elp1 expression in developing trigeminal ganglion tissue.

The expression of Elp1 in developing trigeminal ganglion tissue over the same time course E1.5-3.5 (HH11-20) was also analyzed through immunoblotting (Figure 20). Two different Elp1 antibodies, raised to somewhat overlapping regions of the carboxy terminus of the Elp1 protein, were used to detect Elp1, yielding surprisingly different results. The antibody from Sigma (WH0008518M3) revealed a band at 170 kDa expressed at relatively similar levels at each

timepoint observed (Figure 20). A doublet starts to appear with a band at 150 kDa faintly visible in HH15-18, with more robust expression at HH19/20. Additionally, a band around 250 kDa band showed increased intensity from HH15/16 through HH19/20. However, the LSBio antibody (LS-B571) uncovered a band at 100 kDa that increased in intensity in the HH19/20 sample lane while the doublet band at 85 kDa decreased over time, with faint expression at HH15/16 and expression absent from HH17-20.

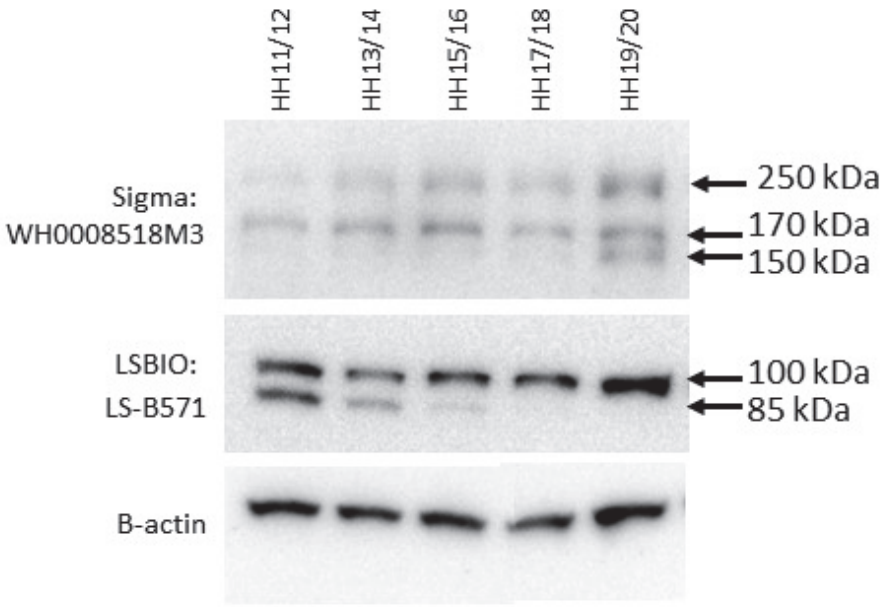

Figure 20: The apparent molecular weight of Elp1 changes throughout early development of the trigeminal ganglion, with various protein sizes observed with different Elp1 antibodies. Immunoblotting of samples collected of trigeminal ganglion cell contributions was performed, followed by probing with different Elp1 antibodies. The Sigma antibody revealed a band with increasing intensities over the timepoints at 250 kDa and a band at 170 kDa, forming a faint doublet with a band at 150 kDa that had higher intensity at HH19/20. The LSBio antibody showed a band at 100 kDa that increases in intensity at HH19/20, with a band at 85 kDa that decreased in intensity and was eventually undetectable by HH17/18.

4.3 Conclusions

Our data revealed Elp1 is ubiquitously expressed, with enrichment in the ectoderm, migratory neural crest cells, and neural crest cells and placode cell-derived neurons within the trigeminal ganglion at the developmental timepoints analyzed. Interestingly, previous studies in the chick trunk showed that Elp1 was not expressed in migratory neural crest cells but was detected in the cytoplasm and axons of neural crest-derived sensory neurons (Hunnicutt et al., 2012). A later study reported Elp1 expression only in post-mitotic neurons of the neural crest-derived dorsal root ganglia (Abashidze et al., 2014). This published immunohistochemistry data, however, used a different Elp1 antibody (no longer commercially available), with an epitope sequence located further upstream than the antibody used in our studies. Therefore, expression differences may be due to epitope location and/or antibody affinities. In addition to the antibodies used, differences between trunk and cranial development are relatively common (D'Amico-Martel & Noden, 1980) and may explain the differences uncovered in Elp1 protein expression in these studies.

Elp1 expression in the trigeminal ganglion has also been studied in the mouse. Elp1 was initially characterized at E10.5 using an *Elp1*^{LacZ} reporter (Leonard et al., 2022). Beta-galactosidase staining was used as a proxy for *Elp1* transcript distribution, and at this timepoint, all neurons of the trigeminal ganglion are placode cell-derived, i.e., equivalent to the timepoints we characterized in chick. The beta-galactosidase staining was enriched throughout the trigeminal ganglion and neural tube, with expression seen in the surrounding cranial mesenchyme (Leonard et al., 2022). Although showing transcript localization, these data are consistent with our chick immunohistochemistry results. However, when examining Elp1 protein expression in the mouse, Elp1 was enriched in the cytoplasm and axons of neurons, generally devoid of staining in the nucleus (Leonard et al., 2022). These findings suggest that differences

seen between transcript and protein localization could be due to post-transcriptional or post-translational modifications.

Interestingly, in the chick, as trigeminal ganglion development continues and coalescence and condensation of placode cell-derived neurons and neural crest cells occurs, Elp1 expression remains the same from HH13-20. However, immunoblotting results suggest changes to Elp1 protein are occurring, possibly through post-translational modifications such as phosphorylation, which has previously described for Elp1 in yeast (Saint-Germain et al., 2004). In addition, the difference in band sizes seen between the two antibodies suggests that there may be proteolytic processing occurring and that the two antibodies may have different affinities for these different forms of Elp1. Furthermore, when the amount of protein lysate is increased, the Sigma antibody additionally detects the 100 and 85 kDa bands, while the LSBio antibody detects the 250, 170, and 150 kDa bands. This difference in detection threshold suggests that the antibodies possess different affinities for the observed Elp1 bands.

Further, when looking at the most recent chick assembly (GRCg6a), three predicted splice variants are present: *Elp1-201*, *Elp1-202*, and *Elp1-203*. Upon aligning the predicted protein sequences of these three splice variants, the amino acid sequences are the same until the carboxy terminus (Figure 21). Coincidentally, the two antibodies used in our studies are designed to recognize sequences in the carboxy terminus. Since the immunogen sequence is proprietary, the exact epitope of these antibodies is unknown. However, when aligning the protein sequences within these regions, neither antibody is likely to detect all three splice variants. The Sigma antibody (WH0008518M3) likely recognizes Elp1-202 and Elp1-203, while LSBio (LS-B571) would be immunoreactive with Elp1-201 and Elp1-203. Therefore, differences noted between immunoblots could be due to antibody recognition and/or a result of alterations in splice variant

expression and/or processing. Taken together, these data are the first to characterize Elp1 expression in the chick trigeminal ganglion.

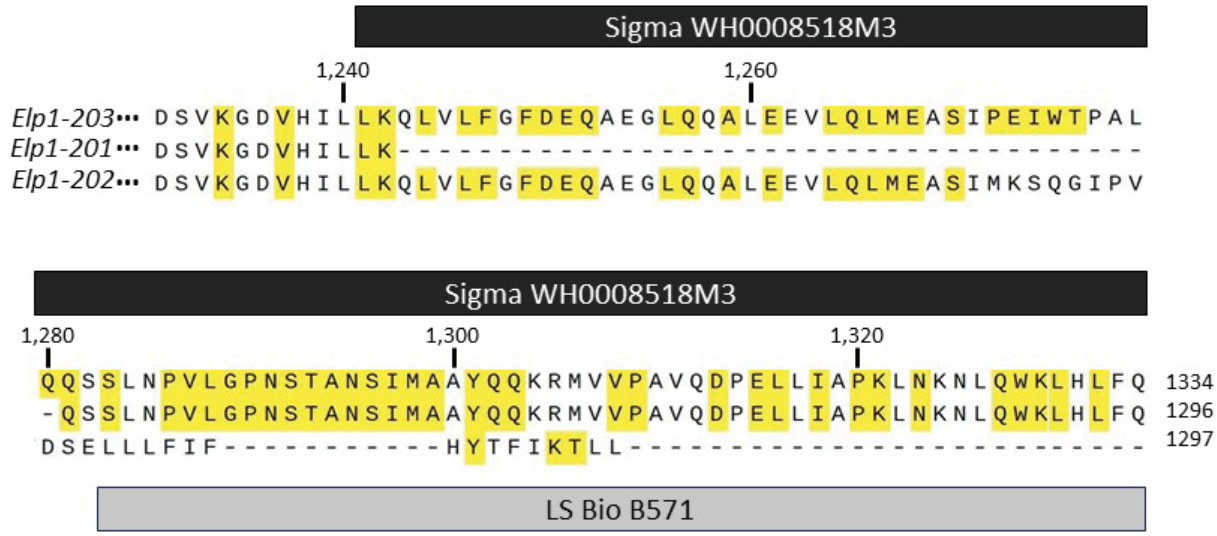

Figure 21: Schematic representation of antibody alignment to predicted protein products from *Elp1* splice variants. Alignment of a portion of the amino acid sequence predicted from the three chick *Elp1* splice variants, Elp1-201, Elp1-202, and Elp1-203, revealed differences at the carboxy terminus of the protein sequences. The immunogen sequence is represented here, aligned with the *Elp1* transcripts. The mouse Sigma antibody (WH0008518M3) was raised to a partial recombinant protein 89 amino acids in length from the human Elp1 protein sequence. The immunogen for the rabbit LSBio antibody (LS-B571) is a 16 amino acid peptide located within the last 50 amino acids of the human Elp1 protein. Yellow highlighting refers to the conserved amino acids between chick and human Elp1 protein sequences.

Chapter 5: Evaluating the efficacy of Elp1 translation-blocking and splice-blocking MOs

5.1 Summary

A technique called ectodermal electroporation permits molecular perturbations in cranial placode cells in the chick. This technique was used to validate two MOs designed for knockdown of chick Elp1 protein levels. MOs are oligos that bind mRNA transcripts, blocking either their translation or splicing, and are routinely used for protein knockdown in models such as the chick, zebrafish, and *Xenopus* (Saint-Germain et al., 2004; Shah et al., 2017; Tandon et al., 2012).

As with all models, there are certain challenges faced when using the chick for molecular manipulations. Assembly of the chicken genome is still ongoing, making verification of the reported sequences an important step when attempting knockdown techniques. For this reason, 5' RACE was performed to validate the reported 5'UTR sequence that the Elp1 translation-blocking MO targets. Additionally, 5' RACE allowed us to confirm if a newly identified *Elp1* splice variant was present in the trigeminal ganglion at the timepoint being studied. Following validation of MO specificity to *Elp1* using NCBI BLAST and 5'RACE, immunoblotting was performed to confirm successful knockdown of Elp1 protein levels in the chick trigeminal ganglion using these MOs. Our results indicate that the MOs are specific to Elp1 and when electroporated into a chick embryo, knockdown is successfully achieved.

5.2 Results

5.2.1 Elp1 translation- and splice- blocking MOs are specific to the chick Elp1 transcripts.

Two lissamine-tagged MOs were designed by GeneTools, LLC to knockdown *Elp1* in the chick. The lissamine tag fluoresces red, providing a way to visualize the cells that received it. One MO

is translation-blocking, designed to target the start site of translation, along with surrounding sequences, within the *Elp1* transcript (Figure 22). The second MO is splice-blocking, targeting the junction between exon 1 and intron 1, predicted to cause inclusion of intron 1 in the mature mRNA and leading to nonsense-mediated decay of the *Elp1* transcript (Figure 22). To ensure specificity of the MOs, both MO target sequences were blasted against the chick genome (*Gallus gallus*) using NCBI BLAST. According to GeneTools, a 14-15 nucleotide consecutive overlap (or 60% identity) with another mRNA sequence is not specific enough to lead to off-target effects (GeneTools). With both MOs, no mRNA sequences above this threshold were identified in the BLAST results.

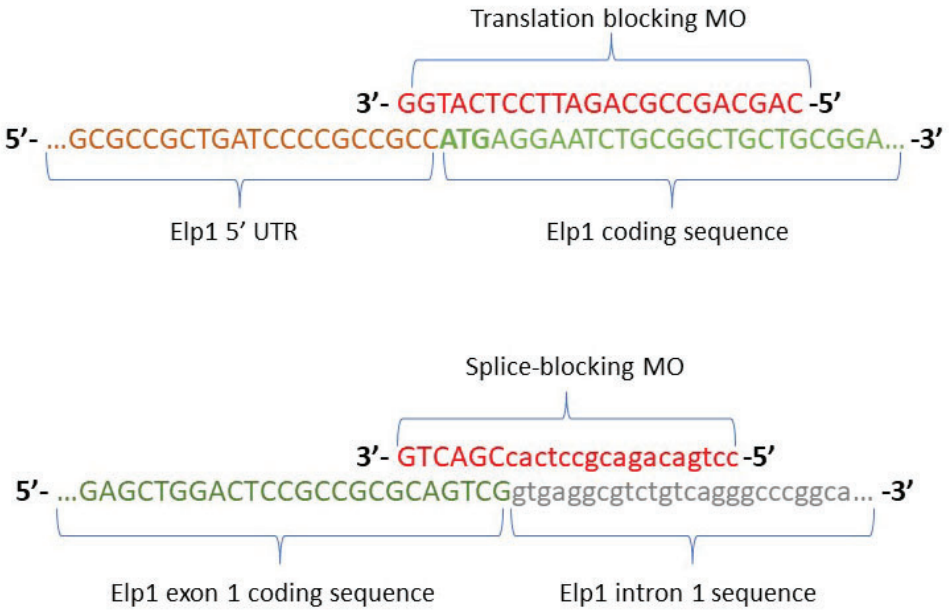

Figure 22: The Elp1 MOs inhibit translation and splicing of *Elp1* transcripts. The translation-blocking MO works by targeting the ATG start site (and sequence up- and downstream) and prevents translation initiation complexes from reaching the *Elp1* start codon. The splice-blocking MO works by targeting the exon/intron junction, inhibiting splice site recognition by the splicing machinery, leading to the inclusion of the targeted intron. Abbreviation: UTR, untranslated region.

5.2.2 5' RACE results confirm reported Elp1-201 sequence in HH19/20 trigeminal ganglion tissue.

Due to initial difficulties showing Elp1 knockdown with the translation-blocking MO, and the knowledge that the chick genome assembly is routinely being updated, 5'RACE was performed to validate the reported sequence to which the translation-blocking MO was designed. After the initial design of the MO, a new genome assembly was released for the chicken (*Gallus gallus*), Galgal4. A computational search of this genome assembly in ENSEMBL revealed an additional predicted splice variant, *Elp1-202*, with a vastly different 5'UTR from *Elp1-201* (Figures 23 & 24). Despite a different 5' UTR, the *Elp1-202* variant has an identical sequence starting at exon 5 of *Elp1-201*, resulting in a 572 nucleotide discrepancy between the two transcripts and a

difference of 151 amino acids (Figure 23). If *Elp1-202* is present in the trigeminal ganglion, it will not be targeted by the designed MOs.

A

Transcript ID	Name	bp	Protein	Biotype	UniProt Match
ENSGALT00000003013.5	ELP1-201	4152	1334aa	Protein coding	F1P5L4
ENSGALT00000104338.1	ELP1-202	3580	1183aa	Protein coding	A0A3Q2UCD8

B

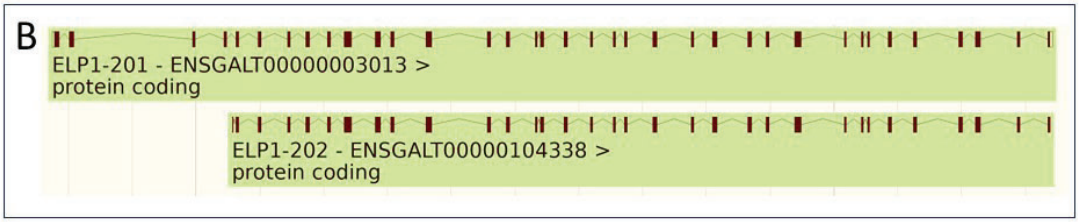

Figure 23: Chick *Elp1* splice variants reported in ENSEMBL. In the genome assembly Galgal4, two splice variants were annotated, *Elp1-201* and *Elp1-202* (A). These variants have complete overlap starting at exon 5 of *Elp1-201* (B), with a difference of 572 nucleotides. This difference causes *Elp1-201* and *Elp1-202* to consist of 4152 and 3580 nucleotides or 1334 and 1183 amino acids respectively.

To verify the sequences reported in ENSEMBL and determine if additional MOs were required, 5'RACE was performed. Gene-specific primers (GSPs) for *Elp1* were designed according to manufacturer's instructions (Takara Bio). GSP1 was designed to recognize Elp1-201 while GSP2 was constructed to identify *Elp1-201* and *Elp1-202* due to the overlap of the transcripts, starting just after ATG of *Elp1-202*. Therefore, if *Elp1-202* is present, two products would be expected from the 5'RACE and should be observed when running the products on a gel.

To determine which transcripts were present, trigeminal ganglion tissue was dissected from E3.5 (HH19-20) embryos and total RNA was extracted, followed by 5' RACE according to the manufacturer's instructions. The products were run on an agarose gel, revealing a band of approximately 320 nucleotides with GSP1 and approximately 700 nucleotides with GSP2, followed by gel extraction (Figure 24). While a faint band at approximately 500 nucleotides can

be seen with GSP2, there was not enough DNA obtained from gel purification to permit sequencing. Additionally, the size band does not align with the predicted size of 353 nucleotides if the GSP2 5'RACE was successful in identifying *Elp1-202*.

After the two 5'RACE products were gel purified, the resulting DNA was cloned into pRACE vectors, and three clones were sent for sequencing (Genewiz). The returned sequences were aligned with the reported sequences from ENSEMBL for *Elp1* and analyzed. The data showed that the *Elp1-201* 5'UTR sequence reported in ENSEMBL was identical to the GSP1 5' RACE results for all clones sequenced, and the sequence returned from GSP2 aligned with the sequence reported for that region of *Elp1-201*, with no *Elp1-202* sequence identified.

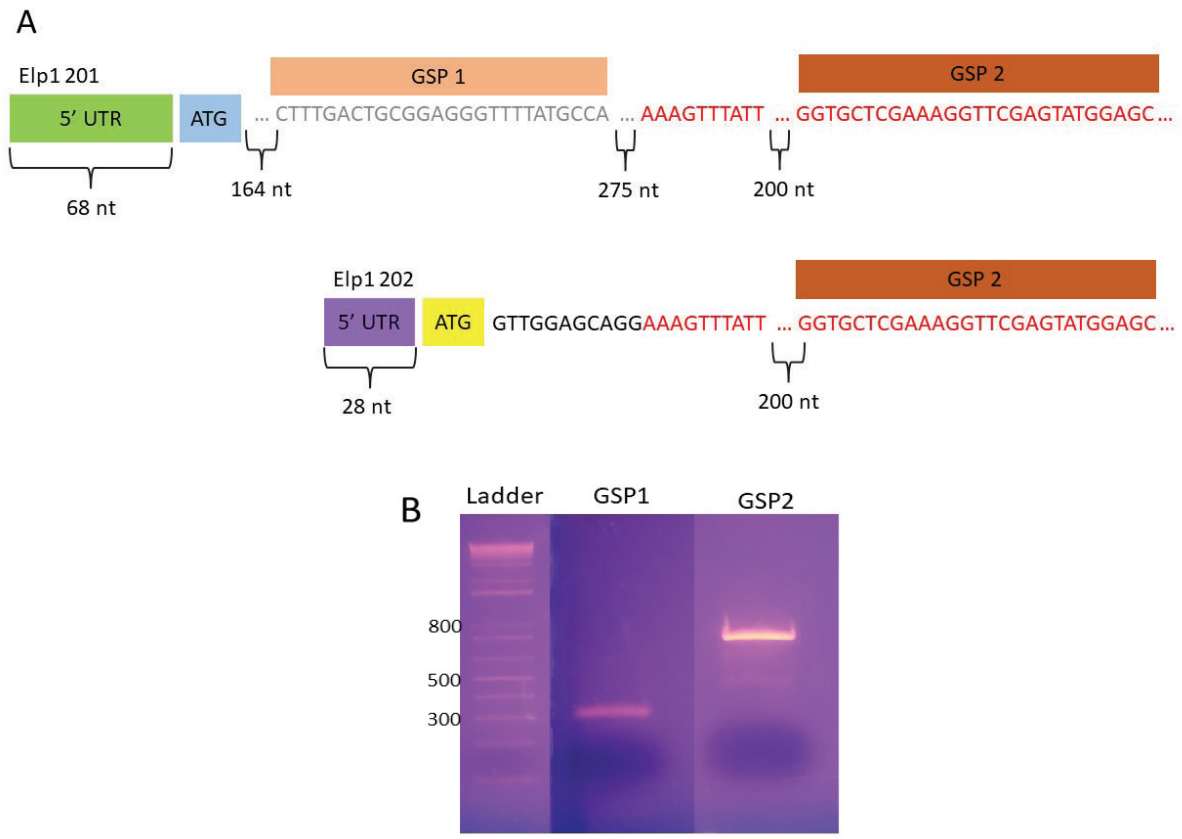

Figure 24: 5'RACE primers designed to both *Elp1-201 and Elp1-202* splice variants only show expression of Elp1-201. 5' RACE primers were designed to recognize two Elp1 splice variants, *Elp1-201 and Elp1-202* (A). GSP1 is specific to *Elp1-201* predicted sequence while GSP2 will pick up both variants if present. (B) 5'RACE, products were run on an agarose gel where a band ~300 nucleotide was seen in the GSP1 lane and bands at ~700 nucleotides and ~500 nucleotides were observed in the GSP2 lane.

5.2.3 Elp1 MOs are effective at reducing Elp1 protein levels in trigeminal placode cells.

A 1:1 mixture of the translation-blocking and splice-blocking MOs, or standard Control MO (GeneTools, LLC), was electroporated at E1 (HH10-11) using a unilateral ectodermal electroporation method (Shah et al., 2017; Shiau et al., 2008) to target trigeminal placode cells prior to delamination. Embryos were then re-incubated and grown to E3.5 (HH19-20). MO presence was confirmed by inspecting the trigeminal ganglion for red fluorescence using a

fluorescent stereomicroscope followed by its dissection (Figure 25). Dissection of trigeminal ganglion tissue was performed using the fluorescent stereomicroscope to ensure only fluorescently labeled tissue was collected.

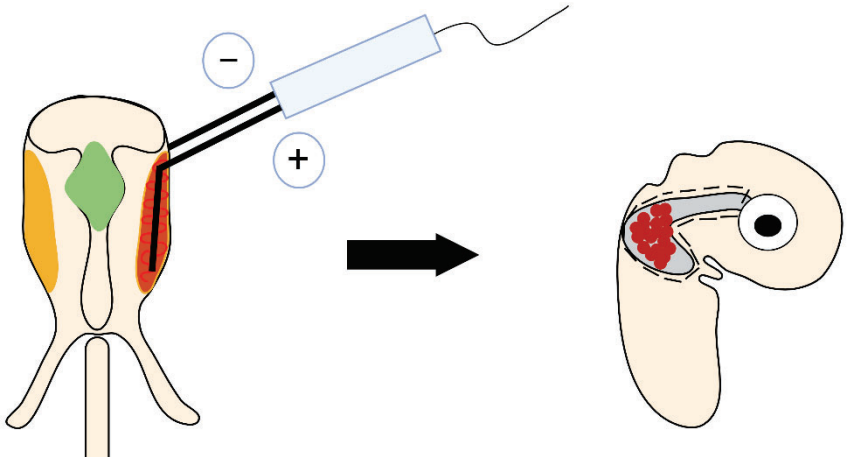

Figure 25: Ectodermal electroporation targeting cranial placode cells, followed by dissection of the trigeminal ganglion. Unilateral electroporation is performed by overlaying the ectoderm with the MO (red) and applying an electric current. The embryos are then re-incubated to E3.5 (HH19-20) and the trigeminal ganglion is dissected under a red fluorescent light to cleanly dissect out the population that has the MO. Created by Biorender.

Following trigeminal ganglion tissue dissection, the tissue was pooled and lysed, with proteins separated by SDS-PAGE. Immunoblotting, further described in Chapter 2, was then performed using the LSBio Elp1 antibody (LS-B571) as it has been previously published for use in immunoblotting (Li et al., 2020). This allowed us to visualize and measure the level of Elp1 reduction to confirm the MOs were effective at reducing Elp1 levels. Immunoblotting data shows six bands immunoreactive to the Elp1 antibody, five of which show varied levels of knockdown ranging from 14-56% (Figure 26). The band at 150 kDa, however, showed no reduction in intensity after introduction of the Elp1 MOs.

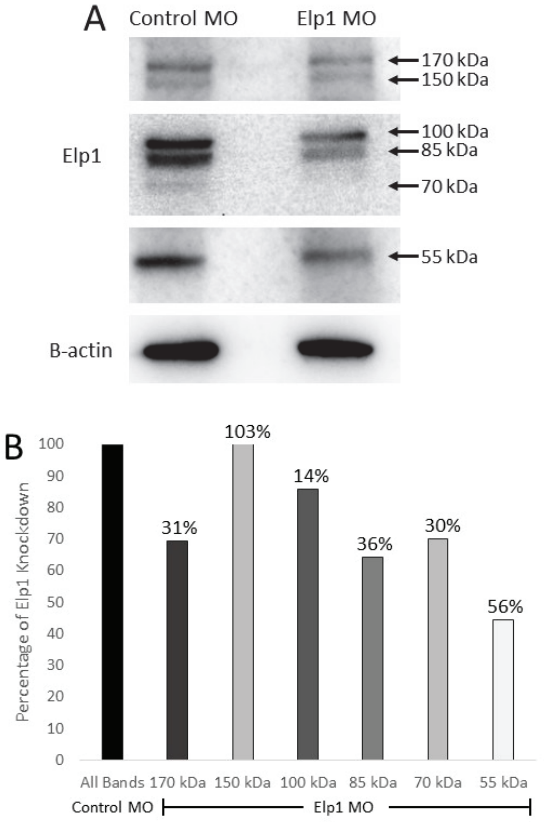

Figure 26: Elp1 MOs reduce Elp1 protein levels in trigeminal ganglion. The knockdown efficiency of a 1:1 ratio Elp1 translation-blocking and splice-blocking MO was assessed using immunoblotting compared standard Control MO. (A). Six bands were immunoreactive to the Elp1 antibody and when normalized to B-actin, 5 showed reduced intensities in the Elp1 MO treated tissue compared to the standard Control MO (B).

5.3 Conclusions

Our NCBI BLAST and 5'RACE data revealed that both Elp1 MOs are specific to *Elp1* reported in the GalGal4 chicken genome assembly. NCBI BLAST results for both MOs showed that according to GeneTools, LLC thresholds for off target prediction, these MOs are specific to *Elp1*. Additionally, the annotated 5'UTR sequence (ENSEMBL) was the same as the sequence we received from all clones obtained from the 5'RACE experiment. Products from 5'RACE did not show the presence of splice variant *Elp1-202* at E3.5 (HH19-20). While a faint band at ~500 nucleotides was present, there was not enough product to yield any DNA after gel purification. However, this band does not correspond to predicted size of *Elp1-202* with GSP2 and is likely a background band. In the time since this experiment was performed, a new chicken genome assembly, GRCg6a, has been released. Examination of these predicted sequences indicated that both MOs would target all three splice variants, if expressed. Additionally, the faint 500 nucleotide band in the GSP2 products does not correspond to predicted product sizes of the new splice variants if GSP2 were used. Immunoblotting then verified knockdown of Elp1 protein in all bands except the 150 kDa band, which is assumed to be a background band since its levels did not change after introduction of the Elp1 MOs.

Collectively, these data validate the use of these MOs in the knockdown of Elp1 in trigeminal placode cells. They were then used to study the effects of reduced Elp1 protein levels in trigeminal placode cells and their derivatives on the formation of the trigeminal ganglion.

Chapter 6: Functional characterization of Elp1 in chick trigeminal ganglion development

6.1 Summary

Evidence suggests that Elp1 is important in trigeminal ganglion development, with a decrease in trigeminal nerve size observed in FD patients along with symptoms suggesting trigeminal nerve dysfunction (Dietrich & Dragatsis, 2016; Gold-von Simson & Axelrod, 2006; Won et al., 2019). Studies have examined the function of Elp1in neural crest cell populations of sensory ganglia using a Wnt1-Cre conditional knockout mouse model in which *Elp1* is deleted from neural crest cells and their derivatives (George et al., 2013; Goffena et al., 2018). Using this model, Elp1 was discovered to function in the neural crest-derived neurons of the trigeminal ganglion, with loss of Elp1 disrupting target tissue innervation (Leonard et al., 2022). To understand the full picture in the trigeminal ganglion, however, the role of Elp1 in placode cell-derived neurons must also be investigated. Currently, there is no trigeminal placode specific Cre driver that can be used to target this cell population in the mouse. Therefore, to study Elp1 in the context of the trigeminal placode cells, we turned to the chick embryo. The chick is an optimal model to study this cell population due to the accessible location of trigeminal placode cells in the surface ectoderm and ability to perform molecular manipulations coupled with continued growth of the embryo to desired developmental timepoints. Using a MO-based knockdown approach, our studies show that decreased Elp1 in trigeminal placode cells causes aberrant trigeminal ganglion formation.

6.2 Results

To determine the function of Elp1 in placode cell-derived neurons of the trigeminal ganglion, ectodermal electroporation, described in Chapter 2, was used to introduce the Elp1 MO into

trigeminal placode cells at E1.5 (HH10-11). Embryos were then re-incubated and grown to desired timepoints to evaluate changes in trigeminal ganglion development. Confocal imaging of whole embryo heads and trigeminal ganglion sections was carried out to examine gross trigeminal ganglion morphology and distribution of placodal neurons and neural crest cells within the forming trigeminal ganglion, respectively.

6.2.1 Elp1 knockdown in trigeminal placode cells decreases the area of the trigeminal ganglion during early stages of trigeminal ganglion assembly.

Initially, placode cell-derived neurons and migratory neural crest cells coalesce to form the trigeminal ganglion anlage (~E2.5, HH15-17). Strikingly, defects are already apparent at these early stages of trigeminal ganglion development when Elp1 is depleted from trigeminal placode cells (Figure 27). Whole-mount immunohistochemical staining for Tubb3 was conducted to label placode cell-derived neurons at this stage. The contralateral control trigeminal ganglion has formed normally, with ophthalmic and maxillomandibular lobes starting to become defined (Figure 27A, arrowhead, arrow, respectively). Elp1 knockdown in trigeminal placode cells, however, negatively impacts the development of the ophthalmic branch of the trigeminal ganglion on the treated side of the embryo, with disorganization of neurons apparent (Figure 27B). Measurement of the area occupied by the experimental and contralateral control side trigeminal ganglion reveals a statistically significant decrease upon Elp1 knockdown compared to control (Figure 27C, $p = 0.0014$). Electroporation of a scrambled control MO into trigeminal placode cells resulted in no phenotypic effect on trigeminal ganglion development, with results comparable to those observed on the contralateral sides of both Elp1 MO- and control MO-treated embryos (Figure 28).

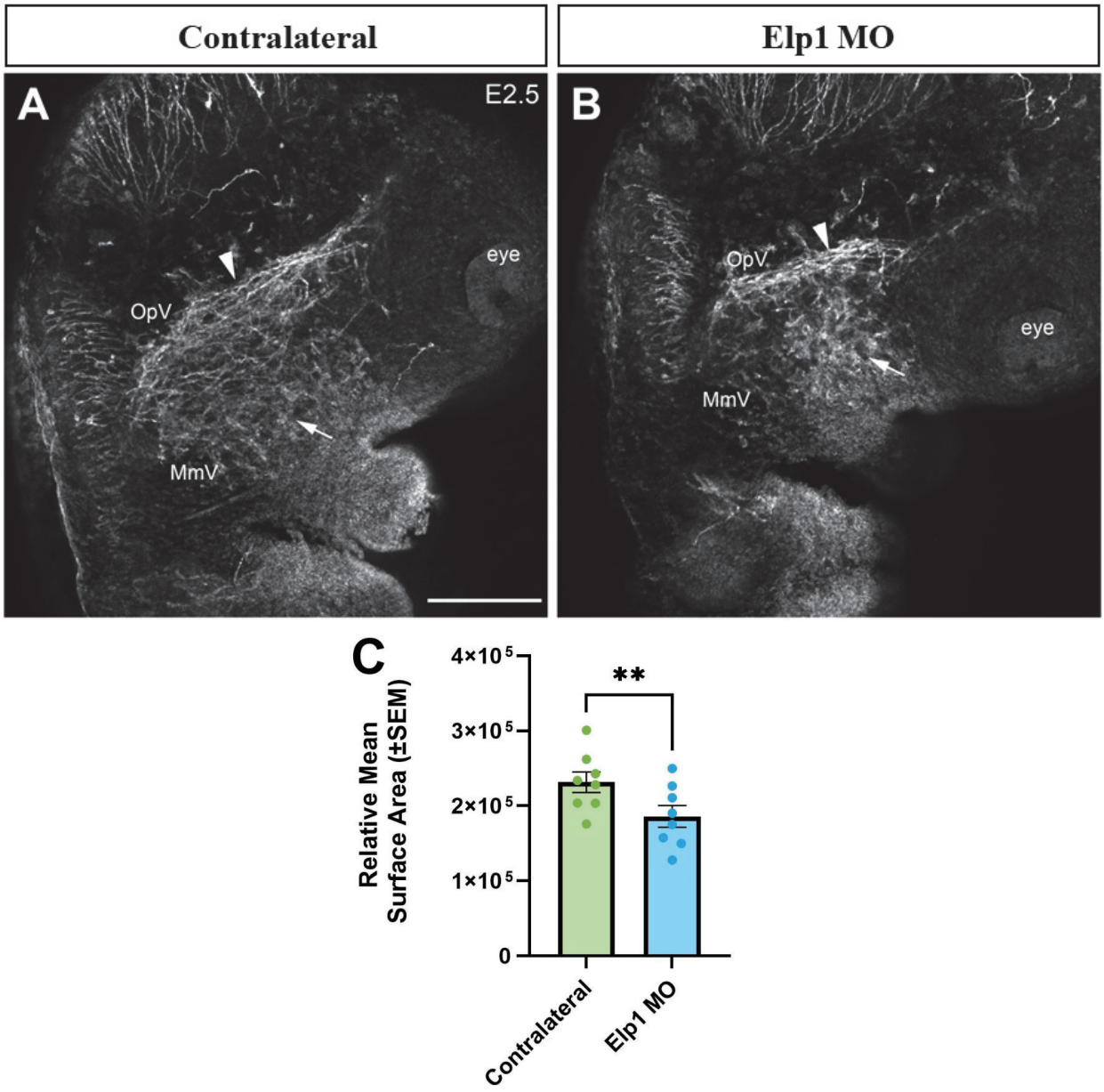

Figure 27: Reduction of Elp1 in trigeminal placode cells decreases trigeminal ganglion area and impacts neuronal organization. Representative max intensity projections of confocal Z-stacks showing the contralateral control (A) or Elp1 MO-treated (B) trigeminal ganglion at E2.5 (HH16) after Tubb3 whole-mount immunohistochemistry (white). Arrowheads point to disorganization of ophthalmic branch projections, while arrows show the forming maxillomandibular branch. Scale bar in (A) is 250µm and applies to (B). (C) Quantification of the area of contralateral (green, n = 7) and Elp1 MO-treated (blue, n = 7) trigeminal ganglia demonstrating statistical significance (p = 0.0014, paired t-test). Abbreviations: OpV = ophthalmic lobe; MmV = maxillomandibular lobe.

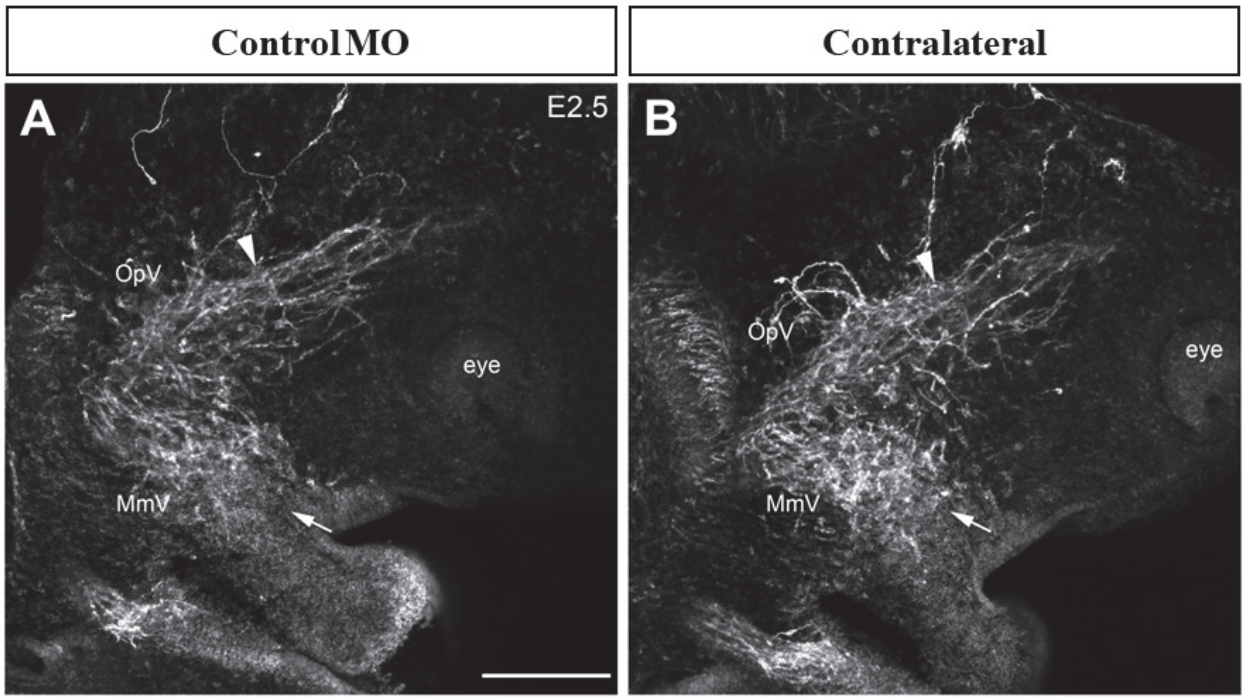

Figure 28: Scrambled Control MO does not alter trigeminal ganglion development. Representative max intensity projections of confocal Z-stacks showing the Control MO-treated (A) or contralateral control (B) trigeminal ganglion at E2.5 (HH16) after Tubb3 whole-mount immunohistochemistry (white). Arrowheads point to normal ophthalmic branch projections, while arrows show a properly forming maxillomandibular branch. Scale bar in (A) is 250μm and applies to (B). Abbreviations: OpV = ophthalmic lobe; MmV = maxillomandibular lobe.

6.2.2 Elp1 knockdown in trigeminal placode cells causes persistent reduction in trigeminal ganglion area and negatively affects innervation of the eye.

One day later, extensive development of the trigeminal ganglion anlage has occurred through further condensation of neural crest cells and placode cell-derived neurons (~E3.5, HH19-20). After immunohistochemical staining for Tubb3 (marking placode cell-derived neurons), the contralateral control trigeminal ganglion possesses distinct ophthalmic, maxillary, and mandibular branches (Figure 29A, arrowhead, arrows, respectively). After Elp1 knockdown in trigeminal placode cells (Figure 29B), the area encompassing the trigeminal ganglion remains significantly reduced (Figure 29C, $p = 0.0425$). Furthermore, evaluation of the forming maxillary and mandibular branches reveals a dispersal of axonal projections (Figure 29B, arrows). However, analysis of the widths for each branch revealed no significant changes (data not shown).

Further examination of the ophthalmic branch innervation of the eye shows normal axonal branching/projections targeting the contralateral control eye (Figure 30A). Innervation of the Elp1 MO-treated side eye, however, is abnormal, with aberrant axonal branching/projections (Figure 30B). Quantification of this region (i.e., area occupied by ophthalmic axons) reveals a statistically significant reduction in the innervation of the eye after Elp1 knockdown (Figure 30C, blue, $p = 0.004$) compared to the contralateral control side (Figure 30C, green).

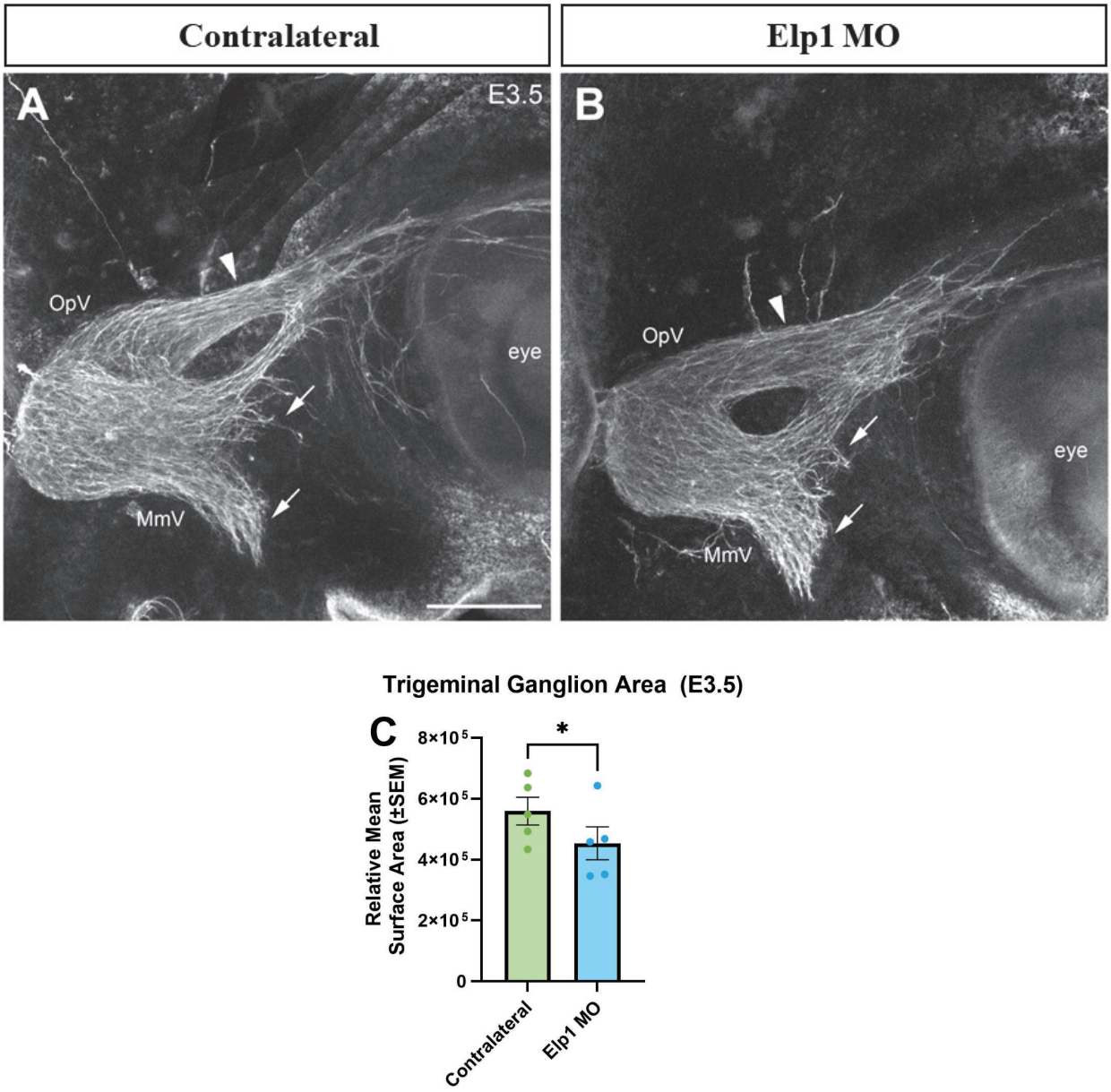

Figure 29: Elp1 depletion reduces the area of the trigeminal ganglion at later developmental stages. Representative max intensity projections of confocal Z-stacks showing the contralateral control (A) or Elp1 MO-treated (B) trigeminal ganglion at E3.5 (HH19-20) after Tubb3 whole-mount immunohistochemistry (white). Arrowheads point to defasciculated and/or dispersed ophthalmic branch axons, while arrows show dispersion of maxillomandibular branch axons. Scale bar in (A) is 250µm and applies to (B). (C) Quantification of the area of contralateral (green, n = 7) and Elp1 MO-treated (blue, n = 5) trigeminal ganglia demonstrating statistical significance (p = 0.0425, paired t-test). Abbreviations: OpV = ophthalmic lobe; MmV = maxillomandibular lobe.

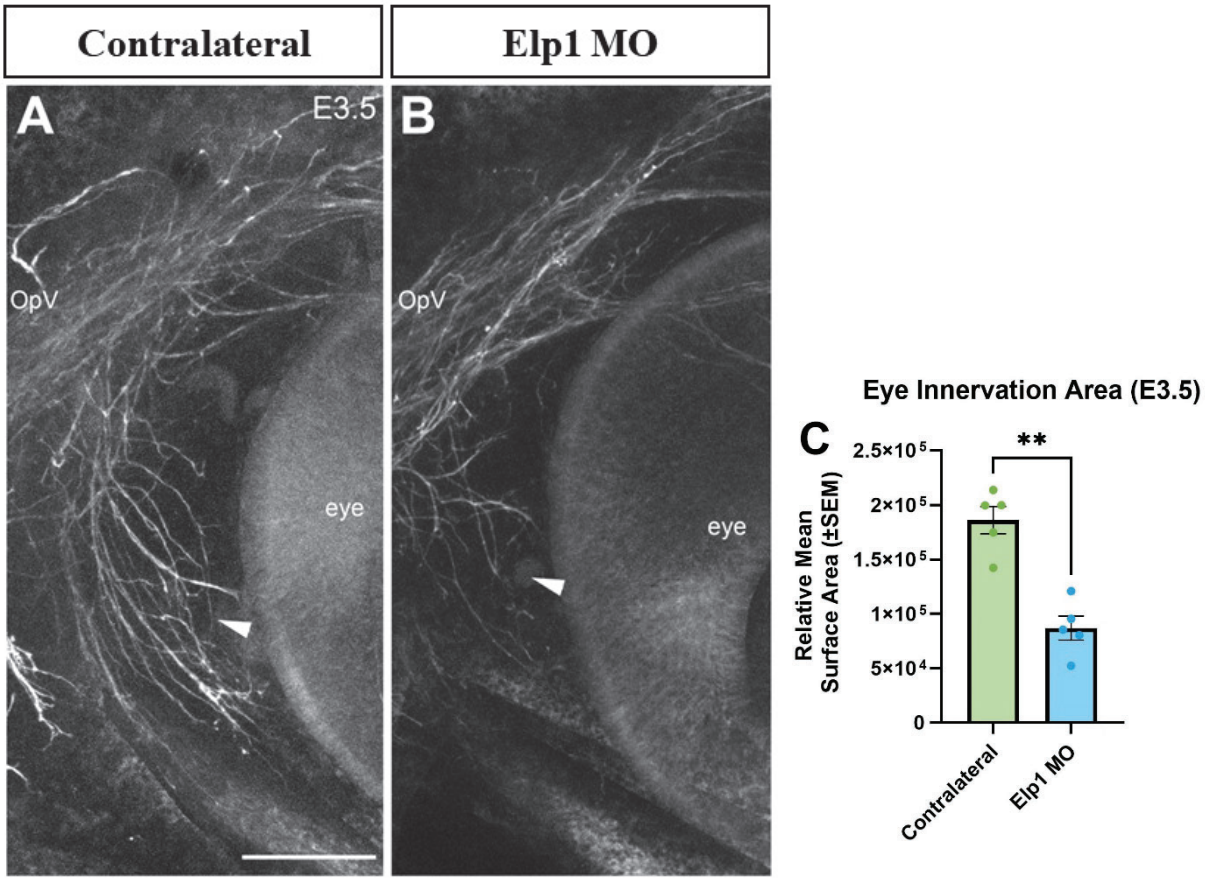

Figure 30: Reduction of eye innervation is observed after Elp1 knockdown. Representative max intensity projections of confocal Z-stacks showing the contralateral control (A) or Elp1 MO-treated (B) trigeminal ganglion at E3.5 (HH19-20) after Tubb3 whole-mount immunohistochemistry (white) with a focus on the innervation of the eye by the ophthalmic branch. Arrowheads point to axonal projections innervating the eye. Scale bar in (A) is 300µm and applies to (B). (C) Quantification of the area of contralateral (green, n = 5) and Elp1 MO-treated (blue, n = 5) ophthalmic innervation of the eye demonstrating statistical significance (p = 0.004, paired t-test). Abbreviations: OpV = ophthalmic lobe.

6.2.3 Deficits in ophthalmic branch innervation persist even after neural crest cell-derived neurons form and contribute to the trigeminal ganglion.

To determine the impact on trigeminal ganglion development at a timepoint when neural crest cells begin contributing to the trigeminal sensory neuron population, Tubb3 whole-mount immunohistochemistry was conducted at E4 (HH24) followed by examination of the medial

nasal branch of the ophthalmic lobe, which is responsible for innervation of the future nose (or beak). Innervation of the contralateral control side (Figure 31A) in comparison to the Elp1 MO-treated side (Figure 31B) reveals continued disorganization of ophthalmic branch projections, with potential changes in axon bundling.

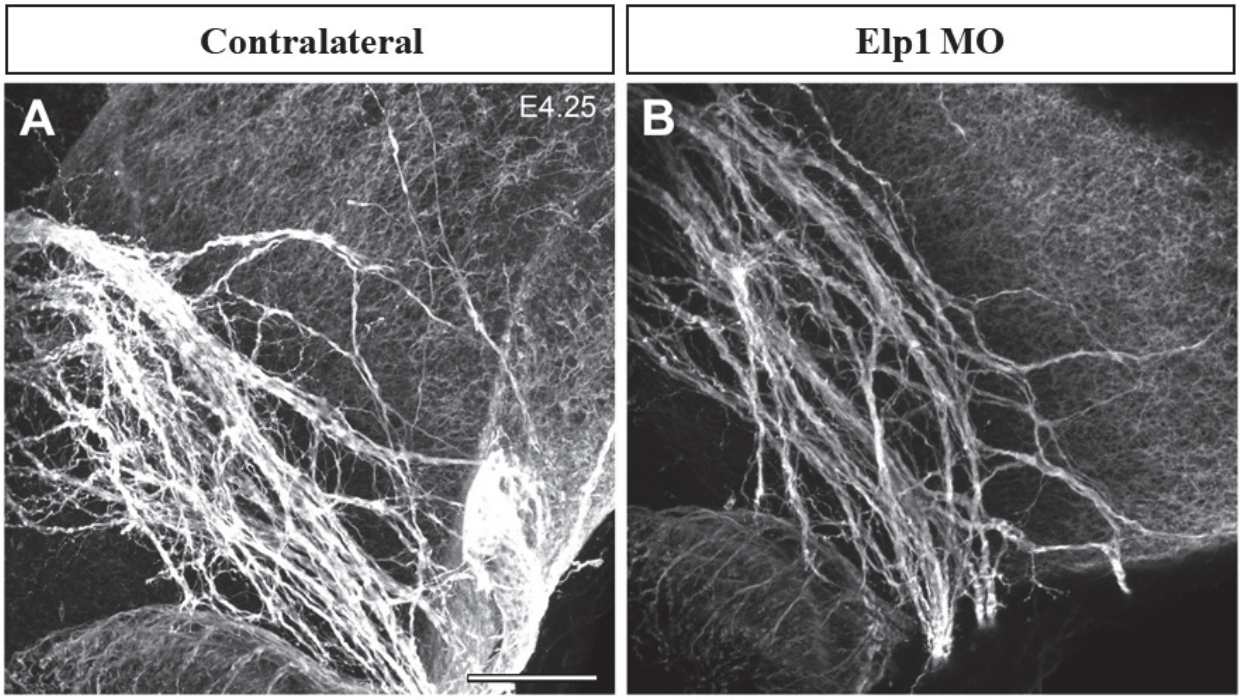

Figure 31: Elp1 knockdown in trigeminal placode cells leads to deficits in the organization of the ophthalmic branch medial nasal nerve. Representative max intensity projections of confocal Z-stacks showing the contralateral control (A) or Elp1 MO-treated (B) ophthalmic branch medial nasal nerve at E4 (HH24) after Tubb3 whole-mount immunohistochemistry (white, n = 2). Scale bar in (A) is 200µm and applies to (B).

6.2.4 Elp1 knockdown in trigeminal placode leads to disorganization of placodal neurons.

To better discern potential changes at the cellular level after Elp1 knockdown, section immunohistochemistry was performed to identify condensing placodal neurons and undifferentiated neural crest cells. At early stages of development (E2.5, HH15-17), the contralateral control trigeminal ganglion shows normal condensation of neural crest cells and

placode cell-derived neurons (Figure 32A-D). Neural crest cells immunoreactive for Sox10 (Figure 32A,C, arrowheads) and placode cell-derived neurons labeled with Tubb3 (Figure 32A,D, arrows) exhibit typical organization, with neural crest cells surrounding placodal neurons (Figure 32A,C,D, arrows and arrowheads, respectively). Evaluation of the Elp1 MO-treated trigeminal ganglion (Figure 32E-H), however, uncovers a change in the arrangement of neural crest cells and placodal neurons after Elp1 knockdown. Condensation of placode cell-derived neurons is negatively impacted, with disbursement of Tubb3 immunoreactive cells observed (Figure 32E,H, arrows). Additionally, axon projections appear disrupted, with some being absent, and those present are disorganized and/or potentially misguided. Furthermore, Sox10-positive neural crest cells appear less condensed (Figure 32E,G, arrowheads).

Within the maxillomandibular lobe of the trigeminal ganglion at a similar stage (Figure 33A,E), the contralateral control side possesses the normal distribution of Sox10-positive neural crest cells (Figure 33A,C, arrowheads) and Tubb3-positive placode cell-derived neurons, with little Tubb3 expression in the ectoderm (Figure 33A,D, arrows). After Elp1 knockdown, however, disorganization and dispersal of neural crest cells and placode cell-derived neurons are also observed (Figure 33E,G,H, arrowheads and arrows, respectively). Moreover, an accumulation of Tubb3-positive cells in the MO-positive ectoderm is also noted, unlike that observed on the contralateral side (Figure 33E,H, asterisk) and with Control MO-treated embryos (not shown).

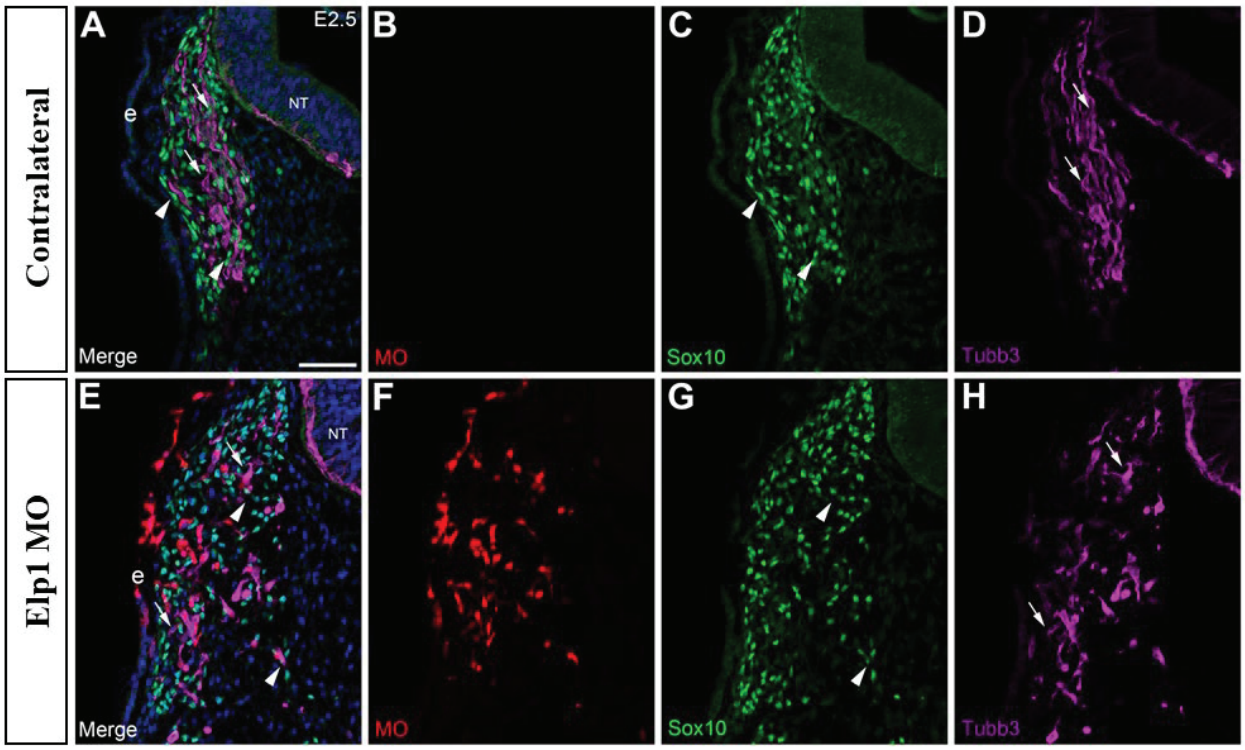

Figure 32: Elp1 knockdown increases cell dispersal within the trigeminal ganglion. Representative transverse section through the forming ophthalmic lobe of the trigeminal ganglion of an Elp1 MO-treated embryo at E2.5 (HH16), with the contralateral control and Elp1 MO-treated sides shown in (A-D) and (E-H), respectively. Immunohistochemistry for Sox10 (C,G, green, labels neural crest cells) and Tubb3 (D,H, purple, labels placode cell-derived neurons) was conducted on tissue sections. MO-positive cells are visualized by the lissamine tag on the MO, which fluoresces red (F; none in B), with corresponding merged images of all channels with DAPI (A,E, blue, marks all nuclei). Arrows point to Tubb3-positive neurons (A,D,E,H), while arrowheads denote Sox10-positive neural crest cells (A,C,E,G). Scale bar in (A) is 50μm and applies to all images. Abbreviations: NT = neural tube; e = ectoderm.

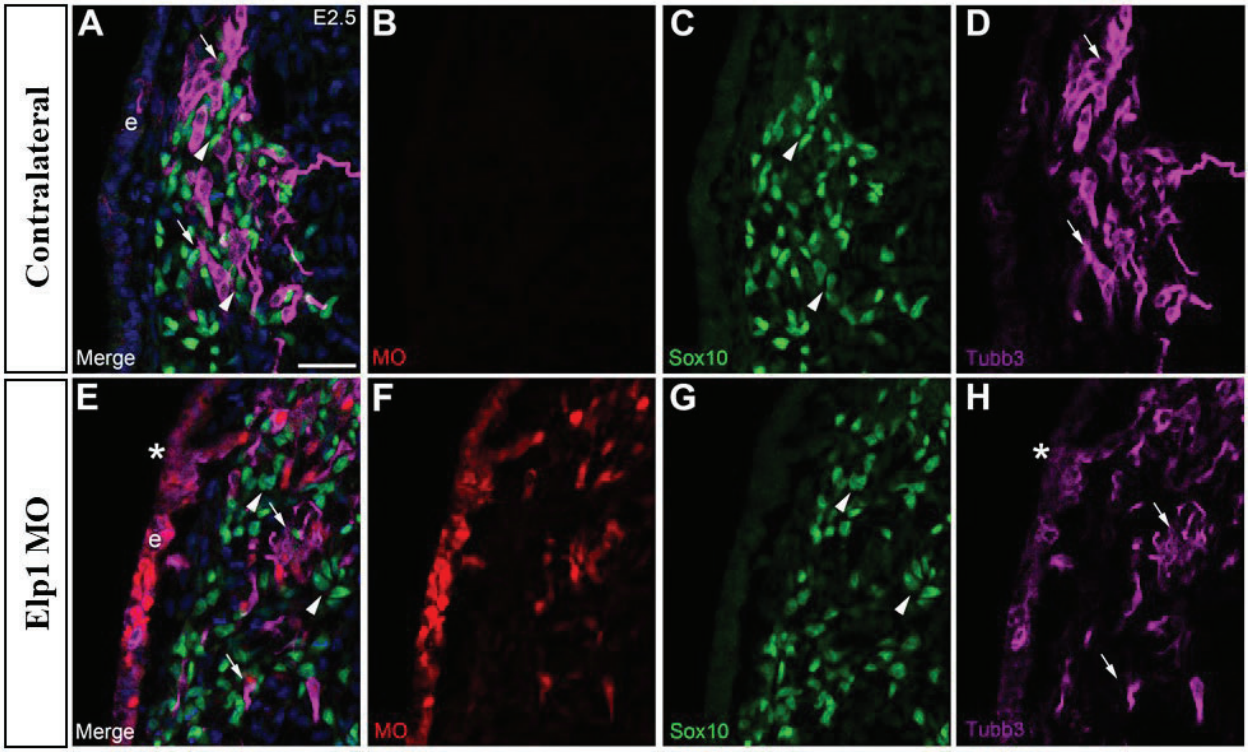

Figure 33: Increased Tubb3 immunoreactivity is observed in the Elp1 MO-positive maxillomandibular placode ectoderm. Representative transverse section through the forming maxillomandibular lobe of the trigeminal ganglion of an Elp1 MO-treated embryo at E2.5 (HH16), with the contralateral control and Elp1 MO-treated sides shown in (A-D) and (E-H), respectively. Immunohistochemistry for Sox10 (C,G, green, labels neural crest cells) and Tubb3 (D,H, purple, labels placode cell-derived neurons) was performed on tissue sections. MO-positive cells are visualized by the lissamine tag on the MO, which fluoresces red (F; none in B), with corresponding merged images of all channels with DAPI (A,E, blue, marks all nuclei). Arrows point to Tubb3 positive neurons (A,D,E,H), while arrowheads denote Sox10-positive neural crest cells (A,C,E,G). Asterisk indicates Tubb3 expression in MO-positive ectoderm (E,H). Scale bar in (A) is 100µm and applies to all images. Abbreviations: e = ectoderm.

6.2.5 Deficits in the trigeminal ganglion body size and neuronal projections are apparent at later developmental timepoints after Elp1 knockdown.

Later in trigeminal ganglion development (E3.5, HH19-20), neural crest cells and placode cell-derived neurons are tightly condensed, and placode cell-derived neurons are extending axons to target tissues. When examining the ophthalmic lobe in cross-section, the contralateral control side trigeminal ganglion is highly condensed and organized (Figure 34A). Here, Sox10 labels neural crest cells (Figure 34A,C) and Tubb3 marks placode cell-derived neurons (Figure 34A,D). In contrast, the Elp1 MO-treated trigeminal ganglion appears smaller in size (Figure 34E). However, overall organization of neural crest cells (Figure 34E,G) and placode cell-derived neurons (Figure 34E,H) appears unchanged at this later stage. Interestingly, a thickening of the MO-positive ectoderm is often observed on the electroporated side (Figure 34E,F, asterisk).

At this same timepoint, the ophthalmic projections are easily distinguishable in cross-sections through the trigeminal ganglion (Figure 35A,E). The projections from the contralateral control side trigeminal ganglion exhibit well-organized Tubb3-positive axons (Figure 35A,D, arrows), with Sox10-positive neural crest cells lining the axons, as expected (Figure 35A,C, arrowheads). After Elp1 knockdown (Figure 35E-H), axon projections identified by Tubb3 immunoreactivity (Figure 35E,H, arrows) are abnormal, with a large degree of disorganization. Moreover, the organization of Sox10-positive neural crest cells along the neuronal projections is also disrupted, with many neural crest cells appearing dispersed (Figure 35E,G, arrowheads). Qualitatively, there is an apparent reduction in neural crest cell number compared to the contralateral control side.

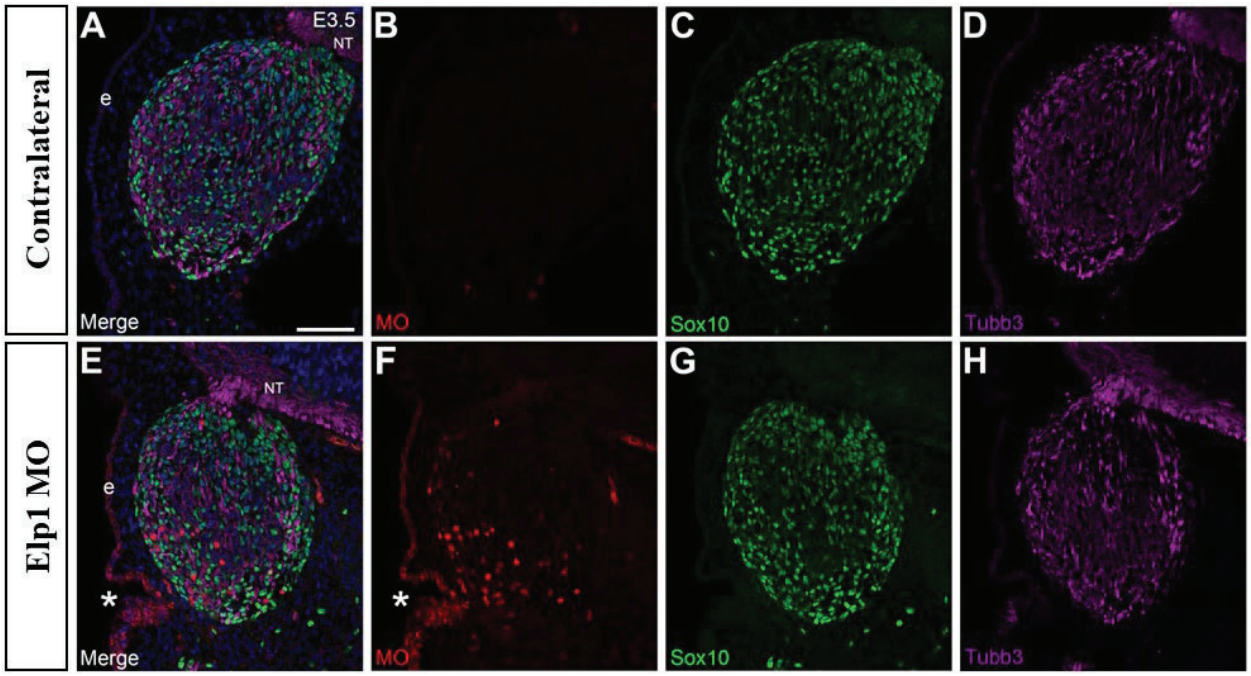

Figure 34: A smaller ophthalmic lobe and thickening of the electroporated ectoderm are observed after Elp1 knockdown. Representative transverse section through the forming ophthalmic lobe of the trigeminal ganglion of an Elp1 MO-treated embryo at E3.5 (HH20), with the contralateral control and Elp1 MO-treated sides shown in (A-D) and (E-H), respectively. Immunohistochemistry for Sox10 (C,G, green, labels neural crest cells) and Tubb3 (D,H, purple, labels placode cell-derived neurons) was carried out on tissue sections. MO-positive cells are visualized by the lissamine tag on the MO, which fluoresces red (F; none in B), with corresponding merged images of all channels with DAPI (A,E, blue, marks all nuclei). Asterisk denotes thickening of MO-positive ectoderm (E,F). Scale bar in (A) is 50μm and applies to all images. Abbreviations: e = ectoderm; NT = neural tube.

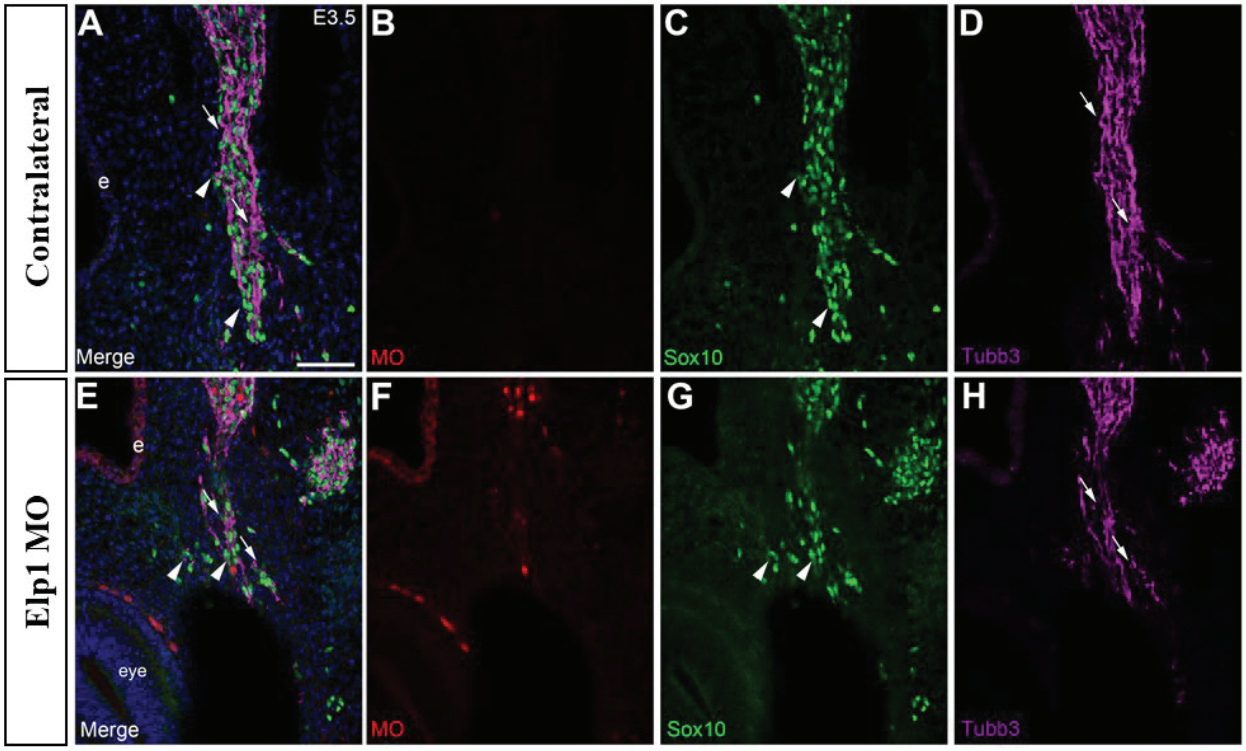

Figure 35: Abnormal outgrowth of neuronal projections and disorganization of neural crest cells is noted after Elp1 knockdown. Representative transverse section through the forming ophthalmic branch of the trigeminal ganglion of an Elp1 MO-treated embryo at E3.5 (HH20), with the contralateral control and Elp1 MO-treated sides shown in (A-D) and (E-H), respectively. Immunohistochemistry for Sox10 (C,G, green, labels neural crest cells) and Tubb3 (D,H, purple, labels placode cell-derived neurons). MO-positive cells are visualized by the lissamine tag on the MO, which fluoresces red (F; none in B), with corresponding merged images of all channels with DAPI (A,E, blue, marks all nuclei). Arrows point to Tubb3-positive neurons (A,D,E,H), while arrowheads denote Sox10-positive neural crest cells (A,C,E,G). Scale bar in (A) is 50μm and applies to all images. Abbreviations: e = ectoderm.

6.3 Conclusions

These studies investigated the effect of reducing Elp1 in trigeminal placode cells on the subsequent development of the trigeminal ganglion in the chick embryo. During the initial formation of the trigeminal ganglion at E2.5 (HH15-17), a reduction in the area occupied by the trigeminal ganglion is observed after Elp1 knockdown. Examination of sections through the trigeminal ganglion at this stage was carried out to provide a cellular explanation for this decrease. These experiments revealed that placode cells may be remaining in the ectoderm, given the increase in ectodermal Tubb3 immunoreactivity seen at this stage, but later undergoing cell death and preventing them from contributing to the trigeminal ganglion. Additionally, both placode cell-derived neurons and neural crest cells appear more spread out, with decreased cellular condensation observed, suggesting the reciprocal interactions between these two populations have been abrogated. This non-cell autonomous effect has been previously observed after knockdown of gene expression in one trigeminal ganglion precursor cell type, leading to defects associated with the other precursor cell type (Shiau & Bronner-Fraser, 2009; Wu & Taneyhill, 2019; Wu et al., 2014).

A day later in development (E3.5, HH19-20), the decrease in area occupied by the trigeminal ganglion persists. Analysis of the area occupied by ophthalmic branches innervating the eye reveals a statistically significant reduction, thus contributing to the overall decrease observed across the entire trigeminal ganglion. Abnormal outgrowth visualized in section further supports defects in axonal development. A thickening of the MO-positive ectoderm was also noted and may be caused by placode cells failing to delaminate properly, a phenomenon that is not a result of the electroporation technique as it is not observed with the use of a Control MO (not shown). However, the presence of MO-positive cells in the trigeminal ganglion anlage

shows that at least a portion of the placode cells delaminate correctly and arrive at their proper destination.

A study in the mouse using a conditional knockout approach in which *Elp1* is deleted from neural crest cells showed that initial formation of the trigeminal ganglion occurred normally (Leonard et al., 2022). Interestingly, our data reveal that knockdown of Elp1 in chick trigeminal placode cells disrupts initial trigeminal ganglion formation. Subsequent development in the mouse showed disorganization and straying of axons with defects in axonal pathfinding and target innervation, also noted in our data.

Additionally, previous studies have evaluated Elp1 function in the context of neural crest cell-derived trunk sensory ganglia in the chick embryo. One group noted a reduction in size of the dorsal root ganglia, with an increase in axon branching from cell bodies (Hunnicutt et al., 2012). This group reported neural crest cells undergo proper induction, delamination, and migration; however, premature neuronal differentiation and neuronal cell death was observed (Hunnicutt et al., 2012). A second group observed increased branching of dorsal root ganglia neurons with misguided axons and aberrant branching seen after Elp1 knockdown (Abashidze et al., 2014). Our findings complement these studies in that placode cells also appear to migrate to the correct location and differentiate into neurons. Moreover, misguided axons with aberrant branching are observed, especially at E2.5 (HH15-17) and in the maxillomandibular branch at E3.5 (HH19-20). Lastly, the changes in size of the trigeminal ganglion we noted may be due to increased neuronal cell death, as this has been reported to contribute to changes seen in trunk sensory nerves after Elp1 knockdown in neural crest cells in the chick embryo (Hunnicutt et al., 2012). Overall, these data provide new and important insights into Elp1 function in the proper

development of not only placode cell-derived neurons, but also the trigeminal ganglion as a whole.

Chapter 7: Future Directions

7.1 Summary

Reciprocal interactions between neural crest cells and trigeminal placode cells are required to form the trigeminal ganglion (D'Amico-Martel & Noden, 1983; Hamburger, 1961; Lwigale, 2001; Shiau & Bronner-Fraser, 2009), which is involved in the perception of many sensations in the head and face, including pain, touch, and temperature (Koontz et al.,2023). While this dual cellular origin of the trigeminal ganglion has been known for decades, the molecules mediating this process remain obscure. The goal of this research was to identify molecules in placode cells contributing to trigeminal ganglion development and elucidate their functions. Using an unbiased RNAsequencing approach carried out at developmental timepoints when only placode cell-derived neurons are present, *Neurog2*, *NeuroD1*, and *Elp1* were identified as potential candidates for trigeminal ganglion development. While Neurog2 and NeuroD1 expression had been evaluated previously (Abu-Elmagd et al., 2001; Xu et al., 2008), Elp1 expression in the chick trigeminal ganglion remained uncharacterized. Moreover, the function of these three proteins in the context of trigeminal placode cells and their neuronal derivatives was not known. To address this, we performed MO-based knockdown experiments in chick trigeminal placode cells and uncovered unique roles for Neurog2, NeuroD1, and Elp1 during chick trigeminal neurogenesis. Our results provide important insight into the function of these critical proteins in chick placode cell-derived neurons during trigeminal ganglion development. This chapter discusses future studies to build on the current work highlighted previously in this dissertation.

7.2 Neurog2 and NeuroD1: Function in trigeminal placode cells

Neurog2 and *NeuroD1* are proneural genes encoding bHLH transcription factors that play an important role in vertebrate neurogenesis. Our work is the first to study their function in the trigeminal ganglion (Bina et al., 2023). Initial experiments were conducted in the chick embryo using Neurog2 or NeuroD1 MOs electroporated into chick trigeminal placode cells followed by immunoblotting to validate knockdown of these proteins in the chick trigeminal ganglion (Chapter 3, Figures 9 and 12, respectively). After confirmation of MO-mediated knockdown, studies investigating the impact of reduced protein levels in trigeminal placode cells were performed. Neurog2 knockdown revealed a smaller trigeminal ganglion, including a decrease in the width of the ophthalmic branch (Chapter 3, Figure 10). While NeuroD1 knockdown also exhibited a reduction in the size of the trigeminal ganglion (Chapter 3, Figures 13 and 14), an increase in the width of the ophthalmic branch was observed (Figure 14). In both cases, the ophthalmic branch innervation around the eye was reduced. These studies provide evidence for the importance of these proteins in trigeminal ganglion formation, revealing both are critical for normal development.

Further characterization of these phenotypic changes will yield insightful information into understanding the developmental processes with which these proteins are associated. Measurements of the whole trigeminal ganglion area must be performed to provide quantitative evidence for the observed qualitative decrease in area noted. Additionally, conducting immunohistochemistry using a nuclear neuronal marker will provide a way to count the number of neurons present to determine if the reduced size is due to a reduction in cell numbers. Next, obtaining cross sections through the trigeminal ganglion will offer insight into changes occurring at the cellular level. Performing immunohistochemistry with markers for neurons and

neural crest cells will help visualize potential phenotypic changes in morphology, intermixing, and condensation of both cell populations. Due to the reciprocal interactions that occur between neural crest cells and placode cells in the formation of the trigeminal ganglion, neural crest cells must also be examined to see if there are non-cell autonomous effects occurring due to disruptions in trigeminal placode cells. Additionally, while Neurog2 knockdown did not show evidence of increased cell death, this has yet to be investigated after NeuroD1 knockdown. Thus, TUNEL staining can be carried out on sections of trigeminal ganglion tissue after NeuroD1 knockdown.

Culturing neurons *in vitro* provides increased resolution with which to visualize individual cells, providing an exceptional method to ascertain subcellular localization of proteins. With this approach, cells are further dispersed than in the condensed trigeminal ganglion, thus allowing for easier visualization of specific locations within a cell. This also allows better characterization of morphological changes such as neurite formation and axon branching, which would be useful in further evaluating phenotypes.

Based on the phenotypic data, defects in axonal outgrowth could be attributed to deficits associated with neurotrophic signaling, cytoskeletal regulation, or other mechanisms. To help identify affected pathways that align with the phenotypes observed after Neurog2 or NeuroD1 knockdown in trigeminal placode cells, ‘omics techniques such as RNAsequencing and mass spectrometry can be employed. This would provide an unbiased method to identify global changes occurring upon depletion of these proteins.

Additional developmental timepoints after Neurog2 or NeuroD1 knockdown must also be characterized as we have only looked at a narrow window of development. Subsequent

timepoints will provide additional information as the trigeminal ganglion becomes more complex with the addition of neural crest cells contributing to the neuronal population.

Lastly, prior research suggests that NeuroD1 is activated downstream of Neurog2 (Abu-Elmagd et al., 2001). To investigate the relationship between Neurog2 and NeuroD1, performing qPCR after Neurog2 knockdown to quantify *NeuroD1* transcript levels will help determine if *NeuroD1* transcripts are altered resulting from Neurog2 knockdown. If qPCR reveals changes in *NeuroD1*, co-electroporation of the Neurog2 MO and a NeuroD1 expression construct can be performed to attempt rescue of phenotypes.

7.3 Elp1: Spatiotemporal expression pattern

Since Elp1 expression had yet to be investigated in the chick trigeminal ganglion, immunohistochemical experiments were first conducted in the trigeminal ganglion and its precursor populations, as discussed in Chapter 4. Results revealed a punctate cellular distribution of Elp1 throughout the timepoints characterized (E1.5-3.5, HH11-20). Elp1 was observed in migrating neural crest cells and presumptive placodal cells in the surface ectoderm, with expression in the latter found more apically at E1.5 (HH11/12) (Chapter 4, Figure 16). During the formation of the trigeminal ganglion from E2-E3.5 (HH13-20), Elp1 cytoplasmic expression was noted in neural crest cells and placode cell-derived neurons (Chapter 4, Figures 17, 18, and 19). Co-localization with the nuclear marker DAPI was also seen in the neural crest cell population throughout the developmental window characterized. To better elucidate the subcellular localization of Elp1, immunohistochemistry with additional antibodies for proteins with known cellular localizations can be used to look for co-expression, which will help identify the subcellular location in which Elp1 is observed.

Additionally, beta-galactosidase staining in an *Elp1*^{LacZ} mouse reporter strain (previously explained in Chapter 4) exhibited differences in cellular localization compared to that noted after immunostaining with the Elp1 antibody (Leonard et al., 2022). However, the beta-galactosidase distribution observed in mouse more closely resembles Elp1 protein expression in the chick embryo as demonstrated by immunohistochemistry. Due to the differences in protein distribution seen in mouse vs. chick, performing fluorescence *in situ* hybridization experiments to visualize *Elp1* transcript localization in the chick embryo will be beneficial to investigate if any transcript and protein localization discrepancies are also present in our model. Reasons for these discrepancies could include modifications that occur to Elp1 post-transcriptionally or post-translationally. As explained in Chapter 4 (Figure 21, multiple *Elp1* splice variants have been identified, with changes among them occurring near the carboxy terminus of the predicted protein products where the commercially available antibodies recognize. Therefore, it is possible that the antibody used may not recognize all forms of chick Elp1.

The immunoblotting results also support the possibility of post-transcriptional and/or post-translational modifications to Elp1. The predicted size of protein products from all the *Elp1* transcripts is ~140 kDa; however, multiple bands at different molecular weights are observed (Chapter 4, Figure 20. The presence of doublets on the blots could be due to changes such as acetylation, phosphorylation, methylation, or glycosylation, as these modifications often cause small shifts in molecular weights observed by immunoblotting. Multiple bands at different molecular weights could also suggest potential proteolytic processing. Therefore, blocking proteolysis, treating samples with enzymes to disrupt modifications like phosphorylation and glycosylation, or enrichment assays for acetylation and methylation to look for post-translational modifications will prove useful moving forward since these changes have not been examined in

the context of Elp1 expression in the trigeminal ganglion. To determine if Elp1 proteolysis is occurring, regions of the SDS-PAGE gel corresponding to the molecular weight of each band could be cut out and mass spectrometry performed to identify the protein sequences of each band. Conversely, an HA-tagged Elp1 could be expressed in the embryo followed by immunoblotting with an antibody to HA. If multiple bands are detected after probing the immunoblot for an antibody specific for HA, this would further support the notion that Elp1 is undergoing proteolytic processing.

7.4 Elp1: Knockdown approach

Our experiments outlined in Chapter 5 validated the MOs to be used to knockdown Elp1 in subsequent experiments. While prior reports investigating Elp1 depletion on the development of chick trunk neural crest derived-dorsal root ganglia used either shRNA or siRNA to knockdown Elp1 (Abashidze et al., 2014; Hunnicutt et al., 2012), we were not able to successfully achieve Elp1 knockdown using the published (and other) shRNAs (see Appendix). No change in *Elp1* transcript or protein levels were noted by qPCR or immunoblotting, respectively, when electroporated trigeminal ganglion tissue was examined. Some reasons for this lack of knockdown could include poor electroporation efficiency, dilution of the vector over time, or Elp1 expression in surrounding cells that were not subject to knockdown but inadvertently included in the dissection.

To obtain greater, sustained knockdown, revisiting the shRNA experiments with a vector like PiggyBac may be of value (Hunnicutt et al., 2012; Lu et al., 2009). Due to its genome incorporating ability, the shRNA continues to be made and persists through development, while MOs are stable for approximately 5-7 days but are eventually packaged into endosomes and degraded, leading to loss of knockdown (GeneTools, LLC). Having persistent knockdown will

allow for the study of later stages in trigeminal ganglion development that is not possible with MOs. Since our first attempts made with shRNA constructs, a finer dissection method (Chapter 5, Figure 25 has now been employed to evaluate Elp1 knockdown in the trigeminal ganglion only, thereby reducing the contribution of Elp1 from surrounding cells. Refinement of dissection techniques coupled with electroporation of a PiggyBac shRNA- or siRNA-based vector may now prove adequate to achieve Elp1 knockdown.

7.5 Elp1: Function in trigeminal placode cells

Using the Elp1 MOs previously validated in Chapter 5, knockdown experiments in trigeminal placode cells were performed to investigate Elp1 function in the placode cell population during trigeminal ganglion development. Analyses after Elp1 knockdown revealed a reduction in the area occupied by the trigeminal ganglion at the timepoints observed (E2.5 (HH15-17) and E3.5 (HH19-20)) (Chapter 5, Figures 27 and 29, respectively). Early trigeminal ganglion development (E2.5, HH15-17) showed decreased condensation of placode cell-derived neurons and neural crest cells and an increase in Tubb3 staining within the ectoderm (Chapter 5, Figure 32 and 33). The next developmental timepoint (E3.5, HH19-20) uncovered a reduced innervation area of the eye along with a decrease in axon projections (Chapter 5, Figures 30 and 35). These results indicate depleting Elp1 in the trigeminal placode cell population disrupts proper trigeminal ganglion development.

Additional investigation of trigeminal ganglion developmental changes after Elp1 reduction is needed to further elucidate the function of this protein. To verify if changes in area are due to decreased cell number, counting neurons on sections after immunohistochemistry using an antibody that recognizes a nuclear neuronal marker such as Six1 or Islet1 can be performed as well as TUNEL staining to look for any increase in cell death. Given the changes

observed in neural crest cells, the number of Sox10-positive neural crest cells must also be counted to explore this cell population. Previous studies investigating Elp1 in trunk neural crest-derived sensory nerves showed increased cell death, leading to our hypothesis that an increase in TUNEL and a decrease in neuronal number would be observed in the trigeminal ganglion (Abashidze et al., 2014; George et al., 2013; Hunnicutt et al., 2012; Leonard et al., 2022). Additionally, TUNEL staining can also be used to help identify if the thickened MO-positive ectodermal cells eventually undergo apoptosis.

The deficits seen in neuron projections upon Elp1 knockdown suggest defects in axon pathfinding and guidance. Neurotrophic receptors such as Tropomyosin receptor kinases (Trks) are important for stimulation of intracellular signaling cascades associated with growth and survival of neuron populations. Elp1 is reported to modulate TrkA/NGF retrograde signaling by regulating the phosphorylation of TrkA receptors in signaling endosomes (Li et al., 2020). One hypothesis is that neurons cannot receive NGF signal (i.e., insufficient TrkA is present to bind NGF), leading to their death. However, findings support defects prior to NGF binding, suggesting additional explanations for the phenotypes seen.

The Wnt1-Cre Elp1 CKO mouse model previously described was used to evaluate the expression of TrkA, B, and C. TrkA immunoreactivity was drastically reduced in the Elp1 CKO compared to the control and a 23% reduction in TrkA neuron numbers was also noted, with no changes seen in TrkB or TrkC (Leonard et al., 2022), consistent with studies in dorsal root ganglia (George et al., 2013). TrkB and TrkC neurons are reportedly born before the TrkA population (Huang et al., 1999a; Huang et al., 1999b) just as the placode cell-derived neurons are born before neural crest cell-derived neurons in the trigeminal ganglion (Méndez-Maldonado et al., 2020). This possible correlation between cellular origin and Trk expression was investigated

in the mouse trigeminal ganglion, revealing that ~75% of the TrkA population are neural crest cell-derived, while ~78% of the TrkB and TrkC neurons are placode cell-derived (Leonard et al., 2022). If this relationship is conserved, it is likely TrkB and/or TrkC neurons will be affected when Elp1 is knocked down in chick trigeminal placode cells. To investigate this, immunohistochemistry on MO-treated tissue using antibodies for TrkA, B, and C can be performed. Both fluorescent intensity and cell numbers for each Trk population can be measured in comparison to the contralateral control trigeminal ganglion to detect potential changes.

Compared to data in the Elp1 CKO, our results show disruption to trigeminal ganglion development at earlier stages. While some differences could be due to species variability, it is likely that many are due to the disruption of placode cell-derived neurons instead of neural crest cells. Noting earlier phenotypic changes is logical because perturbations are occurring to the first population of trigeminal sensory neurons that are present, given that neural crest cells differentiate into neurons later than placode cells (Méndez-Maldonado et al., 2020).

Additionally, data from the Elp1 CKO show the frontal nerve initially extends branching around the eye (but less than control) followed by a retraction of those neurons (Leonard et al., 2022). This demonstrates that at least some neurons can reach their destination initially. Conversely, the medial and lateral nasal nerves fail to form in the mouse. Whereas in our data, innervation, albeit reduced, is observed by all these nerves. The unique phenotypes among branches and between the two cell types investigated suggest a potential difference of the origin of these neuronal derivatives in formation of the different trigeminal ganglion branches. Moreover, previous studies have reported that increases or decreases in axon/neurite branching after Elp1 knockdown vary depending upon context (Abashidze et al., 2014; Hunnicutt et al., 2012; Jackson et al., 2014; Ohlen et al., 2017), which could be due to timepoints examined or the

identity and environment of specific neurons. Later developmental stages comparable to these mouse studies will be beneficial to investigate. Such timepoints would provide additional similarities and differences that will help distinguish potential context-dependent differences of Elp1 function between neural crest and placode cell derivatives of the trigeminal ganglion.

In the chick, gene expression in both neural crest and placode cells contributing to the trigeminal ganglion can be altered using a technique referred to as sequential electroporation in which neural crest cells are electroporated first, followed by placode cells. This is possible due to the anatomy of the chick embryo and the distinct location of neural crest cells (dorsal neural tube) and placode cells (surface ectoderm). Using the shRNA-based approach previously described coupled with different fluorescent reporters will permit distinct labeling of each cell population, allowing us to identify the cellular origin of affected neurons after Elp1 depletion. Knockdown of Elp1 in both neural crest and placode cells destined to form trigeminal ganglion neurons is also closer to recapitulating FD, as the method is inherently mosaic, so there is still some Elp1 expression but both populations of neurons are affected. This allows us to look at Elp1 in all neurons to help determine function and without the other cell type potentially compensating for the deficits of the other. Notably, the use of the chick embryo is better suited for studying FD given the manner in which Elp1 can be perturbed, as described above, compared to any type of conditional knockout mouse in which Elp1 is completely lost in specific cell types.

Additional mechanisms and pathways that may be altered upon Elp1 reduction and are consistent with our results, such as cytoskeletal regulation and cell adhesion, have been previously reported (Abashidze et al., 2014; Goffena et al., 2018; Johansen et al., 2008). Based on our data, defects in axonal outgrowth could arise from issues in cytoskeletal regulation, and the distribution of neural crest cells and placode cell-derived neurons within the trigeminal

ganglion could be disrupted due to defects in cell adhesion. As previously described in Section 7.2, 'omics techniques will aid in elucidating mechanisms and pathways altered after Elp1 knockdown. Proteomics of Elp1 CKO dorsal root ganglia revealed changes associated with axon guidance/pathfinding as well as adhesion molecules (Goffena et al., 2018). Investigating impacted pathways will be very helpful to identify possible mechanisms underlying Elp1 function in the trigeminal ganglion.

7.6 Potential links between Neurog2, NeuroD1, and Elp1

Our Neurog2, NeuroD1, and Elp1 investigations demonstrated the importance of each protein in trigeminal ganglion development. While phenotypic changes observed after knockdown of each protein are not identical, in all three cases, eye innervation deficits and dispersal of neurons are observed (Chapter 3, Figures 10, 14; Chapter 6, Figures 28, 30). Axon growth is regulated by guidance molecules, adhesion proteins, and neurotrophic factors (Deinhardt et al., 2011). It is possible that ophthalmic branch axons reach their target tissues normally but are then retracted due to a compromised cytoskeleton or axon projections are not made and/or maintained due to an inability to sense the environment.

The aberrant innervation of the eye that we observe after knockdown could point to the dysregulation of proteins associated with these processes, such as disruptions to neurotrophic receptors and/or neurotrophins. A lack of neurotrophic support leads to target innervation defects and neuronal cell death. This has yet to be studied, however, in association with Neurog2 and NeuroD1, so work in this area is needed.

Additionally, issues with cytoskeletal regulatory proteins causing cytoskeletal dysregulation may lead to aberrant formation of axonal projections observed. Cytoskeletal changes are critical for neurons to make axons and dendrites from initially immature neurites,

with rearrangements of actin filaments and microtubules dynamically occurring in neurites and in growing axons (Dent et al., 2011). Previous studies in mice (Ma et al., 1998) and *Xenopus* (Seo et al., 2007) demonstrated that cytoskeletal regulators are downstream targets of bHLH transcription factors. Thus, it is possible that placodal neuron morphology is affected due to intracellular changes occurring upon depletion of Neurog2 and/or NeuroD1. Among the downstream targets of Neurogs and NeuroD1 that regulate cell polarity and the cytoskeleton are *STMN2* (Ma et al., 1998) and *DBN1* (Seo et al., 2007). Interestingly, Elp1 is known to directly bind to JNK, which regulates microtubule stability in neurons (Abashidze et al., 2014). Elp1 may play a role in JNK-dependent neuronal functions such as microtubule stabilization of MAP1B and microtubule plasticity via phosphorylation of superior cervical ganglion protein (SCG10 aka STMN2) in growth cones (Abashidze et al., 2014). These results suggest, for the first time, a potential link between Elp1 and Neurog2 through STMN2, providing a testable hypothesis as part of future work.

Another possible relationship among Neurog2, NeuroD1, and Elp1 may be occurring through Pax3. In the dorsal root ganglia, Elp1 is required for proliferation and survival of Pax3-positive neural crest cell progenitors. These studies led to the hypothesis that Elp1 plays a role in acetylation of Pax3, either directly as it contains a W40 domain previously reported to acetylate Pax family members, or indirectly through the Elongator complex (George et al., 2013). In the trigeminal ganglion, Pax3 is expressed in ophthalmic trigeminal placode cells, which are the population of cells that also express Neurog2 since Pax3 is a known activator of Neurog2 (Nakazaki et al., 2008). One possibility is that knockdown of Elp1 causes a decrease in Pax3 acetylation, which in turn decreases transcription of *Neurog2* followed by decreased activation of *NeuroD1*. To investigate these associations, evaluating changes in STMN2 and Pax3 transcripts

and protein after Neurog2, NeuroD1, or Elp1 knockdown must be carried out through qPCR and/or immunoblotting.

7.7 Significance

The trigeminal ganglion houses the cell bodies of the trigeminal nerve, which is responsible for detecting pain, touch, and temperature sensations in the head and face (Koontz et al., 2023). This functionally complex structure is also developmentally complex. Unlike other cranial sensory ganglia, both neural crest cells and placode cells contribute to the neuronal population (D'Amico-Martel & Noden, 1983; Steventon et al., 2014). Additionally, it is the largest and first cranial ganglia to begin forming, making it an ideal model for studying the interactions of neural crest cells and placode cells.

Our studies focused on investigating pathways that control differentiation and maturation of placode cells into trigeminal neurons as well as mechanisms underlying cell morphology changes, and subsequent neural crest-placode cell interactions during ganglia assembly, as these processes are not well defined. Characterization of normal development is essential for understanding diseased states and informs the design of therapeutic treatments. Basic science helps us to understand processes that have yet to be investigated as well as offers connections to other developmental mechanisms.

The chick embryo serves as a powerful model organism for scientific research. It possesses developmental similarities to mammals, sharing some morphological, biochemical, and genetic characteristics (Brugmann et al., 2010). A high level of conservation is present in developmental processes, meaning studies in the chick are applicable to the development of other animals, even humans. Additionally, the chick grows relatively quickly, is large, and develops *in ovo* or outside of the mother, allowing for embryonic manipulations followed by continued

growth to desired timepoints. *Elp1* null mice are embryonic lethal (Chen et al., 2009) while *Neurog2* null mice exhibit impaired delamination of neuronal precursors from placodes (Fode et al., 1998). However, there are no trigeminal specific placode markers that can be used to create conditional knockouts for these proteins in mouse. Therefore, the chick is especially useful to study these proteins in trigeminal placode cells due to this limitation, together with the accessibility of this cell population in the ectoderm, thus allowing for molecular perturbation (Chapter 5, Figure 25).

The studies in this dissertation utilized the chick embryo to provide initial characterization of three novel proteins in trigeminal placode cell neurogenesis. Early trigeminal ganglion assembly was disrupted by knockdown of Neurog2, NeuroD1, or Elp1. Future research will continue to elucidate pathways and potential mechanisms these proteins use during neurogenesis. Taken together, these results reveal Neurog2, NeuroD1, and Elp1 are essential for proper trigeminal ganglion development.

Chapter 8: Appendix: Evaluating methods to knockdown Elp1

8.1 Summary

Successful validation of Elp1 knockdown in the chick required troubleshooting multiple methods to deplete Elp1 from trigeminal placode cells. Initial experiments to assess Elp1 knockdown used 500μm of a translation-blocking Elp1 MO, as recommended by the manufacturer (GeneTools,LLC). Unfortunately, immunoblotting revealed reduction of Elp1 protein was unsuccessful with this concentration. Therefore, additional approaches to permit knockdown were evaluated, as described below.

8.2 Use of shRNA constructs for Elp1 knockdown

We then switched to using shRNA constructs as a previous publication in chick used this method to knockdown Elp1 (Hunnicutt et al., 2012). To this end, we purchased shRNAs (IDT DNA) based on a published sequence (IKP-8 (Elp1 shRNA#2): 5' – AGATCTACGTGTACAGATA – 3') (Hunnicutt et al., 2012), our own design (Elp1 shRNA#1: 5' – CTCAAACAGGCAGTTAATCA – 3'), and a scrambled control (control shRNA: 5' – ACGAACATTATCGGGTAACT – 3'). These were independently cloned into a PiggyBac genome-integration vector (gift from Dr. Frances Lefcort, Montana State University; Lu et al., 2009). Electroporations were performed into trigeminal placode cells using a ratio of 4:1 shRNA to PBase (gift from Dr. Xiaozhong Alec Wang, Northwestern University; Lu et al., 2009). Unfortunately, qPCR and immunoblotting results were inconsistent, and we were unsuccessful in validating changes to Elp1 transcript and protein expression.

8.3 Determination of MO concentration for Elp1 knockdown

After unsuccessful attempts to verify knockdown using shRNA constructs, we returned to MO-mediated knockdown. Different concentrations of our translation-blocking MO and a combination of translation-blocking and splice-blocking MOs were used for ectodermal electroporation (targeting trigeminal placode cells) after which we compared phenotypic changes to trigeminal ganglion development (Figure 36). Whole-mount immunohistochemical staining for Tubb3 was conducted to label placode cell-derived neurons at this stage. In each condition, the contralateral control trigeminal ganglion formed normally, with ophthalmic and maxillomandibular lobes starting to become defined (Figure 36A,C,E, arrowhead, arrow, respectively). Although the combinations resulted in similar phenotypes with disorganization of neurons and a change in size of the ophthalmic branch (Figure 36B,D,F), a greater change in the eye innervation was observed in the presence of a mixture of 1mM translation-blocking and 1 mM splice-blocking MO (Figure 36C,D). This combination was then used for immunoblotting experiments, where successful knockdown of Elp1 protein was observed (Chapter 4, Figure 26).

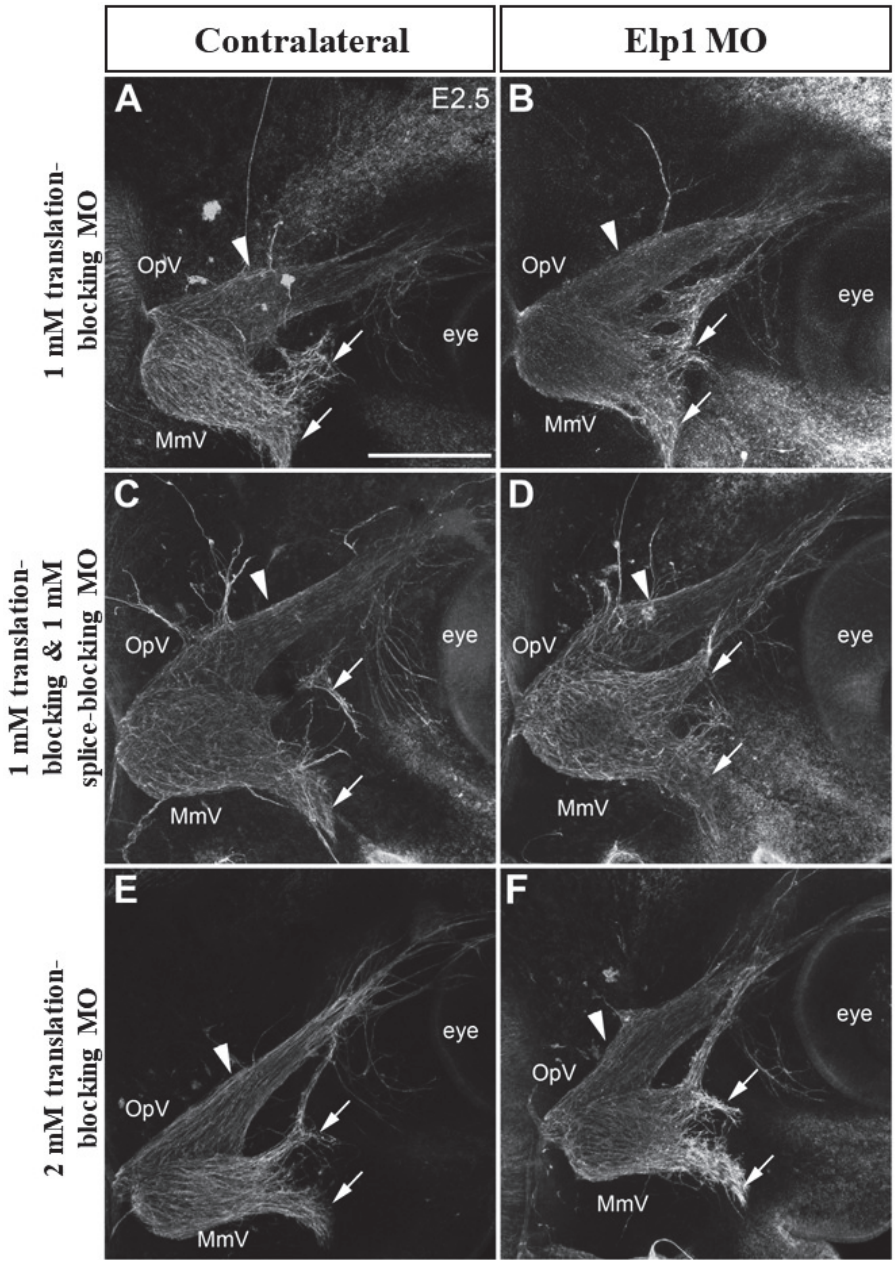

Figure 36: Comparison of trigeminal ganglion phenotypes using different concentrations and combinations of Elp1 MOs. Representative max intensity projections of confocal Z-stacks showing the contralateral control (A,C,E) or Elp1 MO-treated (B,D,F) trigeminal ganglion at E3.5 (HH19-20) after Tubb3 whole-mount immunohistochemistry (white). Arrowheads point to ophthalmic branch axons, while arrows identify maxillomandibular branch axons. Scale bar in (A) is 250μm and applies to (B-F). Abbreviations: OpV = ophthalmic lobe; MmV = maxillomandibular lobe.

Bibliography

Abashidze, A., Gold, V., Anavi, Y., Greenspan, H., & Weil, M. (2014). Involvement of IKAP in Peripheral Target Innervation and in Specific JNK and NGF Signaling in Developing PNS Neurons. *PLoS ONE*, *9*(11), 113428. https://doi.org/10.1371/journal.pone.0113428

Abdel-Fattah, W., Jablonowski, D., Di Santo, R., Thüring, K. L., Scheidt, V., Hammermeister, A., … Stark, M. J. R. (2015). Phosphorylation of Elp1 by Hrr25 Is Required for Elongator-Dependent tRNA Modification in Yeast. *PLOS Genetics*, *11*(1), e1004931. https://doi.org/10.1371/journal.pgen.1004931

Abu-Elmagd, M., Ishii, Y., Cheung, M., Rex, M., Le Rouëdec, D., & Scotting, P. J. (2001). cSox3 expression and neurogenesis in the epibranchial placodes. *Developmental Biology*, *237*(2), 258–269. https://doi.org/10.1006/DBIO.2001.0378

Achilleos, A., & Trainor, P. A. (2012). Neural crest stem cells: discovery, properties and potential for therapy. *Cell Research 2012 22:2*, *22*(2), 288–304. https://doi.org/10.1038/cr.2012.11

Anderson, S. L., Coli, R., Daly, I. W., Kichula, E. A., Rork, M. J., Volpi, S. A., … Rubin, B. Y. (2001). Familial Dysautonomia Is Caused by Mutations of the IKAP Gene. In *Am. J. Hum. Genet* (Vol. 68). Retrieved from https://www.ncbi.nlm.nih.gov/pmc/articles/PMC1274486/pdf/AJHGv68p753.pdf

Axelrod, F. B. (2002). Hereditary sensory and autonomic neuropathies familial dysautonomia and other HSANs. *Clinical Autonomic Research*, *12*(1 SUPPL.), 2–14. https://doi.org/10.1007/s102860200014

Baker, C. V. H., & Bronner-Fraser, M. (2001, April 1). Vertebrate cranial placodes. I. Embryonic induction. *Developmental Biology*, Vol. 232, pp. 1–61. https://doi.org/10.1006/dbio.2001.0156

Baker, C. V. H., Stark, M. R., Marcelle, C., & Bronner-Fraser, M. (1999). Competence, specification and induction of Pax-3 in the trigeminal placode. *Development*, *126*(1), 147–156. https://doi.org/10.1242/dev.126.1.147

Bauer, F., & Hermand, D. (2012). A coordinated codon-dependent regulation of translation by Elongator. *Cell Cycle*, *11*(24), 4524. https://doi.org/10.4161/CC.22689

Begbie, J., Ballivet, M., & Graham, A. (2002). Early steps in the production of sensory neurons by the neurogenic placodes. *Molecular and Cellular Neuroscience*, *21*(3), 502–511. https://doi.org/10.1006/mcne.2002.1197

Betancur, P., Bronner-Fraser, M., & Sauka-Spengler, T. (2010). Genomic code for Sox10 activation reveals a key regulatory enhancer for cranial neural crest. *Proceedings of the National Academy of Sciences of the United States of America*, *107*(8), 3570–3575. https://doi.org/10.1073/pnas.0906596107

Bina, P., Hines, M. A., Sanyal, J., & Taneyhill, L. A. (2023). Neurogenin 2 and Neuronal Differentiation 1 Control Proper Development of the Chick Trigeminal Ganglion and Its Nerve Branches. *Journal of Developmental Biology*, *11*(1). https://doi.org/10.3390/JDB11010008

Breau, M. A., & Schneider-Maunoury, S. (2015). Cranial placodes: Models for exploring the multi-facets of cell adhesion in epithelial rearrangement, collective migration and neuronal movements. *Developmental Biology*, *401*(1), 25–36. https://doi.org/10.1016/j.ydbio.2014.12.012

Bronner, M. E., & LeDouarin, N. M. (2012, June 1). Development and evolution of the neural crest: An overview. *Developmental Biology*, Vol. 366, pp. 2–9. https://doi.org/10.1016/j.ydbio.2011.12.042

Brugmann, S. A., Powder, K. E., Young, N. M., Goodnough, L. H., Hahn, S. M., James, A. W., … Lovett, M. (2010). Comparative gene expression analysis of avian embryonic facial structures reveals new candidates for human craniofacial disorders. *Human Molecular Genetics*, *19*(5), 920–930. https://doi.org/10.1093/HMG/DDP559

Chen, Y.-T., Hims, M. M., Shetty, R. S., Mull, J., Liu, L., Leyne, M., & Slaugenhaupt, S. A. (2009). Loss of Mouse Ikbkap, a Subunit of Elongator, Leads to Transcriptional Deficits and Embryonic Lethality That Can Be Rescued by Human IKBKAP. *Molecular and Cellular Biology*, *29*(3), 736–744. https://doi.org/10.1128/MCB.01313-08

Cheishvili, D., Maayan, C., Cohen-Kupiec, R., Lefler, S., Weil, M., Ast, G., & Razin, A. (n.d.). *IKAP/Elp1 involvement in cytoskeleton regulation and implication for familial dysautonomia*. https://doi.org/10.1093/hmg/ddr036

Close, P., Hawkes, N., Cornez, I., Creppe, C., Lambert, C. A., Rogister, B., … Chariot, A. (2006). Transcription Impairment and Cell Migration Defects in Elongator-Depleted Cells: Implication for Familial Dysautonomia. *Molecular Cell*, *22*(4), 521–531. https://doi.org/10.1016/j.molcel.2006.04.017

Cohen, J. S., Srivastava, S., Farwell, K. D., Lu, H. M., Zeng, W., Lu, H., … Fatemi, A. (2015). ELP2 is a novel gene implicated in neurodevelopmental disabilities. *American Journal of Medical Genetics. Part A*, *167*(6), 1391–1395. https://doi.org/10.1002/AJMG.A.36935

Collins, T. J. (2007). ImageJ for microscopy. *BioTechniques*, *43*(1S), S25–S30. https://doi.org/10.2144/000112517/asset/images/large/figure4.JPEG

Copp, A. J., Greene, N. D. E., & Murdoch, J. N. (2003). The genetic basis of mammalian neurulation. *Nature Reviews Genetics*, *4*(10), 784–793. https://doi.org/10.1038/nrg1181

Cuajungco, M. P., Leyne, M., Mull, J., Gill, S. P., Gusella, J. F., & Slaugenhaupt, S. A. (2001). Cloning, Characterization, and Genomic Structure of the Mouse Ikbkap Gene. In *DNA AND CELL BIOLOGY* (Vol. 20). Retrieved from Mary Ann Liebert, Inc. Pp website: www.liebertpub.com

D'Amico-Martel, A., & Noden, D. M. (1980). An autoradiographic analysis of the development of the chick trigeminal ganglion. *Development*, *55*(1).

D'amico-Martel, A., & Noden, D. M. (1983). Contributions of placodal and neural crest cells to avian cranial peripheral ganglia. *American Journal of Anatomy*, *166*(4), 445–468. https://doi.org/10.1002/aja.1001660406

Deinhardt, K., Kim, T., Spellman, D. S., Mains, R. E., Eipper, B. A., Neubert, T. A., … Hempstead, B. L. (2011). Neuronal growth cone retraction relies on proneurotrophin receptor signaling through Rac. *Science Signaling*, *4*(202). https://doi.org/10.1126/SCISIGNAL.2002060

Dent, E. W., Gupton, S. L., & Gertler, F. B. (2011). The Growth Cone Cytoskeleton in Axon Outgrowth and Guidance. *Cold Spring Harbor Perspectives in Biology*, *3*(3), 1–39. https://doi.org/10.1101/CSHPERSPECT.A001800

Dietrich, P., & Dragatsis, I. (2016). Familial dysautonomia: Mechanisms and models. *Genetics and Molecular Biology*, *39*(4), 497–514. https://doi.org/10.1590/1678-4685-GMB-2015-0335

Duband, J. L. (2010). Diversity in the molecular and cellular strategies of epithelium-to-mesenchyme transitions: Insights from the neural crest. *Cell Adhesion and Migration*, *4*(3), 458–482. https://doi.org/10.4161/cam.4.3.12501

Duband, J. L., & Thiery, J. P. (1982). Appearance and distribution of fibronectin during chick embryo gastrulation and neurulation. *Developmental Biology*, *94*(2), 337–350. https://doi.org/10.1016/0012-1606(82)90352-9

Dude, C. M., Kuan, C. Y. K., Bradshaw, J. R., Greene, N. D. E., Relaix, F., Stark, M. R., & Baker, C. V. H. (2009). Activation of Pax3 target genes is necessary but not sufficient for neurogenesis in the ophthalmic trigeminal placode. *Developmental Biology*, *326*(2), 314. https://doi.org/10.1016/J.YDBIO.2008.11

Fode, C., Gradwohl, G., Morin, X., Dierich, A., LeMeur, M., Goridis, C., & Guillemot, F. (1998). The bHLH protein NEUROGENIN 2 is a determination factor for epibranchial placode-derived sensory neurons. *Neuron*, *20*(3), 483–494. https://doi.org/10.1016/S0896-6273(00)80989-7

Freter, S., Fleenor, S. J., Freter, R., Liu, K. J., & Begbie, J. (2013). Cranial neural crest cells form corridors prefiguring sensory neuroblast migration. *Development (Cambridge)*, *140*(17), 3595–3600. https://doi.org/10.1242/dev.091033

Gaudillière, B., Konishi, Y., De La Iglesia, N., Yao, G. L., & Bonni, A. (2004). A CaMKII-NeuroD Signaling Pathway Specifies Dendritic Morphogenesis. *Neuron*, *41*(2), 229–241. https://doi.org/10.1016/S0896-6273(03)00841-9

George, L., Chaverra, M., Wolfe, L., Thorne, J., Close-Davis, M., Eibs, A., … Lefcort, F. (2013). Familial dysautonomia model reveals Ikbkap deletion causes apoptosis of Pax3+ progenitors and peripheral neurons. *Proceedings of the National Academy of Sciences of the United States of America*, *110*(46), 18698–18703. https://doi.org/10.1073/pnas.1308596110

Goffena, J., Lefcort, F., Zhang, Y., Lehrmann, E., Chaverra, M., Felig, J., … George, L. (2018). Elongator and codon bias regulate protein levels in mammalian peripheral neurons. *Nature Communications*. https://doi.org/10.1038/s41467-018-03221-z

Gold-von Simson, G., & Axelrod, F. B. (2006). Familial Dysautonomia: Update and Recent Advances. *Current Problems in Pediatric and Adolescent Health Care*, *36*(6), 218–237. https://doi.org/10.1016/j.cppeds.2005.12.001

Gutiérrez, J. V., Norcliffe-Kaufmann, L., & Kaufmann, H. (2015). Brainstem reflexes in patients with familial dysautonomia. *Clinical Neurophysiology*, *126*(3), 626–633. https://doi.org/10.1016/j.clinph.2014.06.028

Halmi, C. A., Wu, C. Y., & Taneyhill, L. A. (2022). Neural crest cell-placodal neuron interactions are mediated by Cadherin-7 and N-cadherin during early chick trigeminal ganglion assembly. *F1000Research*, *11*, 1–28. https://doi.org/10.12688/f1000research.122686.2

Hamburger, V. (1961). Experimental analysis of the dual origin of the trigeminal ganglion in the chick embryo. *Journal of Experimental Zoology*, *148*(2), 91–123. https://doi.org/10.1002/jez.1401480202

Hamburger, V., & Hamilton, H. L. (1992). A series of normal stages in the development of the chick embryo. *Developmental Dynamics*, *195*(4), 231–272. https://doi.org/10.1002/aja.1001950404

Hardwick, L. J. A., & Philpott, A. (2015). Multi-site phosphorylation regulates NeuroD4 activity during primary neurogenesis: a conserved mechanism amongst proneural proteins. *Neural Development*, *10*(1). https://doi.org/10.1186/S13064-015-0044-8

Hatta, K., Takagi, S., Fujisawa, H., & Takeichi, M. (1987). Spatial and temporal expression pattern of N-cadherin cell adhesion molecules correlated with morphogenetic processes of chicken embryos. *Developmental Biology*, *120*(1), 215–227. https://doi.org/10.1016/0012-1606(87)90119-9

Hawkes, N. A., Otero, G., Sebastiaan Winkler, G., Marshall, N., Dahmus, M. E., Krappmann, D., … Svejstrup, J. Q. (2002). Purification and characterization of the human elongator complex. *The Journal of Biological Chemistry*, *277*(4), 3047–3052. https://doi.org/10.1074/JBC.M110445200

Higashiyama, H., & Kuratani, S. (2014). On the maxillary nerve. *Journal of Morphology*, *275*(1), 17–38. https://doi.org/10.1002/jmor.20193

Huang, B., Jian, L., & Byström, A. S. (2008). A genome-wide screen identifies genes required for formation of the wobble nucleoside 5-methoxycarbonylmethyl-2-thiouridine in Saccharomyces cerevisiae. *RNA (New York, N.Y.)*, *14*(10), 2183–2194. https://doi.org/10.1261/RNA.1184108

Hou, B., Zhang, D., Zhao, S., Wei, M., Yang, Z., Wang, S., … Jiang, T. (2015). Scalable and DiI-compatible optical clearance of the mammalian brain. *Frontiers in Neuroanatomy*, *9*(FEB). https://doi.org/10.3389/FNANA.2015.00019

Huang, B., Johansson, M. J. O., & Byström, A. S. (2005). An early step in wobble uridine tRNA modification requires the Elongator complex. *Rna*, *11*(4), 424–436. https://doi.org/10.1261/rna.7247705

Huang, C., Chan, J. A., & Schuurmans, C. (2014). Proneural bHLH genes in development and disease. *Current Topics in Developmental Biology*, *110*, 75–127. https://doi.org/10.1016/B978-0-12-405943-6.00002-6

Huang, E. J., Wilkinson, G. A., Fariñas, I., Backus, C., Zang, K., Wong, S. L., & Reichardt, L. F. (1999). Expression of Trk receptors in the developing mouse trigeminal ganglion: in vivo evidence for NT-3 activation of TrkA and TrkB in addition to TrkC. *Development*, *126*(10), 2191–2203. https://doi.org/10.1242/DEV.126.10.2191

Huang, E. J., Zang, K., Schmidt, A., Saulys, A., Xiang, M., & Reichardt, L. F. (1999). POU domain factor Brn-3a controls the differentiation and survival of trigeminal neurons by regulating Trk receptor expression. *Development*, *126*(13), 2869–2882. https://doi.org/10.1242/DEV.126.13.2869

Hunnicutt, B. J., Chaverra, M., George, L., & Lefcort, F. (2012). IKAP/Elp1 Is Required In Vivo for Neurogenesis and Neuronal Survival, but Not for Neural Crest Migration. *PLoS ONE*, *7*(2), e32050. https://doi.org/10.1371/journal.pone.0032050

Jackson, M. Z., Gruner, K. A., Qin, C., & Tourtellotte, W. G. (2014). *A neuron autonomous role for the familial dysautonomia gene ELP1 in sympathetic and sensory target tissue innervation*. https://doi.org/10.1242/dev.107797

Johansen, L. D., Naumanen, T., Knudsen, A., Westerlund, N., Gromova, I., Junttila, M., … Kallunki, T. (2008). IKAP localizes to membrane ruffles with filamin A and regulates actin cytoskeleton organization and cell migration. *Journal of Cell Science*, *121*(6), 854–864. https://doi.org/10.1242/jcs.013722

Karlsborn, T., Tükenmez, H., Mahmud, A. K. M. F., Xu, F., Xu, H., & Byström, A. S. (2014). Elongator, a conserved complex required for wobble uridine modifications in Eukaryotes. *RNA Biology*, *11*(12), 1519–1528. https://doi.org/10.4161/15476286.2014.992276

Kojic, M., & Wainwright, B. (2016). The many faces of elongator in neurodevelopment and disease. *Frontiers in Molecular Neuroscience*, *9*(NOV2016), 1–10. https://doi.org/10.3389/fnmol.2016.00115

Koontz, A., Urrutia, H. A., & Bronner, M. E. (2023). Making a head: Neural crest and ectodermal placodes in cranial sensory development. *Seminars in Cell & Developmental Biology*, *138*, 15. https://doi.org/10.1016/J.SEMCDB.2022.06.009

Lee, J. E., Hollenberg, S. M., Snider, L., Turner, D. L., Lipnick, N., & Weintraub, H. (1995). Conversion of Xenopus ectoderm into neurons by NeuroD, a basic helix-loop-helix protein. *Science (New York, N.Y.)*, *268*(5212), 836–844. https://doi.org/10.1126/SCIENCE.7754368

Lee, T. Y., Cho, I. S., Bashyal, N., Naya, F. J., Tsai, M. J., Yoon, J. S., … Suh-Kim, H. (2020). ERK Regulates NeuroD1-mediated Neurite Outgrowth via Proteasomal Degradation. *Experimental Neurobiology*, *29*(3), 189. https://doi.org/10.5607/EN20021

Leonard, C. E., Quiros, J., Lefcort, F., & Taneyhill, L. A. (2022). Loss of Elp1 disrupts trigeminal ganglion neurodevelopment in a model of familial dysautonomia. *ELife*, *11*. https://doi.org/10.7554/ELIFE.71455

Li, H. J., Ray, S. K., Pan, N., Haigh, J., Fritzsch, B., & Leiter, A. B. (2019). Intestinal Neurod1 expression impairs paneth cell differentiation and promotes enteroendocrine lineage specification. *Scientific Reports 2019 9:1*, *9*(1), 1–11. https://doi.org/10.1038/s41598-019-55292-7

Li, L., Gruner, K., & Tourtellotte, W. G. (2020). Retrograde nerve growth factor signaling abnormalities in familial dysautonomia. *Journal of Clinical Investigation*. https://doi.org/10.1172/jci130401

Lu, Y., Lin, C., & Wang, X. (2009). PiggyBac transgenic strategies in the developing chicken spinal cord. *Nucleic Acids Research*, *37*(21). https://doi.org/10.1093/nar/gkp686

Lwigale, P. Y. (2001). Embryonic origin of avian corneal sensory nerves. *Developmental Biology*, *239*(2), 323–337. https://doi.org/10.1006/dbio.2001.0450

Ma, Q., Chen, Z., Barrantes, I. D. B., De La Pompa, J. L., & Anderson, D. J. (1998). neurogenin1 is essential for the determination of neuronal precursors for proximal cranial sensory ganglia. *Neuron*, *20*(3), 469–482. https://doi.org/10.1016/S0896-6273(00)80988-5

Ma, W., Yan, R. T., Mao, W., & Wang, S. Z. (2009). Neurogenin3 promotes early retinal neurogenesis. *Molecular and Cellular Neurosciences*, *40*(2), 187. https://doi.org/10.1016/J.MCN.2008.10.006

Mass, E., & Gadoth, N. (1994). Oro-dental self-mutilation in familial dysautonomia. *Oral Pathology and Medicine*, *23*(6), 273–276. https://doi.org/10.1111/j.1600-0714.1994.tb00058.x

McCabe, K. L., Sechrist, J. W., & Bronner-Fraser, M. (2009). Birth of ophthalmic trigeminal neurons initiates early in the placodal ectoderm. *Journal of Comparative Neurology*, *514*(2), 161–173. https://doi.org/10.1002/CNE.22004

Méndez-Maldonado, K., Vega-López, G. A., Aybar, M. J., & Velasco, I. (2020). Neurogenesis From Neural Crest Cells: Molecular Mechanisms in the Formation of Cranial Nerves and Ganglia. *Frontiers in Cell and Developmental Biology*, *8*(August). https://doi.org/10.3389/fcell.2020.00635

Morimoto, Y., Fushimi, A., Yamashita, N., Hagiwara, M., Bhattacharya, A., Cheng, J., … Kufe, D. (2022). Addiction of Merkel cell carcinoma to MUC1-C identifies a potential new target for treatment. *Oncogene*, *41*(27), 3511. https://doi.org/10.1038/S41388-022-02361-3

Naftelberg, S., Abramovitch, Z., Gluska, S., Yannai, S., Joshi, Y., Donyo, M., … Ast, G. (2016). Phosphatidylserine Ameliorates Neurodegenerative Symptoms and Enhances Axonal Transport in a Mouse Model of Familial Dysautonomia. *PLOS Genetics*, *12*(12), e1006486. https://doi.org/10.1371/journal.pgen.1006486

Najmabadi, H., Hu, H., Garshasbi, M., Zemojtel, T., Abedini, S. S., Chen, W., … Ropers, H. H. (2011). Deep sequencing reveals 50 novel genes for recessive cognitive disorders. *Nature*, *478*(7367), 57–63. https://doi.org/10.1038/NATURE10423

Nakazaki, H., Reddy, A. C., Mania-Farnell, B. L., Shen, Y. W., Ichi, S., McCabe, C., … Mayanil, C. S. K. (2008). Key basic helix-loop-helix transcription factor genes Hes1 and Ngn2 are regulated by Pax3 during mouse embryonic development. *Developmental Biology*, *316*(2), 510–523. https://doi.org/10.1016/j.ydbio.2008.01.008

Norcliffe-Kaufmann, L., Slaugenhaupt, S. A., & Kaufmann, H. (2017, May 1). Familial dysautonomia: History, genotype, phenotype and translational research. *Progress in Neurobiology*, Vol. 152, pp. 131–148. https://doi.org/10.1016/j.pneurobio.2016.06.003

Ohlen, S. B., Russell, M. L., Brownstein, M. J., & Lefcort, F. (2017). BGP-15 prevents the death of neurons in a mouse model of familial dysautonomia. *Proceedings of the National Academy of Sciences of the United States of America*, *114*(19), 5035–5040. https://doi.org/10.1073/PNAS.1620212114/suppl_file/PNAS.1620212114.SM02.MOV

Otero, G., Fellows, J., Yang, L., De Bizemont, T., Dirac, A. M. G., Gustafsson, C. M., … Svejstrup, J. Q. (1999). Elongator, a multisubunit component of a novel RNA polymerase II holoenzyme for transcriptional elongation. *Molecular Cell*, *3*(1), 109–118. https://doi.org/10.1016/S1097-2765(00)80179-3

Park, B.-Y., & Saint-Jeannet, J.-P. (2010). Induction and Segregation of the Vertebrate Cranial Placodes. *Colloquium Series on Developmental Biology*, *1*(1), 1–83. https://doi.org/10.4199/c00014ed1v01y201007deb003

Perez, S. E., Rebelo, S., & Anderson, D. J. (1999). Early specification of sensory neuron fate revealed by expression and function of neurogenins in the chick embryo. *Development*, *126*(8), 1715–1728. https://doi.org/10.1242/dev.126.8.1715

Pilon, N. (2021). Treatment and Prevention of Neurocristopathies. *Trends in Molecular Medicine*, *27*(5), 451–468. https://doi.org/10.1016/j.molmed.2021.01.009

Planelles-Herrero, V. J., Bittleston, A., Seum, C., Gaitan, M. G., & Derivery, E. (2022). Elongator stabilizes microtubules to control central spindle asymmetry and polarized trafficking of cell fate determinants. *Nature Cell Biology*, *24*(11), 1606–1616. https://doi.org/10.1038/s41556-022-01020-9

Rahl, P. B., Chen, C. Z., & Collins, R. N. (2005). Elp1p, the yeast homolog of the FD disease syndrome protein, negatively regulates exocytosis independently of transcriptional elongation. *Molecular Cell*, *17*(6), 841–853. https://doi.org/10.1016/j.molcel.2005.02.018

Reichardt, L. F. (2006). Neurotrophin-regulated signalling pathways. *Philosophical Transactions of the Royal Society B: Biological Sciences*, *361*(1473), 1545–1564. https://doi.org/10.1098/rstb.2006.1894

Sadaghiani, B., & Thiébaud, C. H. (1987). Neural crest development in the Xenopus laevis embryo, studied by interspecific transplantation and scanning electron microscopy. *Developmental Biology*, *124*(1), 91–110. https://doi.org/10.1016/0012-1606(87)90463-5

Saint-Germain, N., Lee, Y. H., Zhang, Y., Sargent, T. D., & Saint-Jeannet, J. P. (2004). Specification of the otic placode depends on Sox9 function in Xenopus. *Development*, *131*(8), 1755–1763. https://doi.org/10.1242/DEV.01066

Saint-Jeannet, J. P., & Moody, S. A. (2014). Establishing the pre-placodal region and breaking it into placodes with distinct identities. *Developmental Biology*, *389*(1), 13–27. https://doi.org/10.1016/j.ydbio.2014.02.011

Sato, Y., Okamoto, I., Kameyama, H., Kudoh, S., Saito, H., Sanada, M., … Ito, T. (2020). Integrated Immunohistochemical Study on Small-Cell Carcinoma of the Lung Focusing on Transcription and Co-Transcription Factors. *Diagnostics*, *10*(11). https://doi.org/10.3390/DIAGNOSTICS10110949

Schindelin, J., Arganda-Carreras, I., Frise, E., Kaynig, V., Longair, M., Pietzsch, T., … Cardona, A. (2012). Fiji - an Open Source platform for biological image analysis. *Nature Methods*, *9*(7), 676–682. https://doi.org/10.1038/NMETH.2019

Seo, S., Lim, J. W., Yellajoshyula, D., Chang, L. W., & Kroll, K. L. (2007). Neurogenin and NeuroD direct transcriptional targets and their regulatory enhancers. *The EMBO Journal*, *26*(24), 5093. https://doi.org/10.1038/SJ.EMBOJ.7601923

Shah, A., Schiffmacher, A. T., & Taneyhill, L. A. (2017). Annexin A6 controls neuronal membrane dynamics throughout chick cranial sensory gangliogenesis. *Developmental Biology*, *425*(1), 85–99. https://doi.org/10.1016/j.ydbio.2017.03.011

Shiau, C. E., & Bronner-Fraser, M. (2009). N-cadherin acts in concert with Slit1-Robo2 signaling in regulating aggregation of placode-derived cranial sensory neurons. *Development*, *136*(24), 4155–4164. https://doi.org/10.1242/dev.034355

Shiau, C. E., Lwigale, P. Y., Das, R. M., Wilson, S. A., & Bronner-Fraser, M. (2008). Robo2-Slit1 dependent cell-cell interactions mediate assembly of the trigeminal ganglion. *Nature Neuroscience*, *11*(3), 269–276. https://doi.org/10.1038/nn2051

Simoes-Costa, M., & Bronner, M. E. (2015). Establishing neural crest identity: a gene regulatory recipe. *Development*, *142*(2), 242–257. https://doi.org/10.1242/dev.105445

Simões-Costa, M., & Bronner, M. E. (2013). Insights into neural crest development and evolution from genomic analysis. *Genome Research*, *23*(7), 1069–1080. https://doi.org/10.1101/gr.157586.113

Simpson, C. L., Lemmens, R., Miskiewicz, K., Broom, W. J., Hansen, V. K., van Vught, P. W. J., … Al-Chalabi, A. (2009). Variants of the elongator protein 3 (ELP3) gene are associated with motor neuron degeneration. *Human Molecular Genetics*, *18*(3), 472–481. https://doi.org/10.1093/HMG/DDN375

Singh, A., Mahesh, A., Noack, F., de Toledo, B. C., Calegari, F., & Tiwari, V. K. (2022). Tcf12 and NeuroD1 cooperatively drive neuronal migration during cortical development. *Development (Cambridge, England)*, *149*(3). https://doi.org/10.1242/DEV.200250

Singh, S., & Groves, A. (2016). The Molecular Basis of Craniofacial Placode Development. *Wiley Interdisciplinary Reviews: Developmental Biology*, *5*(3), 363–376. https://doi.org/10.1002/wdev.226.

Slaugenhaupt, S. A., Blumenfeld, A., Gill, S. P., Leyne, M., Mull, J., Cuajungco, M. P., … Gusella, J. F. (2001). Tissue-Specific Expression of a Splicing Mutation in the IKBKAP Gene Causes Familial Dysautonomia. In *Am. J. Hum. Genet* (Vol. 68). Retrieved from https://www.ncbi.nlm.nih.gov/pmc/articles/PMC1274473/pdf/AJHGv68p598.pdf

Solinger, J. A., Paolinelli, R., Klöß, H., Scorza, F. B., Marchesi, S., Sauder, U., … Cassata, G. (2010). The Caenorhabditis elegans Elongator Complex Regulates Neuronal α-tubulin Acetylation. *PLOS Genetics*, *6*(1), e1000820. https://doi.org/10.1371/JOURNAL.PGEN.1000820

Stark, M. R., Sechrist, J., Bronner-Fraser, M., & Marcelle, C. (1997). Neural tube-ectoderm interactions are required for trigeminal placode formation. *Development*, *124*(21), 4287–4295. https://doi.org/10.1242/DEV.124.21.4287

Steventon, B., Mayor, R., & Streit, A. (2014). Neural crest and placode interaction during the development of the cranial sensory system. *Developmental Biology*, *389*(1), 28–38. https://doi.org/10.1016/j.ydbio.2014.01.021

Strug, L. J., Clarke, T., Chiang, T., Chien, M., Baskurt, Z., Li, W., … Pal, D. K. (2009). Centrotemporal sharp wave EEG trait in rolandic epilepsy maps to Elongator Protein Complex 4 (ELP4). *European Journal of Human Genetics : EJHG*, *17*(9), 1171–1181. https://doi.org/10.1038/EJHG.2008.267

Svejstrup, J. Q. (2007, June 1). Elongator complex: how many roles does it play? *Current Opinion in Cell Biology*, Vol. 19, pp. 331–336. https://doi.org/10.1016/j.ceb.2007.04.005

Tandon, P., Showell, C., Christine, K., & Conlon, F. L. (2012). Morpholino injection in Xenopus. *Methods in Molecular Biology*, *843*, 29–46. https://doi.org/10.1007/978-1-61779-523-7_4

Theveneau, E., & Mayor, R. (2012, June 1). Neural crest delamination and migration: From epithelium-to-mesenchyme transition to collective cell migration. *Developmental Biology*, Vol. 366, pp. 34–54. https://doi.org/10.1016/j.ydbio.2011.12.041

Trigeminal Neuralgia: Symptoms, Causes, Treatment & Surgery. (n.d.). Retrieved April 8, 2024, from https://my.clevelandclinic.org/health/diseases/15671-trigeminal-neuralgia-tn

Vega-Lopez, G. A., Cerrizuela, S., Tribulo, C., & Aybar, M. J. (2018). Neurocristopathies: New insights 150 years after the neural crest discovery. *Developmental Biology*, *444*(May), S110–S143. https://doi.org/10.1016/j.ydbio.2018.05.013

Vermeiren, S., Bellefroid, E. J., & Desiderio, S. (2020). Vertebrate Sensory Ganglia: Common and Divergent Features of the Transcriptional Programs Generating Their Functional Specialization. *Frontiers in Cell and Developmental Biology*, *8*(October). https://doi.org/10.3389/fcell.2020.587699

Won, E., Palma, J.-A., Kaufmann, H., Milla, S. S., Cohen, B., Norcliffe-Kaufmann, L., … Lui, Y. W. (2019). Quantitative magnetic resonance evaluation of the trigeminal nerve in familial dysautonomia. *Clinical Autonomic Research*, *29*, 469–473. https://doi.org/10.1007/s10286-019-00593-0

Wu, C., & Taneyhill, L. A. (2019). Cadherin-7 mediates proper neural crest cell–placodal neuron interactions during trigeminal ganglion assembly. *Genesis*, *57*(1), e23264. https://doi.org/10.1002/dvg.23264

Wu, C. Y., Hooper, R. M., Han, K., & Taneyhill, L. A. (2014). Migratory neural crest cell αN-catenin impacts chick trigeminal ganglia formation. *Developmental Biology*, *392*(2), 295–307. https://doi.org/10.1016/j.ydbio.2014.05.016

Xu, Hong, Dude, C. M., & Baker, C. V. H. (2008). Fine-grained fate maps for the ophthalmic and maxillomandibular trigeminal placodes in the chick embryo. *Developmental Biology*, *317*(1), 174–186. https://doi.org/10.1016/j.ydbio.2008.02.012

Xu, Huisha, Lin, Z., Li, F., Diao, W., Dong, C., Zhou, H., … Long, J. (2015). Dimerization of elongator protein 1 is essential for Elongator complex assembly. *Proceedings of the National Academy of Sciences of the United States of America*, *112*(34), 10697–10702. https://doi.org/10.1073/pnas.1502597112